

Dissertation
submitted to the
Combined Faculty of Natural Sciences and Mathematics
of the Ruperto Carola University Heidelberg, Germany
for the degree of
Doctor of Natural Sciences

Presented by

B.A. Holly Amelia Rebecca Giles

born in Portsmouth

Oral examination: Feb 20, 2021 (to discuss)

Drug - microenvironment - gene interactions in Chronic
Lymphocytic Leukemia

Referees: Dr. Judith Zaugg
Prof. Dr. Michael Boutros

To Mum, Dad and Milly x

Acknowledgements

I would like to thank

List of publications

Thesis related

- Peter-Martin Bruch*, Holly A. R. Giles*, Carolin Kolb, Sophie Herbst, Tina Bećirović, Tobias Roider, Junyan Lu, Sebastian Scheinost, Lena Wagner, Jennifer Huellein, Ivan Berest, Mark Kriegsmann, Katharina Kriegsmann, Christiane Zgorzelski, Peter Dreger, Judith Zaugg, Carsten Müller-Tidow, Thorsten Zenz, Wolfgang Huber, Sascha Dietrich et al. "Mapping drug-microenvironment-genetic interplay in CLL reveals trisomy 12 as a modulator of microenvironmental signalling." *bioRxiv*. DOI: 10.1101/2021.07.23.453514

Other contributions

The author of this thesis also contributed to a number of other projects throughout the PhD. The following have been published:

- Berest, Ivan*, Christian Arnold*, Armando Reyes-Palomares, Giovanni Palla, Kasper Dindler Rasmussen, Holly Giles, and Peter-Martin Bruch et al. 2019. "Quantification Of Differential Transcription Factor Activity And Multiomics-Based Classification Into Activators And Repressors: DiffTF". *Cell Reports* DOI: 10.1016/j.celrep.2019.10.106
- Lu, Junyan*, Ester Cannizzaro*, Fabienne Meier-Abt, Sebastian Scheinost, Peter Martin Bruch, Holly A. R. Giles, and Almut Lütge et al. 2021. "Multi-Omics Reveals Clinically Relevant Proliferative Drive Associated With Mtor-MYC-OXPHOS Activity In Chronic Lymphocytic Leukemia". *Nature Cancer*. DOI: 10.1038/s43018-021-00216-6

List of other contributions and achievements

Conference Talks and Posters

I have additionally presented at the following meetings during my PhD:

- 19th International EMBL PhD Symposium 2017
- Molecular Medicine Partnership Unit (MMPU) Summer Research Meeting 2018
- ASCONA Workshop: Statistics for Medical Data Science 2019
- MMPU Summer Research Meeting 2019

Courses and Conferences

During my PhD, I attended the following courses and conferences:

2017:

- Huber Group Retreat, Dubrovnik *12th - 15th Sept 2017*
- EMBL EIPP Predoc Course, Heidelberg *1st Oct - 15th Dec 2017*
- EMBL PhD Symposium, Heidelberg *19th - 21st Oct 2017*

2018:

- Huber-Dietrich SOUND retreat, Black Forest *19th - 20th Feb 2018*
- EMBL Biocomputing Retreat, Black Forest *19th - 21st Mar 2018*
- EMBL Course: Statistical Methods in Bioinformatics, Heidelberg *25th - 27th Apr 2018*

- EMBL Course: GitLab, Heidelberg *Apr 2018*
- EMBL Course: Using the Cluster, Heidelberg *May 2018*
- Quantitative Genomics Conference, London *14th Jun 2018*
- EMBL Genome Biology Retreat, Boppard *21st - 22nd Jun 2018*
- CSAMA Bioinformatics Course, Brixen *9th - 13th Jul 2018*
- EMBL Course: ATACseq Analysis, Heidelberg *10th - 14th Sept 2018*
- Lymphoid Malignancies Conference, Dublin *29th - 30th Sept 2018*
- EMBL Predoc Retreat, Pilsen *4 - 5th Oct 2018*
- MMPU Winter Research Day, Heidelberg *16th Nov 2018*
- EMBL PhD Symposium, Heidelberg *21st - 24th Nov 2018*
- EBI Bioinformatics Course, Cambridge *26th Nov - 2nd Dec 2018*

2019:

- EMBL Biocomputing Retreat, Black Forest *18th - 20th Feb 2019*
- Therapeutic targeting of the Tumour Microenvironment in Leukaemia, London *24th - 26th Feb 2019*
- EMBL Genome Biology Retreat *28th - 29th Mar 2019*
- MASAMB (Mathematical and Statistical Aspects of Molecular Biology), Cambridge *25 - 26th Apr 2019*
- MMPU Summer Research Day, Heidelberg *10th May 2019*
- Huber Group Retreat, Mallorca *20th - 24th May 2019*
- ASCONA 2019: Statistics for Medical Data Science *17th - 21st Jun 2019*
- EMBL Course: Corporate Winter School, Heidelberg *Sept 2019 and Feb 2020*

2020:

- Modern Statistics for Modern Biology Course *May - Jul 2020*

Software

During my PhD, I have published the following software:

- **Giles, Holly A. R.** and Peter M. Bruch, 2021. CLLCytokineScreen2021: Complete data and executable scripts to reproduce the figures and analysis presented in Bruch and Giles et al. 2021. <https://github.com/Huber-group-EMBL/CLLCytokineScreen2021>
- **Giles, Holly A. R.** and Peter M. Bruch, 2021. CLLCytokineScreen2021Shiny: Shiny app to explore the dataset presented in Bruch and Giles et al. 2021. https://www.imbi.uni-heidelberg.de/dietrichlab/CLL_Microenvironment/

Responsibilities

- **Coordinator, EMBL PhD Symposium 2018** My role as Coordinator involved managing a team of 30 fellow PhD students to plan and implement a large-scale conference, with over 220 attendees and a budget of over €60000.
- **External Consultant, Merck KGaA** I advised Merck regarding the implementation of the project proposal I submitted as part of Team Healthy Lives at the 2018 Merck Innovation Cup.

Awards

- **Joachim-Herz Add-on Fellowship for Interdisciplinary Life Science 2019, €12000** In 2019 I was awarded the Joachim-Herz Add-on Fellowship, which funds interdisciplinary research and qualification (e.g. stays at a research lab and participation in conferences) over a period of two years.
- **Merck Innovation Cup, €5000** As part of a team of six, I competed in the Merck Innovation Cup, winning first prize in the Healthy Lives category for our business proposal for a new pharmaceutical product to improve our preparedness for future viral pandemics.

Contributions

Unless stated otherwise, the computational methods, statistical inference and regression modelling presented here were primarily conceptualised, performed, and interpreted by me, with support from my supervisors Dr. Wolfgang Huber and Dr. Sascha Dietrich. This shiny app and software documentation was assembled by me, using the scripts generated with Peter-Martin Bruch for the manuscript Bruch and Giles et al. 2021. Processing of screening data and clinical data was performed by my colleague in the Department of Medicine, University of Heidelberg, Peter Martin-Bruch. Where stated, figures were jointly produced with Peter Martin-Bruch and with input from Wolfgang Huber and Sascha Dietrich for the manuscript Bruch and Giles et al. 2021. Junyan Lu provided advice and code to support regression modelling. Ivan Berest and Christian Arnold supported processing and analysis of ATAC sequencing datasets.

The experiments described in this thesis were generated as follows. The drug - stimulus perturbation assay was performed primarily by Peter Martin-Bruch, with support from Dr. Sascha Dietrich, Carolin Kolb, Dr. Sebastian Scheinhost and Lena Wagner. Additional follow-up experiments presented in this thesis were performed by colleagues at EMBL and the Department of Medicine, University of Heidelberg:

- The Spi-B and PU.1 shRNA Knockdowns were performed by Tina Becirovic and Sophie Herbst
- The immunohistochemistry (IHC) staining of CLL and non-neoplastic lymph nodes were performed by Mark Kriegsmann, Katharina Kriegsmann and Christiane Zgorzelski
- The Ibrutinib - IL4 - STAT6i interaction assay on CLL PMBCs was performed by Peter-Martin Bruch
- The joint RNAseq - ATACseq - Mass Spectrometry of treated CLL PMBC samples

was performed by Peter-Martin Bruch and Nayara Trevisan Doimo de Azevedohe
I supported the initiation and experimental design of these follow-up experiments, in
addition to analysis and interpretation of the resulting data.

xi

Zusammenfassung

Abstract in German Aktuelle Entwicklungen im Bereich der “omic”-Technologien tragen wesentlich zur Beschleunigung des Fortschritts in der Krebsforschung bei etc

Abstract

[IN PROGRESS] Chronic Lymphocytic Leukaemia is a malignancy of mature B lymphocytes, characterised by the accumulation of malignant cells within the blood, bone marrow and lymph nodes. The disease pathogenesis is driven by multiple factors, including molecular features, signalling via the B cell receptor (BCR) and interactions with non-neoplastic cells within the lymphoid tissues (known as the tumour microenvironment). The impact of individual genetic features and microenvironmental signals has been well-characterised, and CLL represents a success story in linking advances in molecular understanding to improvements in clinical approaches. However, very few studies have studied these features integratively, and systematic investigations of the influence of cell-intrinsic and cell-extrinsic features on CLL are lacking. To investigate the integrative impact of these features on CLL biology, in this thesis I analyse screening data of primary patient samples, combined with multi-omics profiles of the same samples. The screen was performed using 12 drugs co-applied with 17 individual microenvironmental stimuli on CLL peripheral blood mononucleated cells ($n = 192$). I combined this data with whole-exome sequencing, DNA-methylation, RNA-sequencing and copy number variant data of matching tumour samples, and additional ATAC-sequencing and RNA-sequencing data for validation work. The screening data is complemented with *in vivo* data on clinical outcomes, and IHC of patient lymph nodes stained for pSTAT6, pIRAK4 and STAT6. I apply statistical inference and regression modelling to integrate multiple data types, with the aim of finding new drivers and mechanisms of drug resistance in CLL. Profiling responses to microenvironmental stimulation across the heterogeneous patient cohort delineates four patient subgroups that have differential disease progression dynamics, and molecular profiles, suggesting the dynamics of the microenvironment is important to disease outcomes. I perform a systematic survey of genetic determinants of microenvironmental response and identify trisomy 12 as a modulator of microenvironmental stimulation. The data suggest that the activity of the transcription factors Spi-B and PU.1 may mediate this effect. I generate a map of interactions

between microenvironmental signalling pathways and drugs, and identify novel drug - resistance mechanism including the effect of interferon gamma on ibrutinib toxicity. I demonstrate how drug - microenvironment interactions can be further modulated by molecular features, and identify drug resistance mechanism that occur in suggests of CLL cases. For example, TLR activity induces resistance to fludarabine in IGH-U and triomsy 12 patients, but not in IGHV-M. I demonstrate the *in vivo* relevance of these findings within CLL-infiltrated lymph nodes, which show higher levels of IL4 and TLR signalling compared to non-neoplastic samples ($p<0.001$). Elevated IL4 signalling in CLL -infiltrated lymph nodes correlates with poorer outcomes ($p=0.038$). CLL represents a prototypic model for the study of cell-intrinsic and cell-extrinsic features in cancers. This data set represents an important resource for exploring the impact of these features and I have published the dataset and reproducible analyses as part of an online git repository () and interactive shiny app(). Collectively, these results demonstrate the integrative impact of molecular features and microenvironmental stimuli on drug response and propose potential novel drivers and drug resistance mechanisms and strategies for targeting these in future work.

Table of Contents

Acknowledgements	i
List of publications	iii
List of other contributions and achievements	v
Contributions	ix
Zusammenfassung	xiii
Abstract	xv
List of Abbreviations	xxii
1 Introduction	1
1.1 Chronic Lymphocytic Leukemia (CLL)	1
1.1.1 Disease characteristics	1
1.1.2 Cell of Origin	2
1.1.3 IGHV status	3
1.1.4 The central role of BCR signalling	4
1.1.5 Recurrent genetic features in CLL	6
1.2 Therapies in CLL	11
1.2.1 Chemotherapy and chemoimmunotherapy	11
1.2.2 Targeted therapies	11
1.2.3 Management algorithm	12
1.3 The tumour microenvironment in CLL	14
1.3.1 The role of the tumour microenvironment in CLL	14
1.3.2 Components of the tumour microenvironment	14

1.3.3	Microenvironmental pathways	16
1.3.4	The influence of the microenvironment on drug response	18
1.3.5	Modelling the tumour microenvironment	19
1.4	CLL as a model for studying tumour biology	21
1.5	Background to the approaches used in this thesis	22
1.5.1	<i>Ex-vivo</i> drug perturbation screens	22
1.5.2	Multiomics profiling and integration of multiple datatypes	23
1.5.3	Mathematical modelling	24
1.6	Summary of this thesis	26
2	Methods	29
2.1	Experimental methods:	29
2.1.1	Combinatorial Drug - Stimulus Perturbation Screen	29
2.1.2	Follow - up investigations	31
2.2	Additional Data and Data availability	34
2.3	Data processing	34
2.3.1	Screening data	34
2.3.2	Follow - up investigations	35
2.4	Statistical Analysis	37
2.4.1	Analysis of Screening Data	37
2.4.2	Analysis of follow-up data	40
3	Data	47
3.1	Experimental overview	47
3.1.1	Drug-stimulus combinatorial perturbation assay and patient sample multi-omic profiling	47
3.1.2	Additional datasets	49
3.2	Data Processing	49
3.2.1	Processing the raw values obtained from the screen	49
3.2.2	Quality control and data reproducibility	50
3.3	Characteristics of drugs used in the screen	50
3.3.1	The panel of drugs	51
3.3.2	Assessing drug response	51
3.4	Characteristics of stimuli used in the screen	52
3.4.1	The panel of stimuli	52
3.4.2	Assessing stimulus response	53
3.5	Characteristics of patient samples used in the screen	53

3.5.1	Overview of the molecular profiles of the patient samples	53
3.6	Making the data and associated analysis available	54
3.6.1	Shiny app	55
3.6.2	Online code repository	57
4	Ex-vivo sensitivity to microenvironmental stimulation in primary CLL cells	61
4.1	Proliferating responses to the panel of stimuli	62
4.1.1	<i>ex vivo</i> assay demonstrates functional diversity of cytokines and microenvironmental stimuli	62
4.1.2	Microenvironmental response profiling identifies discrete patient subgroups	63
4.2	Functional characterisation of patient clusters	65
4.2.1	C1 - C4 show distinct response profiles with the panel of stimuli	65
4.2.2	The clusters show differences in disease dynamics	66
4.2.3	The clusters show differential responses to drugs <i>in vitro</i>	68
4.2.4	The clusters are enriched for different genetic features	69
4.2.5	GSEA of DE genes between subgroups	71
4.3	Summary	73
5	Genetic modulators of responses to microenvironmental stimulation	77
5.1	Systematic analysis of the effect of genetic features on responses to stimuli	78
5.1.1	Univariate analysis identifies IGHV status and trisomy 12 as key modulators of microenvironmental response	78
5.1.2	Multivariate analysis of gene - stimulus associations confirms IGHV status and trisomy 12 as key modulators of stimulus response	79
5.1.3	Response to TLR stimulation is dependent on IGHV status, trisomy 12 and mutations in DNA Damage Response genes	80
5.2	Investigating trisomy 12 as a modulator of microenvironmental response	83
5.2.1	Trisomy 12 is a modulator of microenvironmental response	83
5.2.2	<i>STAT6</i> , <i>IRAK4</i> and <i>SMAD3</i> are more highly expressed in trisomy 12 CLL	84
5.2.3	Classification analysis identifies trisomy 12 phenocopies that show increased expression of <i>IRAK4</i> and <i>SMAD3</i>	86
5.2.4	Spi-B and PU.1 TFs show higher binding site accessibility in trisomy 12 CLL	88
5.2.5	Spi-B and PU.1 targets are enriched for immune signalling pathways	91

5.2.6 Double knockdown of Spi-B and PU.1 reduces proliferation of trisomy 12 cell lines	92
5.3 Summary	93
6 Molecular and microenvironmental modulators of drug response in CLL	95
6.1 The impact of microenvironmental stimuli on drug response	96
6.1.1 Linear modelling maps interactions between drugs and stimuli	96
6.1.2 Drug - stimulus interactions can be categorised by their mode of action	97
6.1.3 Investigating specific drug-stimulus interactions indicates that INF γ induces resistance to ibrutinib <i>in vitro</i>	99
6.2 Genetic modulators of drug response	102
6.2.1 Univariate analysis identifies trisomy 12 as a key modulator of drug response	102
6.3 The modulatory effect of mutations on drug - stimuli interactions	104
6.3.1 Patient - specific linear modelling identifies drug - stimulus - gene interactions	104
6.3.2 Patient - specific drug - stimulus interactions of clinical interest	107
6.4 Summary	109
7 Discussion	113
References	115
Appendix	153
Figures	153
Tables	154

List of Abbreviations

AML	Acute myeloid leukaemia
AKT	Protein kinase B
ATACseq	Assay for Transposase-Accessible Chromatin using sequencing
ATP	Adenosine triphosphate
AUC	Area under curve
BAFF	B cell-activating factor
BCR	B-cell receptor
BH	Benjamini-Hochberg
BMSC	Mesenchymal bone marrow stromal cell
BTK	Brutons tyrosine kinase
CD40L	CD40 Ligand
CDF	Cumulative Distribution Function
ChIPseq	Chromatin immunoprecipitation sequencing
CLL	Chronic lymphocytic leukemia
CNV	Copy number variation
CI	Confidence Interval
CpG ODN	CpG oligodeoxynucleotides
DMSO	Dimethyl sulfoxide
DNA	Deoxyribonucleic acid
DNaseq	DNA sequencing
ERK	Ras-dependent extracellular signal-regulated kinase
FACS	Flourescence-activated cell sorting
FBS	Fetal bovine serum
FDA	Federal Drug Administration
FDC	Follicular dendritic cell
FDR	False discovery rate
GSEA	Gene set enrichment analysis
HR	Hazard ratio

HS-5 CM	HS-5 Conditioned Medium
IFN γ	Interferon γ
Ig	Immunoglobulin
IGHV	Immunoglobulin heavy chain variable region
IHC	Immunohistochemistry
IL	Interleukin
JAK	Janus kinase
M-CLL	CLL with somatic hypermutations in IGHV loci
U-CLL	CLL without somatic hypermutations in IGHV loci
MACS	Magnetic-activated cell sorting
MAPK	Mitogen-activated protein kinase
MRD	Minimal residual disease
MSCs	Mesenchymal stromal cells
NF κ B	Nuclear factor kappa-light-chain-enhancer of activated B cells
NLC	nurselike cell
NOTCH	Neurogenic locus notch
OS	Overall survival
PBMC	Peripheral blood mononuclear cells
PCA	Principal component analysis
PKC	Protein kinase C
PLC- γ 2	phospholipase C γ 2
PI3K	Phosphoinositide 3-kinase
RNA	Ribonucleic acid
RNAseq	RNA sequencing
SDF1 α	Stromal Cell-Derived Factor-1 alpha
SF3B1	Splicing factor 3B subunit 1
STAT	Signal transducer and activator of transcription
SYK	Spleen tyrosine kinase
TF	Transcription factor
TGF β	Transforming growth factor β
Th cell	T-helper cell
TLR	Toll-like receptor
TSS	Transcription start site
TTFT	Time to first treatment
TTT	Time to next treatment
U-CLL	CLL without somatic hypermutations in IGHV loci

VST	Variance Stabilising Transformation
WES	Whole exome sequencing
WGS	Whole genome sequencing
WT	Wild type
ZAP70	Tyrosine-protein kinase ZAP-70

Chapter 1

Introduction

1.1 Chronic Lymphocytic Leukemia (CLL)

1.1.1 Disease characteristics

Chronic lymphocytic leukaemia (CLL) is a malignancy of mature B cells, characterised by the progressive accumulation of malignant lymphocytes in the blood, bone marrow and lymph nodes (Kipps et al. 2017). The malignant cells can be distinguished by expression of CD5, CD19, and CD23, and by lower levels of membrane IgM, IgD, and CD79B (Matutes et al. 1994; Moreau et al. 1997; Chiorazzi, Rai, and Ferrarini 2005) (Figure 1.1).

The disease pathogenesis is driven by multiple factors, including molecular features, signalling via the B cell receptor (BCR) and interactions with non-neoplastic cells within the lymphoid tissues (known as the tumour microenvironment) (Kipps et al. 2017). Whilst the majority of CLL cells are in a resting state (B. T. Messmer et al. 2005; Defoiche et al. 2008), evidence suggests that CLL cells migrate towards lymph nodes where they form proliferation centres (Granziero et al. 2001; B. T. Messmer et al. 2005), similar to germinal centres in healthy lymph nodes, which can show a daily birth rate of up to 3.3% of the tumour (Herndon et al. 2017).

CLL is the most common leukaemia in the West, accounting for 37% of leukaemia cases and ~19,000 newly detected cancers in the US in 2016 (Kipps et al. 2017; Dubois et al. 2020). The risk of developing CLL is twice as high for men than women, and more likely with increasing age (Siegel et al. 2012; Nabhan et al. 2014; Y. Li et al. 2015; Pulte et al. 2015). Chemotherapy (Robak 2005; Chang and Kahl 2012; Lukenbill and

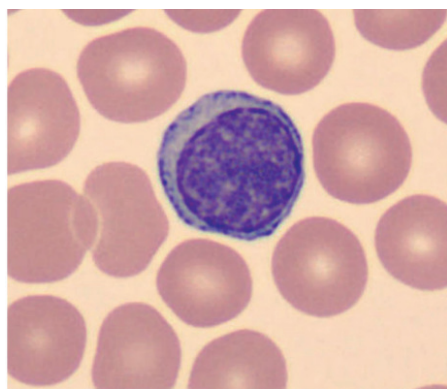


Figure 1.1: Wright–Giemsa-stained blood smear of a CLL malignant B cell, depicting typical morphology. *Figure reproduced with permission from Kipps et al. (2017).*

Kalaycio 2013) and chemoimmunotherapy (M. Hallek et al. 2010; Goede et al. 2014; Hillmen et al. 2015) has been the mainstay of therapy for many years. More recently, the central role of BCR signalling in disease pathogenesis has been appreciated and new drugs targeting this pathway have improved patient outcomes. The overall 5-years relative survival for CLL is 84% (Miller et al. 2019).

In spite of this, CLL is widely considered to be incurable (Bosch and Dalla-Favera 2019), and treatment regimens induce significant side-effects. Moreover, the disease is characterised by its clinical heterogeneity (Miller et al. 2019) and there is significant variation in disease progression amongst patients. Some patients harbour indolent disease, and can be followed by a watch-and-wait approach, sometimes going decades without requiring treatment. Others may need immediate treatment and survival can be short (Miller et al. 2019). There is a clinical need to understand the underlying biology of the disease, with a view to understanding the causes of this clinical heterogeneity and to improving patient outcomes and experiences.

1.1.2 Cell of Origin

Identifying the cell of origin of a cancer can help explain disease pathogenesis, and understand the different subtypes, and their associated prognosis. Various studies have established mature CD5+ B cells as the cell of origin in CLL (Bosch and Dalla-Favera 2019).

In healthy tissues, these mature B cells are derived from haematopoietic stem cells in

the bone marrow (Kondo 2010; Fischer et al. 2020). These stem cells develop in multiple stages, where each stage is defined by rearrangements within the immunoglobulin heavy chain and light chain loci (Pelanda and Torres 2012) that encode components of the BCR. The aim of this process is to generate a large BCR repertoire, capable of recognising a range of foreign antigens.

Developing B cells in the bone marrow undergo positive and negative selection, ensuring that each BCR binds effectively to foreign antigen, whilst eliminating those that bind strongly to self-antigen (Lebien and Tedder 2008; Mårtensson et al. 2010). These immature B cells then migrate to the lymph nodes and spleen where they differentiate into mature cells that are considered to be antigen “naive”(Chung, Silverman, and Monroe 2003).

B cells are later activated when they encounter their respective antigen. When activated, the B cells form germinal centres, which are specialised microenvironments within the lymph node that facilitate extensive proliferation. Here they undergo a process called affinity maturation, in which the loci encoding components of the BCR undergo somatic hypermutation to optimise BCR antigen specificity (Shlomchik and Weisel 2012). This process generates short-lived plasmablasts which provide immediate protection, along with plasma cells and memory B cells procuring longer-term immunity (Nutt et al. 2015).

1.1.3 IGHV status

The two major subtypes of CLL can be defined by whether the B cell of origin has undergone this process of somatic hypermutation within a germinal centre. This is reflected in the degree of mutation of the immunoglobulin heavy-chain variable region (IGHV) genes. Evidence suggests that IGHV-mutated (IGHV-M) CLLs (60% of cases) are derived from antigen-experienced B cells. On the other hand, there is continued debate as to whether IGHV-unmutated (IGHV-U) CLLs derive from naive B cells that have yet to transit through the germinal centre, or germinal-centre, antigen-experienced B cells (Klein et al. 2001).

The two subtypes show distinct clinical and molecular properties. In contrast to IGHV-M CLLs, IGHV-U CLLs have a higher proportion of high-risk genetic lesions, more commonly undergo clonal evolution and consequently have a shorter time to first treatment (TTFT) and less favourable overall survival (OS) (Hamblin et al. 1999; Damle et al. 1999; Landau et al. 2013; Puente et al. 2015; Bosch and Dalla-Favera 2019). Their

differential antigen experience also affects how they respond to signals from the microenvironment, including stimulation of the BCR.

1.1.4 The central role of BCR signalling

The BCR pathway is central to the process of selection, development, proliferation and survival of CLL clones (Chiorazzi and Ferrarini 2003; Stevenson and Caligaris-Cappio 2004; Agathangelidis et al. 2012; Jan A. Burger and Chiorazzi 2013; Iacobelli et al. 2015; Dubois et al. 2020). Evidence of the importance of this pathway comes from the observation that BCRs of CLL cells show a biased selection of IGHV and IGLV κ/λ genes. This generates BCRs that are remarkably similar across patients (Kipps et al. 1989; Fais et al. 1998; Widhopf et al. 2004; B. T. Messmer et al. 2004; K. Stamatopoulos et al. 2007), suggesting that BCR binding to certain antigens may drive selection and proliferation of CLL clones. Other compelling studies have shown that BCR signalling genes are upregulated in CLL cells taken from lymph nodes (Herishanu et al. 2011) and that cells from IGHV-U CLL patients (with poorer outcomes), also show activation of BCR-related genes (Rosenwald et al. 2001). The success of BCR inhibitors in the clinic (John C. Byrd et al. 2013), also underlines the critical importance of this pathway in CLL.

Figure 1.2 shows a schematic of the BCR pathway itself. The BCR is a multimeric complex consisting of surface immunoglobulin (Ig), which recognises antigen, plus the Ig- α /Ig- β hetero-dimers, known as CD79A and CD79B. The BCR may bind to external antigens within the microenvironment (Binder et al. 2010) or intra-BCR self-antigens (Minden et al. 2012), which in turn recruits SYK and the Src kinase LYN. These kinases phosphorylate motifs located on the cytoplasmic tails of CD79A and CD79B, initiating a signalling cascade involving a number of proteins and pathways. These include the proteins BTK (Herman et al. 2011) and PI3K (Longo et al. 2007) which activate a number of downstream pathways and players including PLC γ 2, calcium signalling, PKC, NF κ B signalling, ERK and MAPKs, and nuclear transcription (Jan A. Burger and Chiorazzi 2013; Dubois et al. 2020).

There are two types of BCR signalling in healthy and CLL B cells: ligand-dependent “active” signalling that relies on antigen-binding, and ligand-independent “tonic” signalling (Lam, Kühn, and Rajewsky 1997; Kraus et al. 2004). Whilst active signalling engages the entire signalling cascade described above, tonic signalling activates only a subset of these. Kraus et al. (2004) showed that tonic signalling is important for prolonged B cell survival whereby PI3K signalling is thought to play a key role in delivering survival

signals (L. Srinivasan et al. 2009; Pua et al. 2019). Both these modes of BCR signalling are believed to impact of the survival and growth of the tumour, although the dominant mode remains a matter of debate (Jan A. Burger and Chiorazzi 2013).

The different clinical properties of IGHV-M and IGHV-U CLLs are believed to be determined by in part by their differential response to BCR stimulation, which is influenced by their cell of origin (Jan A. Burger and Chiorazzi 2013). IGHV-U CLLs have not undergone somatic hypermutation and consequently express low-affinity BCRs that are frequently activated by numerous antigens and auto-antigens in the microenvironment (Borche et al. 1990; Bröker et al. 1988; Sthoeger et al. 1989; Hervé et al. 2005; Myhrinder et al. 2008; Chu et al. 2008; Binder et al. 2010; Krysov et al. 2010; Kostareli et al. 2012). In contrast, IGHV-M BCRs only recognise highly specific antigens, which either occur infrequently or induce anergy due to high-affinity binding (Chiorazzi and Ferrarini 2003; Stevenson and Caligaris-Cappio 2004; Chiorazzi, Rai, and Ferrarini 2005; Jan A. Burger and Chiorazzi 2013). IGHV-M CLL clones therefore are more stable and expand at a slower rate.

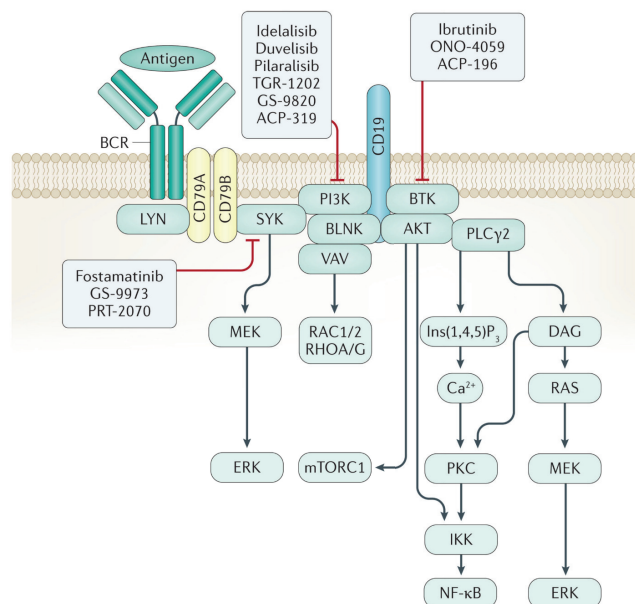


Figure 1.2: Graphical depiction of the BCR pathway. *Figure reproduced with permission from Kipps et al. (2017)*

1.1.5 Recurrent genetic features in CLL

The genomic landscape of CLL has been thoroughly characterised in a number of studies, including two seminal papers involving >500 CLL samples (Landau et al. 2015; Puente et al. 2015). Such studies have indicated that CLL shows a lower mutational load than other lymphoid neoplasms (Vogelstein et al. 2013; Alexandrov et al. 2013; Bosch and Dalla-Favera 2019), in which a relatively large number of genes are rarely mutated (Fabbri and Dalla-Favera 2016). A small number of driver genes are mutated in a significant proportion of cases, though a common genetic event which can accounts for most cases of CLL has not been identified (Fabbri and Dalla-Favera 2016). These genetic alterations encompass chromosomal alterations, mutations, alterations in miRNA expression and epigenetic modifications (Kipps et al. 2017).

Somatic Mutations

There are many recurrent somatic mutations in CLL, and these centre on several major pathways and functions that are frequently altered (Figure 1.3). (Puente et al. 2015; Fabbri and Dalla-Favera 2016; Kipps et al. 2017). These pathways include Notch signalling, DNA damage response, RNA processing, NF κ B signalling, BCR signalling, WNT signalling and chromatin modification (Kipps et al. 2017; Bosch and Dalla-Favera 2019).

Within these pathways, most mutations are rare and only a few occur at a frequency >5% (Bosch and Dalla-Favera 2019). One landmark study indicated the most frequent mutations occur in *NOTCH1* (12.6% of cases), *ATM* (11%), *BIRC3* (8.8%) and *SF3B1* (8.6%), although these frequencies are dependent disease stage and treatment status (Puente et al. 2015). The functional role and prognostic importance of a number of these putative driver mutations has been established, and are discussed below.

Notch signalling The Notch pathway activates genes required for proliferation, metabolism and survival, including *MYC*, via the activation of the *NOTCH1* transmembrane receptor (Guruharsha, Kankel, and Artavanis-Tsakonas 2012). Mutations in *NOTCH1* are very common in CLL (~4-20%) (Fabbri et al. 2011; Puente et al. 2011, 2015; Landau et al. 2013, 2015). A number of other recurrent mutations also centre on Notch deregulation, indicating that this pathway is disrupted in many CLL cases (Fabbri and Dalla-Favera 2016). *NOTCH1* mutations occur more often in IGVH-U CLLs and are associated with a less favourable OS (Fabbri et al. 2011). *NOTCH1* mutants also respond less-well to anti-CD20-based therapies, due to decreased surface expression of CD20 (Fabbri et

al. 2011; Rossi et al. 2012).

DNA Damage Response A number of frequently occurring mutations disrupt the DNA damage response, the most clinically important of which is *TP53*. *TP53* is known as the “guardian of the genome,” owing to its role as a tumour suppressor gene protecting genome integrity by preventing mutation. Despite being a tumour suppressor, *TP53* mutations can have a dominant negative effect on function, such that loss of genomic stability occurs even when a single allele is mutated (Zenz et al. 2008). *TP53* is an important prognostic marker, as dysregulation of its function is associated with resistance to DNA-damaging agents (chemotherapy and radiotherapy) (Zenz et al. 2008; Dicker et al. 2009; Rossi et al. 2009), and cases with *TP53* mutations at diagnosis often show shorter TTFT and a less favourable OS (H. Döhner et al. 2000; Zenz et al. 2008; Rossi et al. 2013; Puente et al. 2015).

Upstream of *TP53*, the tumour suppressor *ATM* is also frequently mutated in CLL (Bosch and Dalla-Favera 2019). *ATM* activates the DNA damage response upon recognition of DNA double strand breaks (Austen et al. 2005; Shiloh and Ziv 2013). Similarly to *TP53* mutants, *ATM*-disrupted CLLs also show genomic instability and these mutations are associated with shorter TTFT and OS, and chemoresistance (Austen et al. 2005; Stankovic and Skowronska 2014).

POT1 is also involved in genomic stability, and is mutated in around 3 – 7% of cases (Bosch and Dalla-Favera 2019; Ramsay et al. 2013). *POT1* mutations disrupt telomere protection, leading to increased structural aberrations and chromosomal breaks (Ramsay et al. 2013). Mutations in *POT1* are associated with IGHV-U CLL and advanced clinical stage (Ramsay et al. 2013).

RNA processing 30% of CLL tumours harbour mutations disrupting RNA processing and the spliceosome machinery (Puente et al. 2011, 2015; Wang et al. 2011; Quesada et al. 2012; Fabbri and Dalla-Favera 2016). *SF3B1* mutations are the most frequent to occur, and are found in 10% of cases, usually in IGHV-U CLLs (Puente et al. 2011, 2015; Wang et al. 2011; Quesada et al. 2012; Fabbri and Dalla-Favera 2016). The *SF3B1* gene encodes part of the U2 snRNP complex which is involved in RNA splicing (Shin and Manley 2004), though the functional implication of *SF3B1* mutations are yet to be established, and many transcripts show abnormal splicing in *SF3B1* cases (Quesada et al. 2012). The presence of *SF3B1* mutations is associated with a decreased TTFT and unfavourable OS (Bosch and Dalla-Favera 2019).

NF κ B signalling A wide range of mutations across various pathways converge on the

activation of NF κ B (Fabbri et al. 2011; Puente et al. 2011, 2015; Wang et al. 2011; Quesada et al. 2012; Landau et al. 2015), including *BIRC3* and *MYD88*. For example, certain mutations in *MYD88* result in increased binding to IRAK1 and higher activation of NF κ B (Puente et al. 2011). However, the role and prognostic importance of NF κ B activation in CLL is still unclear (Bosch and Dalla-Favera 2019).

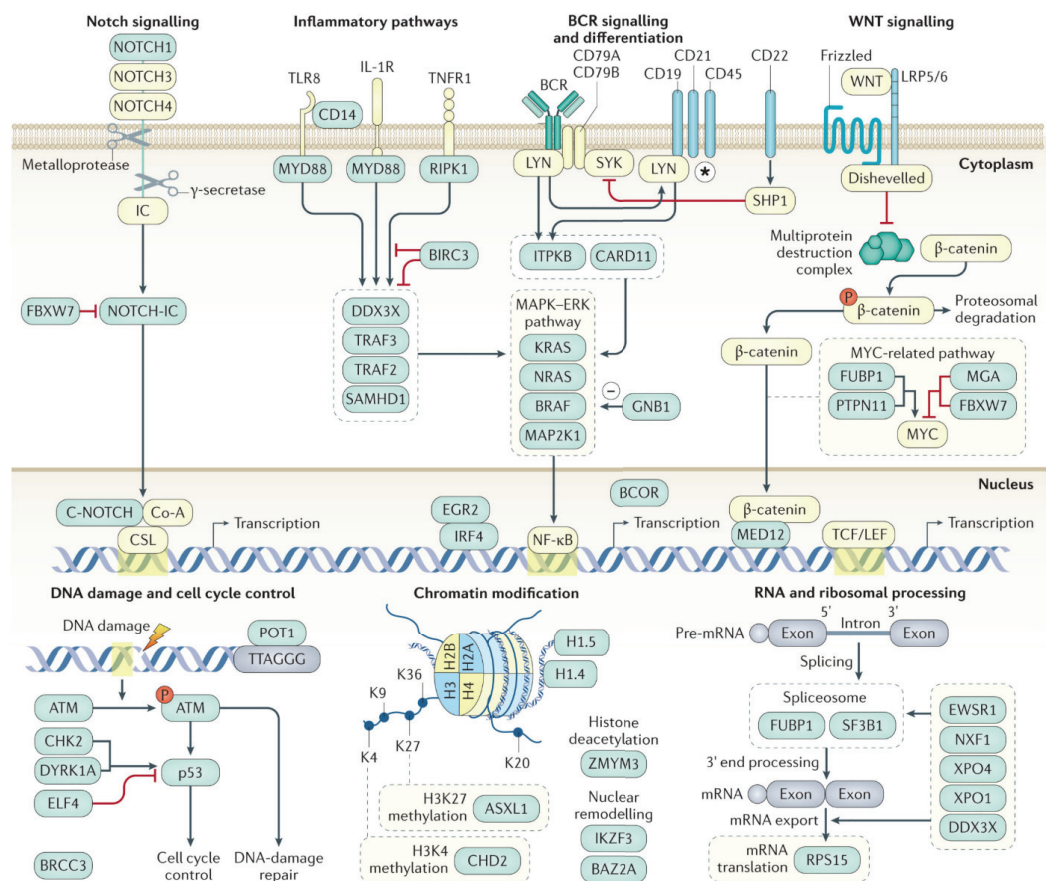


Figure 1.3: Graphical depiction of commonly mutated genes in CLL, grouped into cellular pathways (blue boxes). Minus sign indicates negative regulation. *Figure reproduced with permission from Kipps et al. (2017)*.

Structural Aberrations

In addition to the aforementioned mutations, a number of common structural aberrations confer similar disruption to normal B cell function. The key structural aberrations and their prognostic value were set out in a landmark paper by H. Döhner et al. (2000), as follows.

del(11q) Deletions of chromosome 11q (del(11q)) are fairly common (~10%) in CLL, and are believed to target the *ATM* gene in the 11q22-23 region (H. Döhner et al. 2000; Austen et al. 2005; Bosch and Dalla-Favera 2019). del(11q) is usually monoallelic, but can also be associated with mutations in the remaining *ATM* allele (~30% of cases) (Austen et al. 2005). In certain instances, the deleted region does not include *ATM* but rather *BIRC3*, a negative regulator of the NF κ B pathway (Rossi et al. 2012). Cases with del(11q) or *ATM* lesions have a shorter TTFT and OS, especially if the lesion is biallelic (Austen et al. 2005; Skowronska et al. 2012; Stankovic and Skowronska 2014; Nadeu et al. 2016).

del(17p) Deletion of chromosomal region 17p13 (del(17p)) is found in 1 – 20% of cases, depending on the stage of the disease and most common in chemo-refractory cases (H. Döhner et al. 2000; Zenz et al. 2008, 2010; Stilgenbauer et al. 2014). The target of this lesion is thought to be *TP53*; the deleted region consistently includes the *TP53* locus (Hartmut Döhner et al. 1995), and around 80% del(17p) cases also have missense mutations in the second *TP53* allele (Zenz et al. 2008; Gonzalez et al. 2011; Trbusek et al. 2011). Del(17p) CLLs show increased genomic instability (L. Yu et al. 2017), resistance to chemotherapy and, correspondingly, a shorter TTFT and a less favourable OS (H. Döhner et al. 2000; Zenz et al. 2008; Rossi et al. 2013; Puente et al. 2015).

del(13q) Deletion in the 13q14 region (del(13q)) is the most common genetic lesion in CLL (~50–60% of cases) (H. Döhner et al. 2000). Experiments to determine the minimal deleted region identified that this invariably contains *DLEU1* and *DLEU2*, two long non-coding RNA genes, and the microRNA gene cluster *MIR15A–MIR16-1* (Kalachikov et al. 1997; Migliazza et al. 2001; Calin et al. 2002; Palamarchuk et al. 2010). *in vitro* studies have demonstrated the role of these genes in regulation of the cell cycle and apoptosis (Cimmino et al. 2005; Bosch and Dalla-Favera 2019). In some CLL cases, del(13q) is the sole genetic abnormality, indicating that this lesion may be involved in early CLL development (H. Döhner et al. 2000; Landau et al. 2015). Moreover, conditional deletion of the equivalent minimal deleted region in mice recapitulated CLL initiation and progression, and these mice developed clonal lymphoproliferations (Migliazza et al. 2001; Klein2010?). del(13q) CLLs have the best prognosis, with prolonged TTFT, and OS compared to tumours with other lesions (H. Döhner et al. 2000; Rossi et al. 2013).

The incompletely understood role of trisomy12

Complete duplication of chromosome 12 (trisomy 12) is observed in ~15% of CLL cases at diagnosis (H. Döhner et al. 2000). Despite its recurrence, there is currently no functional explanation for this lesion (Bosch and Dalla-Favera 2019), although a number of features have been observed. Trisomy 12 is more common in IGHV-M CLLs than IGHV-U (Hamblin et al. 1999), and is thought to confer an abnormal cellular morphology (Bosch and Dalla-Favera 2019). Previous work in our lab has also demonstrated that trisomy 12 CLLs show a specific signalling signature and distinct transcriptomic (Dietrich et al. 2017) and proteomic profiles (Herbst 2020; Meier-Abt et al. 2021), including differential expression of genes within the BCR, PI3K, AKT, and mTOR signaling and chemokine signaling pathways. Moreover, trisomy 12 CLLs show higher sensitivity to BCR inhibitors, indicating that BCR signalling may be amplified in these cases (Dietrich et al. 2017).

Traditionally trisomy 12 has been classified as an intermediate-risk lesion (H. Döhner et al. 2000): these cases have a higher proliferative capacity, but are more treatable with chemotherapeutics and BCR inhibitors. However, *NOTCH1* mutations are frequently observed in trisomy 12 cases, and this is associated with poorer outcomes (Balatti et al. 2012; Del Giudice et al. 2012).

Epigenetic alterations

In addition to genetic lesions, the epigenome is also modified in CLL and samples typically show global hypomethylation combined with local hypermethylation (Wahlfors et al. 1992; Cahill et al. 2013; Ziller et al. 2013; Kipps et al. 2017; Bosch and Dalla-Favera 2019). Studies investigating the epigenome in CLL have proven revealing, in particular, higher levels of intra-sample methylation heterogeneity have been shown to be associated with high-risk genetic lesions and poorer prognosis (Landau et al. 2014).

Moreover, methylation signatures have been used to classify distinct clinical CLL subgroups (Kulis et al. 2012; Bhoi et al. 2016), as they are useful to trace the cell of origin. For example, CLL cells from distinct patients originate from many different B cell maturation states, possibly reflecting the biological and phenotypic heterogeneity of CLL (Oakes et al. 2016). Accordingly, IGHV-U CLLs have a distinct methylation signature to IGHV-M CLLs, and these patterns correspond approximately to those of pre-germinal centre or post-germinal centre memory B cells, respectively (Kulis et al. 2012; Oakes

et al. 2016). Epigenetic studies have also revealed the relationship between certain genetic lesions and specific epigenetic signatures, for example *MYD88* mutations and trisomy 12 (Beekman et al. 2018). The CLL epigenome can also be modulated by drugs and thus is of increasing clinical interest (Timp and Feinberg 2013; Beekman et al. 2018; Gaiti et al. 2019).

1.2 Therapies in CLL

Extensive work to uncover the molecular drivers of CLL has led to the development of several therapeutic strategies. CLL represents a successful example of how developing a complex understanding of the biological characteristics of a disease can lead to significantly improved patient outcomes (Yosifov et al. 2019). Treatment of CLL patients can be via chemotherapy, chemoimmunotherapy or targeted therapies that inhibit specific pathways (Kipps et al. 2017; Jan A. Burger 2020). Additionally, allogeneic stem cell transplantation is increasingly considered as an alternative option in relapsed or refractory patients (Kipps et al. 2017).

1.2.1 Chemotherapy and chemoimmunotherapy

Chemotherapy has been the standard of care for CLL for many decades, either with purine analogues such as fludarabine or alkylating agents such as chlorambucil (Robak 2005; Lukenbill and Kalaycio 2013). Chemoimmunotherapy has also benefited many patients owing to the rapid improvements to monoclonal antibody technology and the development of anti-CD20 treatments, such as rituximab (Yosifov et al. 2019; Robak et al. 2010). However, patients with higher risk lesions such as *TP53* and del(17p) do not respond well to chemoimmunotherapy, and require alternative therapeutic options (Zenz et al. 2010).

1.2.2 Targeted therapies

More recently, the importance of BCR signalling and upregulation of anti-apoptotic proteins in CLL expansion has been increasingly realised and led to the development of therapies targeting these pathways. Drugs targeting BCR signalling and BCL-2 have changed the treatment landscape dramatically (Scheffold and Stilgenbauer 2020). Three main drug classes that target BCR signalling have been developed for CLL: BTK inhibitors, PI3K inhibitors and SYK inhibitors (De Rooij et al. 2012; Kipps et al. 2017).

Ibrutinib is a BTK inhibitor approved for use as an initial therapy and for patients who are refractory to chemoimmunotherapy (John C. Byrd et al. 2013; John C. Byrd et al. 2014). Despite such success, complete remission is rare and many patients continue to harbour minimal residual disease within the bone marrow (John C. Byrd et al. 2013), requiring continued therapy for years (John C. Byrd et al. 2013; Woyach and Johnson 2015). Resistance can also occur via the acquisition of mutations in BTK or PLC γ 2 (Woyach and Johnson 2015) genes. Treatment initiation with ibrutinib is associated with a concomitant increase in the absolute lymphocyte count in the blood (Woyach et al. 2014), thought to be caused by the inhibition of chemokine receptor signalling leading to the release of malignant B cells from the lymph nodes into the peripheral blood.

Idelalisib also acts to inhibit BCR signalling and chemokine signalling (Hoellenriegel et al. 2011), via inhibition of PI3K. Whilst the drug is highly efficacious in CLL (Furman et al. 2014; Brown et al. 2014), idelalisib demonstrates more toxicities and lower efficacy than BTK inhibitors and thus is generally used as an alternative therapy in patients for whom BTK inhibitors are unsuitable (Ghia et al. 2020; Jan A. Burger 2020).

Other drugs targeting SYK, downstream of BTK, have also shown promise in Phase I/II clinical trials (Friedberg et al. 2010), though none are licenced as yet.

Aside from BCR inhibitors, BCL-2 inhibitors such as venetoclax, have also shown good efficacy in CLL. Venetoclax is thought to induce apoptosis in CLL cells, by acting as a BH3 mimetic interfering with the ability of BCL-2 to sequester BIM (Moore et al. 2007). This makes venetoclax an attractive alternative in patients with relapsed or refractory disease (Roberts et al. 2016), or who have del(17p) i.e. loss of *TP53* (Stilgenbauer et al. 2016). Complete remissions are observed in ~20% patients (Roberts et al. 2016) which is higher than with other targeted therapies, and minimal residual disease in the bone marrow is less common (Roberts et al. 2016).

1.2.3 Management algorithm

The decision to initiate therapy is guided by the stage of disease, evidence for rapid disease progression or disease-related symptoms (Michael Hallek et al. 2008; Kipps et al. 2017). Disease stage is determined by an index such as the Rai staging system, which categorises patients based on disease severity (Kipps et al. 2017). The choice of therapy accounts for certain mutations, in particular the presence of *TP53* or del(17p) mutations, the age of the patient and the objective of therapy. IGHV status is also increasingly used for patient stratification (Figure 1.4, (Kipps et al. 2017)).

CLL is a manageable disease, with a well-established arsenal of treatments and associated management algorithm. However, treatments are harsh, and the disease is still considered incurable (Bosch and Dalla-Favera 2019). Many cases develop resistance to therapy, both via acquired mutations and through survival signals provided by the microenvironment (see section 1.3.4) and minimal residual disease within the bone marrow is common. Collectively, these lead to relapse or required prolonged therapy and its associated toxicities. There remains a clinical need to improve patient outcomes and experience.

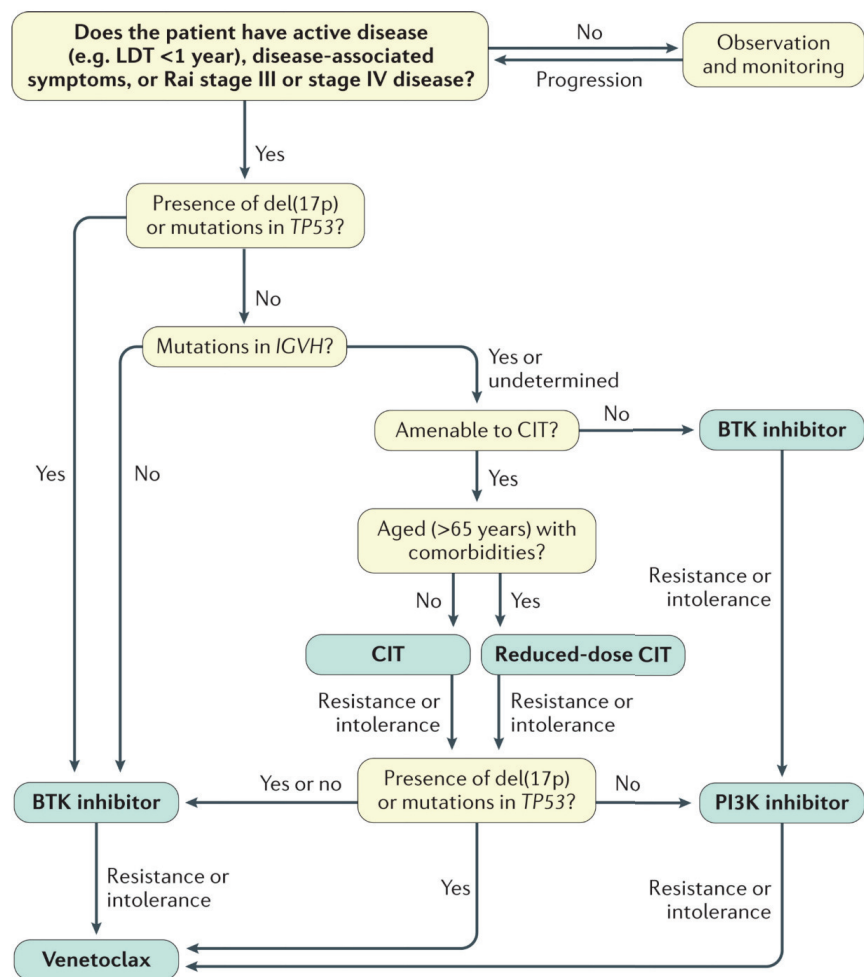


Figure 1.4: Management algorithm for patients with CLL. CIT (chemoimmunotherapy), LDT (lymphocyte doubling time). *Figure reproduced with permission from Kipps et al. (2017) .*

1.3 The tumour microenvironment in CLL

1.3.1 The role of the tumour microenvironment in CLL

In addition to genetic aberrations, the tumour microenvironment is an important driver of disease pathogenesis in CLL (Ten Hacken and Burger 2016). The term microenvironment encompasses the set of non-neoplastic cells within the lymphoid tissues, including the bone marrow and lymph nodes, that provide survival signals to the tumour, leading to clonal expansion and drug resistance (Jan A. Burger and Gribben 2014). Malignant B cells engage in a dialogue with the non-neoplastic cells, via cell-cell contacts and soluble factors, including chemokines, integrins, cytokines and survival factors, centring on a number of important pathways including BCR signalling and tissue homing chemokine receptors (Ten Hacken and Burger 2016).

The importance of the microenvironment in CLL pathogenesis was first recognised in studies that showed CLL cells rapidly undergo apoptosis *in vitro*, whilst their survival can be extended by stimulation or by co-culture with nurselike cells (NLCs) or mesenchymal bone marrow stromal cells (BMSCs) (Collins et al. 1989; Jan A. Burger et al. 2000; Kurtova et al. 2009; Deaglio and Malavasi 2009; Purroy et al. 2015). This observation indicated that the ability of CLL to progressively accumulate *in vivo* may be highly dependent on external stimulation, rather than some cell-intrinsic feature of the tumour. Building on these observations, further *in vitro* studies have shown a number of cell types and soluble factors belonging to the microenvironment are also capable of protecting the tumour cells from drugs and chemotherapeutic agents. Many CLL patients continue to harbour minimal residual disease (MRD), in which a fraction of the malignant cells remain whilst the patient is in remission and eventually lead to relapse (Hayden et al. 2012). It is believed that the tumour microenvironment provides a sanctuary for the malignant B cells to shield from the effects of therapy (Dubois et al. 2020).

1.3.2 Components of the tumour microenvironment

Lymph Nodes Over the last two decades, significant progress has been made in unravelling this complex cross-talk and many of the important cellular and molecular components have been defined and studied. Malignant B cells circulate through the blood in a resting state, and follow chemokine gradients towards the lymph nodes to form “proliferation centres” (Figure 1.5), similar to germinal centres (Herishanu et al. 2011). Studies using deuterated water labelling have shown that up to 3% of the clone is ac-

tively proliferating within the lymph node (B. T. Messmer et al. 2005; Herndon et al. 2017). Cross-talk with the non-neoplastic cells in the lymph node shapes the transcriptomic profile of the malignant B cells, and leads to upregulation of the BCR pathway Mittal et al. (2014), a central driver of CLL pathogenesis.

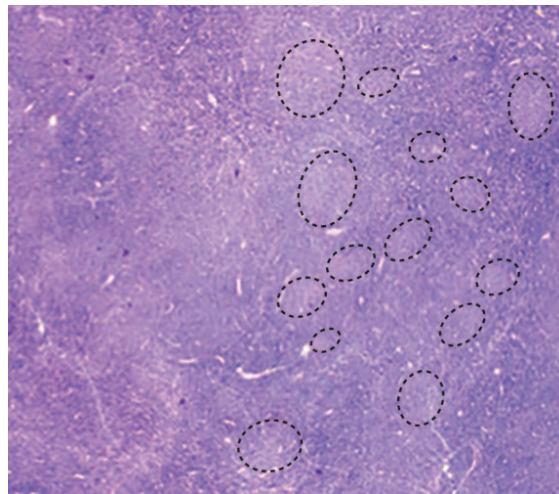


Figure 1.5: Haematoxylin and eosin stain of CLL-infiltrated lymph node tissue section, showing pale-staining proliferation centres (circled). *Figure reproduced with permission from Kipps et al. (2017) .*

Bone marrow The bone marrow is also known to be important, and several studies have shown *ex vivo* BMSCs to protect CLL cells against the drug toxicity (Kay et al. 2007; Kurtova et al. 2009). However, gene expression changes are less pronounced within the bone marrow compared to the lymph node (Herishanu et al. 2011).

Cellular components Within these compartments, the CLL cells engage in a dialogue with mesenchymal stromal cells (MSCs), NLCs and follicular dendritic cells (FDCs), in concert with T cells, natural killer cells (NK cells) and components of the extracellular matrix (Ten Hacken and Burger 2016). NLCs are of monocytic origin: their critical role in CLL was first demonstrated by the observation that peripheral blood-derived monocytes differentiate into NLCs, and that these cells prolong CLL cell survival *ex vivo* (Jan A. Burger et al. 2000). They are also found within the lymphoid tissues of CLL patients (Tsukada et al. 2002; Bürkle et al. 2007). MSCs, which include BMSCs, are frequently observed within the secondary lymphatic tissues of CLL patients. Many studies have demonstrated the ability of these cells to inhibit spontaneous and drug-induced apoptosis in *in vitro* CLL co-cultures Kurtova et al. (2009).

FDCs are important for tissue homing and retention of CLL cells within tissues. In healthy tissues, they are usually found within germinal centres (Allen and Cyster 2008), and present unprocessed antigen to B cells. In CLL they play an important role within the secondary lymphoid organs, having a protective effect on CLL via cytokine secretome, adhesion molecules and the activation of BCR signalling (Dubois et al. 2020). CLL co-culture with FDCs leads to inhibition of spontaneous apoptosis and upregulation of anti-apoptotic MCL (I. M. Pedersen et al. 2002).

The T cell compartment is also altered in CLL, first described by Scrivener et al. (2003). T cells have been observed to have pro-tumour and anti-tumour behaviour. On the one hand, higher numbers of CD4+ T-helper (Th) cells are seen in CLL patient blood samples (Palma et al. 2017; Elston et al. 2020), and in line with this, Th cell cytokines have been shown to provide pro-survival signals *in vitro*, for example IL4 from Th2 cells (Dancescu et al. 1992; Bhattacharya et al. 2015; Aguilar-Hernandez et al., n.d.). Activated CD4+ T-cells in murine xenograft models (Bagnara et al. 2011; Os et al. 2013) of CLL have also been shown to increase survival and growth of the tumour. On the other hand, there is evidence of increased antigen-experienced CD8+ T cells in CLL, which control tumour growth in a CLL mouse model (Roessner and Seiffert 2020; Grioni et al. 2021).

1.3.3 Microenvironmental pathways

Cross-talk between these non-neoplastic cells and the malignant B cells can occur directly, via cell-cell contacts and adhesion molecules, indirectly, via soluble factors that bind to receptors on the CLL cells, or through the exchange of material held in extracellular vesicles (Guarini et al. 2008; Oppezzo and Dighiero 2013; Crompton et al. 2017). Collectively these induce pathway activation (most importantly BCR and NF κ B (Herishanu et al. 2011)) and gene expression modifications with the CLL cells, leading to chemotaxis, homing to lymphoid tissues and survival of the tumour cells (Dubois et al. 2020). Figure 1.6 depicts an overview of this cross-talk.

Cell-cell contacts The importance of direct contact between cells became clear with observations that the ability of MSCs to provide efficient rescue from spontaneous and drug-induced apoptosis is dependent on direct contact and can be blocked by separation through a filter (L. Lagneaux et al. 1998; Jan A. Burger et al. 2000; Kay et al. 2007; Kurtova et al. 2009; Ding et al. 2009). Likewise, FDCs also operate through direct contact, as evidenced by the observation that contact with HK cells (an FDC cell line) protects against CLL cells from apoptosis (I. M. Pedersen et al. 2002).

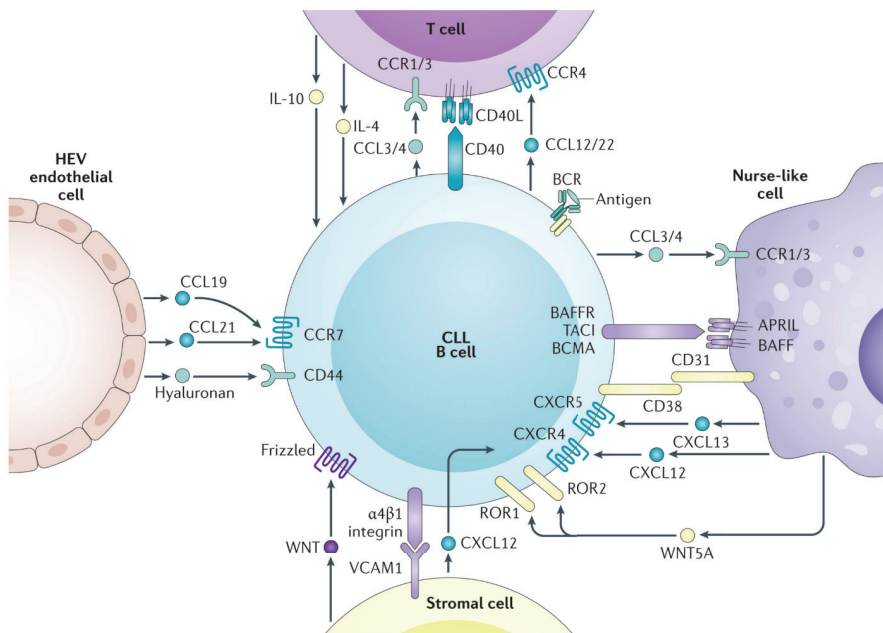


Figure 1.6: Graphic summarising soluble factors and cell-cell contacts involved in cross-talk between CLL cells and non-neoplastic cells of the tumour microenvironment *Figure reproduced with permission from Kipps et al. (2017)*.

This direct contact operates through a number of receptor-receptor interactions. For example, CLL-stromal cell binding involves β 1 integrin (ITGB1, or CD29) and β 2 integrin (ITGB2, or CD18) (L. Lagneaux et al. 1999). VLA-4 is also an important integrin for retention of CLL cells within the lymph nodes and bone marrow, by interacting with its ligand VCAM-1 (or CD106) on stromal cells (J. A. Burger et al. 2001).

These cell-cell interactions then lead to pathway activation (including BCR (Basile Stamatopoulos et al. 2015) and TLR (Schulz et al. 2011)), gene expression changes and epigenetic changes (Vangapandu et al. 2017; Xu et al. 2018) within the tumour cells. For example, contact between CLL B cells and MSCs alters the transcriptomic profile of the cells (Schulz et al. 2011; Mangolini et al. 2018), leading to increased expression of anti-apoptotic proteins such as BCL2 (Nwabo Kamdje et al. 2012; Patel et al. 2014), BCL-XL (Patel et al. 2014; Amigo-Jiménez et al. 2015), MCL1(Kurtova et al. 2009; Amigo-Jiménez et al. 2015), and β -catenin (Mangolini et al. 2018).

Soluble Factors NLCs, MSCs, FDCs and T cells also secrete soluble factors that have a protective effect on the tumour. For example, MSCs secrete a number of cytokines. One of the most widely studied is SDF1- α (or CXCL12), which interacts with CXCR4 on

CLL cells (Jan A. Burger, Burger, and Kipps 1999; J. A. Burger et al. 2001; Kay et al. 2007), stimulating the PI3K (M. Burger et al. 2005), STAT3 (Jan A. Burger, Burger, and Kipps 1999), and p44/42 MAPK (Jan A. Burger et al. 2000) pathways which activates BTK (Montresor et al. 2018), ERK (D. Messmer et al. 2011), and AKT (O’Hayre et al. 2010). FDCs on the other hand secrete B cell-activating factor (BAFF), which has been shown to increase survival of CLL cells through the activation of canonical NF κ B signalling (Nishio et al. 2005). A number of Th T-cell-derived cytokines have also been shown to increase CLL viability *in vitro*, including IFN γ (Buschle et al. 1993), IL15 (Trentin et al. 1996), IL21 (Totero et al. 2006; Pascutti et al. 2013), IL4 (Dancescu et al. 1992; Bhattacharya et al. 2015; Aguilar-Hernandez et al., n.d.), IL2 (Decker et al. 2010) and CD40L (Kitada et al. 1999; Pascutti et al. 2013; Bhattacharya et al. 2015). Certain soluble factors can also increase apoptosis and act against the tumour, including TGF β (Lotz, Ranheim, and Kipps 1994).

1.3.4 The influence of the microenvironment on drug response

In addition to their effect of spontaneous apoptosis, the cell types and soluble factors outlined above have also been shown to impact on drug-induced apoptosis *in vitro*. For example, NLCs and stromal cells have been shown to mediate ibrutinib resistance [Cheng et al. (2014); /; Guo et al. (2017)], and the chemotherapeutics fludarabine, oxaliplatin, chlorambucil, cyclophosphamide and doxorubicine show reduced efficacy in stromal cell co-cultures (Kay et al. 2007; Kurtova et al. 2009; Mraz et al. 2011; W. Zhang et al. 2012). A number of soluble factors also induce resistance to drugs *in vitro*. These include decreased efficacy of fludarabine and venetoclax in the presence of TLR stimulation (Fonte et al. 2013; Kalles D. Jayappa et al. 2017) and reduced sensitivity to ibrutinib in the presence of IL4 (Aguilar-Hernandez et al., n.d.) and BAFF (McWilliams et al. 2019).

Evidence of microenvironmentally-induced drug resistance *in vivo* is less prevalent, although there is widespread consensus that the microenvironment, in particular the lymph node, plays an important role in patient outcomes. Low rates of complete response and the inevitability of relapse in CLL have implicated the protective niche in enabling MRD (O’Brien and Kay 2011; Hayden et al. 2012). A number of studies have shown enlarged lymph nodes are associated with MRD (Moreton et al. 2005), in particular, incomplete response to ibrutinib is associated with persistently enlarged lymph nodes (Ahn et al. 2018). MSCs have also been shown to protect CLL cells taken from patients before and after *in vivo* fludarabine therapy (Trimarco et al. 2015).

In light of this, an important goal in CLL research is to develop strategies to overcome microenvironmentally-induced drug resistance. Targeting microenvironmental signalling in the lymph node tissue could be key to achieving long term remission and cure (Hayden et al. 2012) and thus there is a need for combinatorial therapies that aim to eliminate CLL cells in the lymph node and reduce CLL load in the peripheral blood. For example, Guo et al. (2017) have proposed cerdulatinib as a potential CLL therapy. Cerdulatinib is a dual inhibitor of the BCR pathway and the JAK-STAT pathway, capable of inducing cell death whilst also inhibiting the protective effects from the microenvironment.

The development of rational strategies to target the microenvironment requires a more comprehensive understanding of drug – microenvironment interactions, and how these interplay with molecular features. Some studies have worked in this direction, for example Kallesh D. Jayappa et al. (2018) tested the impact of several agonists on ibrutinib and venetoclax. In a larger scale approach, Gimenez et al. (2020) applied machine learning to identify drugs targeting proteins involved in microenvironmental signalling, and later screened these drugs in combination with venetoclax and ibrutinib, for activity against CLL in the presence of stromal cells.

Previous work in our lab probed drug activity in CLL peripheral blood mononuclear cell (PBMC) samples in the context of BMSC co-culture in a large-scale screen of 81 CLL patients (Herbst 2020). Similar larger scale systematic studies of drug – microenvironment interactions, particularly in the context of molecular features, are required.

1.3.5 Modelling the tumour microenvironment

A major goal of current research in CLL is to unravel the complexity of CLL-microenvironment cross-talk and its role in drug response. Many studies have applied a range of strategies to mimic the pro-survival effect of the microenvironment, each with their own advantages (Crassini et al. 2017; Scielzo and Ghia 2020).

Stimulation with soluble factors One such strategy is to stimulate individual pathways in CLL samples *ex vivo* in order to elucidate their impact on CLL survival and drug response. For example, studies of BCR, TLR, CD40L and interleukin stimulation (Muzio et al. 2009; Crassini et al. 2017; Scielzo and Ghia 2020) have proven critical in demonstrating the marked effect each of these have on CLL survival and the key downstream pathways involved (in particular NF κ B and MAPK) (Crassini et al. 2017). This strategy allows a direct understanding of cause and effect, with the caveat that accurately

mimicking cytokine concentrations *in vitro* is challenging, and that the activity of certain stimuli may be altered in the absence of other signals.

Co-culture Stimulation studies omit the impact of cell-cell contacts and thus co-culturing CLL cells with cell lines can provide a more complete picture. Various co-culture systems have been developed in order to mimic different components of the microenvironment, including stromal cells, T cells, endothelial cells, NLCs and FDCs (Panayiotidis et al. 1996; L. Lagneaux et al. 1998; I. M. Pedersen et al. 2002; Kurtova et al. 2009; B. Stamatopoulos et al. 2010; Basile Stamatopoulos et al. 2012; Asslaber et al. 2013; Hamilton et al. 2012; Crassini et al. 2017).

3D Models In recent years, interest has developed in the use of 3D culture systems, to create yet more *in vivo*-like models of the microenvironment (Jensen and Teng 2020; Scielzo and Ghia 2020). Static 3D approaches involve the use of scaffolds or the generation of spheroids, recapitulating the complexity of the protective niche to a greater degree (Farinello et al. 2018; Scielzo and Ghia 2020). More ambitious still is the development of dynamic 3D cultures, through the use of bioreactors and microfluidics. These systems attempt to capture the influences of gravity, flow and mechanical stresses, to study the phenotypic changes that occur as CLL cells traffic through and communicate with the non-neoplastic tissues (Walsby et al. 2014; Scielzo and Ghia 2020).

in vivo murine models Murine models to investigate CLL-microenvironment interactions are also possible (D. Lu et al. 2004; Enzler et al. 2009; Herishanu et al. 2011; Fedorchenko et al. 2013; Simonetti et al. 2014; Crassini et al. 2017), though the value of these models can be hampered by species-specific biological differences (Simonetti et al. 2014) and *in vitro* modelling is often a more accurate approach (Crassini et al. 2017).

Of the many strategies to model the microenvironment, the reductionist approach of stimulating individual pathways is a useful tool to demonstrate direct causal relationships between signal and response. So far, most of these studies have investigated individual stimuli. Larger scale systematic studies of stimuli in other lymphomas have proven successful, such as work by Carey et al. (2017) to functionally screen many immune stimuli in Acute Myeloid Leukaemia (AML), suggesting that similar approaches could be valuable in CLL.

Moreover, most of these studies have been performed in smaller patient cohorts, omitting the influence of the molecular heterogeneity of CLL. Indeed, integrative studies of the interplay between external stimuli and cell-intrinsic features in CLL are lacking. A

few studies have identified interactions between genetic features and the microenvironment, for example, Martínez-Trillos et al. (2016) have established a link between MYD88 mutations and TLR response, and Chatzouli et al. (2014) demonstrated a link between IGHV status and the response to TLR activation. In addition, Mansouri et al. (2016) have discussed the convergence of mutations and external signals on the NF κ B pathway.

The importance of interplay between microenvironment and molecular features in CLL survival and drug response is abundantly clear. However, a systematic study of the integrative influence of mutations and signals, particularly in the context of drug response, is missing in CLL.

1.4 CLL as a model for studying tumour biology

CLL represents a valuable model system in cancer and studies of CLL can offer proof-of-principle for the application of new approaches in other entities. Primary PMBC samples are relatively simple to obtain, as CLL is the most common leukaemia and biopsies are performed by taking blood samples rather than intrusive operations. In addition, multiple biopsies can be taken over the course of a patient's monitoring and therapy. The samples themselves can survive *ex vivo* for several days, even in basic culture condition, making it relatively simple to perform experiments on primary samples.

For example, the work by J. Lu et al. (2021) to decipher a new multi-omic marker of disease aggression not only represents an important advance in our understanding of CLL drive, it also demonstrates an integrative approach to the study of cancer which could be useful in other cancers, particular where the heterogeneity of outcome remains unexplained.

Moreover, CLL is widely viewed as the prototypic disease for studying the integrative role of cell-intrinsic and cell-extrinsic features in disease initiation, expansion and drug response (Mansouri et al. 2016; V. K. Srinivasan et al. 2020; **Opezzo2021?**). Thus, studies seeking to integrate the impact of cell-intrinsic and cell-extrinsic features on CLL survival and drug response are important in the study of CLL and beyond.

1.5 Background to the approaches used in this thesis

This thesis explores drug - microenvironment - gene interplay in CLL through the analysis of *ex vivo* perturbation assays combined with multi-omic profiling of patient samples. Background information on these experimental approaches, and associated data analysis, is outlined below.

1.5.1 *Ex-vivo* drug perturbation screens

Drug perturbation screens have been invaluable in identifying pathway dependencies, biomarkers and potential therapies in CLL (Bosch and Dalla-Favera 2019). Drug perturbation screens are usually performed in microtiter plates that contain a grid of wells suitable for performing an array of pharmacological or genetic experiments (Letai 2017). Tumour cells, either cell lines or primary samples, can be deposited in each well to test their sensitivity to a set of compounds of interest. Tumour cells are incubated with each of the compounds, commonly dissolved in an aqueous solution of dimethyl sulfoxide (DMSO). After a set amount of time has passed to allow the cells to respond to the compound, the effect of each compound is measured. This “read-out” can take a number of forms. For example the morphology of the cells can be imaged (Snijder et al. 2017; Herbst 2020), or the cell viability can be measured via the number of cells or the level of adenosine triphosphate (ATP) in the well (Dietrich et al. 2017).

High-throughput drug screens of cancer cell lines have been widely used to link drug responses to molecular features (Barretina et al. 2012; Basu et al. 2013; Garnett et al. 2012; Iorio et al. 2016). However, cell lines do not capture the genetic heterogeneity of a cancer (Goodspeed et al. 2016), and thus drug screening of primary samples can be more valuable (Dietrich et al. 2017; Tyner et al. 2013; Pemovska et al. 2013; Snijder et al. 2017). In the case of CLL, screening primary samples has the caveat that CLL cells do not proliferate *ex vivo* (Collins et al. 1989) and thus read-outs need to be taken on the basis of the rate of apoptosis relative to controls, rather than proliferation rate.

A few *ex vivo* perturbation screens have also investigated the impact of microenvironmental stimulation on cancer biology, for example Carey et al. (2017)’s functional screen of 94 cytokines in primary AML samples. Studies of stimuli are much rarer despite the well-recognised role of the microenvironment across haematological malignancies and other cancers.

Drug perturbation assays are also suited to combinatorial approaches, most commonly

to test the efficacy of pairs of drugs in order to identify synergistic combinations (Axelrod et al. 2014; Lukas et al. 2020). Combinatorial screening to test drug efficacy in the context of microenvironmental stimulation is also possible, though rare.

1.5.2 Multiomics profiling and integration of multiple datatypes

Multi-omics profiling of samples, in combination with *ex vivo* perturbation screening, is a powerful approach to link cell phenotypes with molecular features in cancer.

The disease pathogenesis and drug response of a cancer is determined by complex interactions between mutations, epigenetic alterations, gene expression, metabolic abnormalities, and aberrant signalling functions (Anda-Jáuregui and Hernández-Lemus 2020). Thus, the study of tumour biology, and indeed CLL biology, requires integrative methodologies and analyses to decipher this complex network (Du and Elemento 2015).

Enter multi-omics, an approach to studying biological systems that utilises multiple “omic” layers to study biological entities (Anda-Jáuregui and Hernández-Lemus 2020; Menyhárt and Gyrfy 2021). These “omic” layers can encompass next-generation sequencing technologies, including DNA sequencing (DNAseq) and RNA sequencing (RNAseq) and high-throughput proteomics and metabolomics, along with newer single cell technologies and other sequence-based approaches such as ChIPseq (chromatin immunoprecipitation sequencing) and ATACseq (Assay for Transposase-Accessible Chromatin using sequencing) (Anda-Jáuregui and Hernández-Lemus 2020). A number of methods have been built to integrate these diverse data types, calling on tools from statistics, probability, machine learning and network analysis (Hernández-Lemus 2013, 2014; Argelaguet et al. 2018; Anda-Jáuregui and Hernández-Lemus 2020).

In CLL, studies have profiled each of these layers independently, including the genomic (Landau et al. 2015; Puente et al. 2015), transcriptomic (Ferreira et al. 2014; Zenz et al. 2019), epigenomic (Rendeiro et al. 2016, 2020; Beekman et al. 2018; Mallm et al. 2019) and proteomic landscapes (Herbst 2020; Meier-Abt et al. 2021).

Building on these studies, multi-omics approaches have the power to identify causal relationships between phenotypic layers of CLL, and thus have led to important biological insights and clinical perspectives (Dietrich et al. 2017; Berest et al. 2019; Lipsky et al. 2020; Herbst 2020; J. Lu et al. 2021). For example, a recent study in our lab integrated multiple data types to identify a novel biological axis, termed CLL proliferative drive, which is strongly associated with disease outcome (J. Lu et al. 2021). Other

multi-omics studies have identified markers of drug response (Dietrich et al. 2017). Integration of ATACseq and RNAseq has also been used to determine differences in transcription factor (TF) activity in CLL between the two major subtypes (IGHV-M and IGHV-U) (Berest et al. 2019). These studies highlight the importance of integrative approaches to gain further insights into CLL pathogenesis, especially with a view towards more personalised treatment strategies for patients.

1.5.3 Mathematical modelling

A number of mathematical tools are valuable in analysing complex multi-omics datasets. In this thesis, linear regression with and without lasso penalisation is used extensively to model the impact of the microenvironment and molecular features on drug response and a basic background to these approaches is outlined below.

**** Basic linear regression **** Linear regression involves fitting a linear model to a dataset, to model the process that generated the data. For example, equation (1.1) describes a basic model to map the values of X , to the values of Y :

$$Y = \beta_0 + \beta_1 X + \epsilon \quad (1.1)$$

This model specifies two components: the linear predictor $\beta_0 + \beta_1 X$ and the error ϵ . The linear predictor can be compared to the equation for a straight line ($Y = mX + c$), where β_0 represents the intercept (c), and β_1 , the gradient (m). The error ϵ can be modelled by sampling from a normal distribution e.g. $N(0, \sigma^2)$, a normal distribution with mean zero and variance σ^2 .

Thus, we can model a variable Y via an expected value derived from the X independent variable(s), plus a random value derived from normal distribution with specified variance (Walker 2018; Huber and Holmes 2019).

Multiple Linear Regression and Interaction Effects In certain cases, multiple independent variables may be predictors of the value of Y . In these cases, multiple linear regression is required, involving more than one explanatory variable. The basic model, for two independent variables X_1 and X_2 , is denoted as follows:

$$Y = \beta_0 + \beta_1 X_1 + \beta_2 X_2 + \epsilon \quad (1.2)$$

In some cases, the effect of an independent variable on Y may depend on the value of another independent variable. For example, the effect of a drug on the viability of a CLL cell may depend on whether *TP53* is mutated. Such “interactions”

between independent variables can also be accounted for within linear models. These interactions are denoted as the product of two or more independent variables:

$$Y = \beta_0 + \beta_1 X_1 + \beta_2 X_2 + \beta_3 X_1 X_2 + \epsilon \quad (1.3)$$

Here $X_1 X_2$ represents the interaction, and β_3 is the associated regression coefficient. Higher-order interactions with more terms are also possible.

Generalised Linear Models Not all dependent variables (Y) can be assumed to derive from sampling a normal distribution, as in equation (1.1). For example, if Y is binary and takes only the values 0 or 1, a Bernoulli distribution is more appropriate. Generalised linear modelling builds on linear regression such that the response variable can have an error distribution other than the normal distribution (Nelder and Wedderburn 1972). A number of distributions are possible, including the binomial, Poisson and gamma distributions. Where Y is categorical, binomial or multinomial distributions are valuable; for count data, the Poisson distribution is often used.

Lasso Regularisation When fitting such models to a particular dataset, it is important to avoid overfitting the data. Overfitting occurs when a model conforms too precisely to the dataset in hand. The model may not be representative of other datasets, and thus any predictions made using model are not reliable. Regularisation is an important tool to minimise such issues (Kumar n.d.).

Regularisation adds a penalty term to the best fit model. This reduces the influences of dependent variables on the value of Y , by compressing the coefficients. This often acts to reduce the number of predictors and to generate a lesser variance with the test dataset. There are two main methods for this, named L1 Lasso Regression and L2 Ridge Regression. The models described in this thesis use Lasso Regression, which is more interpretable than Ridge Regression.

Lasso regularisation shrinks coefficients towards a central point, by adding a penalty to each coefficient, equal to the absolute value of its magnitude. This shrinkage approach means than some coefficients are reduced to 0 and are eliminated from the model, generating models that are sparse and have fewer parameters (Tibshirani 1996; Kumar n.d.).

This can make models simpler to interpret and can be useful in cases where the dependent variables are highly correlated, as in these cases only one of the correlated variables will usually be assigned a coefficient. This also has the caveat that the correlated features may each independently effect Y , but only one of these variables will be

deemed important by the model. It is also often impossible to determine whether one or all the correlated variables are truly influencing Y . Thus, it is important to bear in mind that whilst modelling approaches have proven invaluable in advancing our understanding of biological processes, careful interpretation is required.

1.6 Summary of this thesis

In this thesis, I investigate interplay between molecular features and microenvironmental signals and their influence on viability and drug response in a large CLL patient cohort. Layer by layer, I aim to establish an integrative understanding of survival and drug resistance pathways in CLL.

I employ a large-scale screening dataset of 192 primary CLL samples, which quantifies the effects of 17 microenvironmental stimuli, both alone and in combination with 12 drugs. I combine the screening data with multi-omic profiles for each of the patient samples, consisting of whole-exome sequencing, DNA-methylation, RNA-sequencing and copy number variant data. The screen serves as a reductionist model of signalling via soluble factors in the microenvironment, in a cohort of patient samples that encompasses the clinical and molecular heterogeneity of CLL. I investigate the influence of microenvironmental stimulation on spontaneous and drug-induced apoptosis, and how this can be further modulated by molecular features.

Several signalling pathways and genetic features emerge as key players in CLL-microenvironment cross-talk, and in microenvironmental mechanisms of drug resistance. The above experiments are complimented by immunohistochemistry (IHC) stains of healthy and CLL-infiltrated lymph nodes to investigate the *in vivo* activity of selected pathways. To supplement the large scale screening approach, I also make use of RNAseq, ATACseq, Mass Spectrometry and ChIPseq datasets of CLL patient samples to validate individual findings at a mechanistic level.

The thesis is structured as follows:

Chapter 1: Introduction Overview of the background information and surrounding literature of the project.

Chapter 2: Methods Overview of the experimental and analytical methods used in this thesis.

Chapter 3: Data Overview of the datasets employed in this thesis, and the correspond-

ing public code repository and shiny app.

Chapter 4: *Ex-vivo sensitivity to microenvironmental stimulation in primary CLL cells*

Phenotypic profiling of the responses of CLL samples to the panel of microenvironmental stimuli.

Chapter 5: Genetic modulators of responses to microenvironmental stimulation

Integration of the screening data with patient sample multi-omic profiles to perform a comprehensive survey of molecular determinants of stimulus response.

Chapter 6: Molecular and microenvironmental modulators of drug response in CLL

Mapping of drug - microenvironment interactions and how these can be further modulated by molecular features

Chapter 7: The impact of IL4 on ibrutinib efficacy

A follow - up investigation into

IL4-induced resistance to the BCR inhibitor ibrutinib

Chapter 8: Discussion

A discussion of the findings, the strengths and weakness of

the approaches and their context within the field and surrounding literature.

Chapter 2

Methods

Methods in quotation marks are taken from cited text and I have authored the original text, unless stated otherwise. Where a method was performed as part of a publication, this is cited at the end of the paragraph.

2.1 Experimental methods:

2.1.1 Combinatorial Drug - Stimulus Perturbation Screen

Preparation of patient samples

Section 3.1.1. Peripheral blood samples were obtained from 192 patients (Appendix Table 7.1). A Ficoll gradient (GE Healthcare) was used to separate the samples and subsequently mononuclear cells were cryopreserved. Patient samples were selected based on number of cells available in the tumour bank. On screening days, samples were thawed and DMSO was removed. Primary patient samples were next incubated on a roll mixer at room temperature in cell culture medium for a duration of three hours. This process ensured that any remaining DMSO was removed and that cell counts would only include those that survived the freezing process. 20 cell lines were also included in the screen, but were excluded from downstream analysis due to lack of response to stimulation (Bruch and Giles et al. 2021).

Preparation of screening plates

Section 3.1.1. Drugs and stimuli were first selected and ordered from Selleckchem, MedChemExpress and Sigma-Aldrich. Drugs were initially dissolved in DMSO and stored at -20°C. For a list of drugs, concentrations and sources see Appendix Table 7.2. Recombinant cytokines and stimulatory agents were dissolved according to protocol defined by the manufacturer. Appendix Table 7.3 provides a detailed list of concentrations and sources. In addition, HS-5 conditioned medium (HS-5 CM) was produced by incubating the stromal cell line HS-5 for four days at 37°C and 5% CO₂. The resulting supernatant was centrifuged and stored at -20°C and the final concentration of HS-5 CM used in the screen was 20%.

Drugs were pre-plated in 384-well polypropylene storage plates (Greiner Bio-One Cat. No. : 781271), which were stored at -20°C. Storage plates were thawed on day of use, and diluted in serum free RPMI with or without corresponding stimuli (Bruch and Giles et al. 2021)..

Drug - stimulation combinatorial assay

Section 3.1.1. 5 μ l of this drug-stimulation dilution was added into each well of the 384-well assay plates (Greiner Bio-One Cat. No. 781904), followed by 20 μ l of cell suspension. Final DMSO concentration did not exceed 0.3% and the final cell concentration was 8 x 10⁵ cells/ml. Screening was performed in RPMI-1640 (Gibco by Life Technologies, final concentration of 100 Units/ml) supplemented with Penicillin Strep-tomycin (Gibco, 100 μ g/ml), L-Glutamine (Gibco, 2mM), and pooled, heat-inactivated and sterile filtered human type AB male off-the-clot serum (PAN Biotech, Cat. No. P40-2701, Lot. No. P-020317, 10%). One well was used per drug, concentration and stimulus (Appendix Figures 7.1, 7.2, 7.3), such that each patient sample was screened on two plates. Samples were incubated at 37°C and 5% CO₂ for 48 hours. Cell viability was determined using the ATP-based CellTiter-Glo assay (Promega, Cat. No. G7573). Luminescence was measured for the drug-stimulation assays using a Perkin Elmer En-Vision, with a measurement time of 100ms per well. 15 drugs, in two concentrations, alone and in combination with 18 stimuli were studied, across 192 patient samples. Carfilzomib, panobinostat and venetoclax were removed from downstream analysis as they showed inconsistent toxicity depending on used media, as well as Bead immobilised anti-IgM due to storage instability. 12 drugs and 17 stimuli were used in all downstream analyses (Bruch and Giles et al. 2021). *The screen was primarily designed and performed by Peter-Martin Bruch.*

2.1.2 Follow - up investigations

Spi-B and PU.1 shRNA Knockdowns

Section 5.2.6. “shRNAs directed against PU.1 (shRNA: 5'-GAAGAAGCTCACCTACCAGTT-3')²¹ and Spi-B (shRNA: 5'-CAAGGTTCCCTCTTGTCAAGAT-3')²² were integrated into the pLKO.1 vector backbone (Addgene plasmid #10878) according to the manufacturer’s protocol using pLKO.1-scramble shRNA (Addgene plasmid #1864) as control.

Lentiviruses were produced by co-transfected psPAX2 (4.8 μ g; Addgene plasmid #12260), pMD2.G (3.2 g; Addgene plasmid #12259) and one of the cloned shRNA plasmids (8 μ g) to HEK 293T cells. Virus-containing medium was collected 48 and 72 hours post transfection and concentrated via ultracentrifugation. The target cells were transduced in 96-well plates and sufficient amounts of virus were added to transduce about 80% of the cells. Spinoculation was performed in the presence of polybrene (SU-DHL 4, SU-DHL 5: 8 μ g/mL; SU-DHL 2: 12 μ g/mL) for 45 minutes at 3,200g. At 72 hours post infection, the cells were selected with puromycin (0.5 μ g/mL). For the PU.1/Spi-B Double-KD, the Spi-B-KD cell lines were additionally transduced with the PU.1-KD lentivirus in the same manner as in the first transduction. Knockdown efficiencies were confirmed by PU.1 and Spi-B western blots.” Bruch and Giles et al. 2021. *Original text written by Master’s Student Tina Becirovic. Experiment performed by Tina Becirovic and Sophie Herbst.*

IHC staining of lymph nodes for STAT6, pSTAT6 and pIRAK4

Section ???. “Lymph node biopsies of CLL-infiltrated and non-neoplastic samples were formalin fixed and paraffin embedded, arranged in Tissue Microarrays and stained for pSTAT6 (ab28829, Abcam) and pIRAK4 (ab216513, Abcam). The slides were analysed using QuPath (Bankhead et al. 2017) and the recommended protocol.” Bruch and Giles et al. 2021. *Original text written by Peter-Martin Bruch. Experiment performed by Mark Kriegsmann, Katharina Kriegsmann and Christiane Zgorzelski.*

Ibrutinib - IL4 - STAT6i interaction assay

[Section 7 method]

Preparation of samples for ATACseq, RNAseq and Mass Spectrometry treated with DMSO, ibrutinib, IBET-762 and IL4

Sections 5.2.4 and ?? Peripheral blood was taken from four CLL patients and separated by Ficoll gradient (GE Healthcare), mononuclear cells were cryopreserved on liquid nitrogen. Samples were later thawed from frozen following the protocol described in Dietrich et al. (2017), and MACS-sorted for CD19 positive cells (Miltenyi autoMACS). The cells were resuspended in RPMI (GIBCO, Cat. No. 21875-034), with the addition of 2mM glutamine (GIBCO, Cat. No. 25030-24), 1% Pen/Strep (GIBCO, Cat. No. 15140-122) and 10% pooled, heat-inactivated and sterile filtered human type AB male off the clot serum (PAN Biotech, Cat. No. P40-2701, Lot.No:P-020317). 5ml of cell suspension was cultured in 6-well plates (Greiner Bio-One Cat. No. 657160). To prepare the treatments, ibrutinib (Selleckchem, Cat.No. S2680), IBET-762 (Selleckchem, Cat. No. S7189) and IL4 (Sigma-Aldrich, Cat.No.SRP3093 Lot. No. 0712AFC14) were dissolved in DMSO (SERVA, Cat. No. 20385) and stored at - 20°C. After thawing, ibrutinib, IBET-72 and IL4 were prediluted in DMSO and added to the plates. Control wells were treated with DMSO in the same concentration as with treatments. In both treatments and control, the final DMSO concentration was 0.2%. Cells were then added and incubated at 37°C and 5% CO₂ for 6 hours. The final cell concentration was 2 x 10⁶ cells/ml and the final treatment concentrations were ibrutinib (500nM), IBET-72 (), IL4 (). After treatment, cell viability and purity was assessed using FACS. All samples had a viability over 90% and over 95% of CD19+/CD5+/CD3- cells (Bruch and Giles et al. 2021).

The four control samples were analysed as part of the investigation of TF activity in trisomy 12 CLL (section 5.2.4). For the analysis of the interaction between ibrutinib, IBET-762 and IL4, all 32 control and treated samples were used (Chapter ??). *Text adapted from extract originally published in Berest et al. (2019). Original text authored by myself and Peter-Martin Bruch. Experiment performed by Peter-Martin Bruch.*

ATACseq library generation and sequencing of CLL PMBCs treated with DMSO, ibrutinib, IBET-762 and IL4

Sections 5.2.4, 6.2.1 and ?? ATACseq libraries were generated as described previously (Buenrostro et al. 2013). Cell preparation and transposition was performed according to the protocol, starting with 5 x 10⁴ cells per sample. Purified DNA was stored at -20°C until library preparation was performed. To generate multiplexed libraries, the transposed DNA was initially amplified for 5x PCR cycles using 2.5 μL each of 25 μM PCR Primer 1 and 2.5 μL of 25 μM Barcoded PCR Primer 2 (included in the Nextera

index kit, Illumina, San Diego, CA, USA), 25 μ L of NEBNext High-Fidelity 2x PCR Master Mix (New England Biolabs, Boston, Massachusetts) in a total volume of 50 μ L. 5 μ L of the amplified DNA was used to determine the appropriate number of additional PCR cycles using qPCR. Additional number of cycles was calculated through the plotting of the linear Rn versus cycle, and corresponds to one-third of the maximum fluorescent intensity. Finally, amplification was performed on the remaining 45 μ L of the PCR reaction using the optimal number of cycles determined for each library by qPCR (max. 13 cycles in total). The amplified fragments were purified with two rounds of SPRI bead clean-up (1.4x). The size distribution of the libraries was assessed on Bioanalyzer with a DNA High Sensitivity kit (Agilent Technologies, Santa Clara, CA), concentration was measured with Qubit DNA High Sensitivity kit in Qubit 2.0 Flurometer (Life Technologies, Carlsbad, CA). Sequencing was performed on NextSeq 500 (Illumina, San Diego, CA, USA) using 75bp paired-end sequencing, generating 450 million paired-reads per run, with an average of 55 million reads per sample.” (Berest et al. (2019); Bruch and Giles et al. 2021) *Original text written by Nayara Trevisan Doimo de Azevedohe of the EMBL Genomics Core Facility. Experiment performed by Nayara Trevisan Doimo de Azevedohe and Peter-Martin Bruch.*

RNAseq library generation and sequencing of CLL PMBCs treated with DMSO, ibrutinib, IBET-762 and IL4

Sections ???. “RNAseq library generation for the CLL dataset treated with ibrutinib RNA was isolated using the miRNeasy Mini Kit (QIAGEN, Cat. No. 217004), starting with 1×10^7 cells per sample. Cells were lysed in QIAzol Lysis reagent and homogenized using QIAshredder (QIAGEN, Cat. No. 79654), homogenized cell lysates were stored at 80°C until RNA extraction. RNA extraction was performed according to miRNeasy protocol and purified RNA was stored at 80°C until further processing. RNA integrity was checked using the RNA Nano 6000 Assay Kit of the Bioanalyzer 2100 system (Agilent Technologies, Santa Clara, CA), and concentration was measured with Qubit RNA Assay Kit in Qubit 2.0 Flurometer (Life Technologies, Carlsbad, CA). Stranded mRNA-Seq libraries were prepared from 250ng of total RNA using the Illumina TruSeq RNA Sample Preparation v2 Kit (Illumina, San Diego, CA, USA) implemented on the liquid handling robot Beckman FXP2. Obtained libraries that passed the QC step, which was assessed on the Agilent Bioanalyzer system, were pooled in equimolar amounts. 1.8 pM solution of each pool of libraries was loaded on the Illumina sequencer NextSeq 500 High output and sequenced uni-directionally, generating 450 million reads per run,

each 85 bases long.” (Berest et al. 2019). *Original text written by Nayara Trevisan Doimo de Azevedohe of the EMBL Genomics Core Facility. Experiment performed by Nayara Trevisan Doimo de Azevedohe and Peter-Martin Bruch.*

Proteomics

[Section 7 ADD]

2.2 Additional Data and Data availability

Patient sample multi-omic profiles Whole-exome sequencing, DNA-methylation, RNA-sequencing and copy number variant data were taken from the PACE repository (Oles et al. 2021).

Clinical data on patient samples Clinical follow-up data was available for some of the 192 patients, taken from PACE (Oles et al. 2021) including TTT (n = 188), TTFT (n = 189) and OS (n = 192). LDT (n = 115) was taken from [].

CLL PMBC ATACseq data The external ATACseq dataset analyses in section 5.2.4 was generated by Rendeiro et al. (2016) and downloaded from the European Genome-phenome Archive (EGA, EGAD00001002110).

Spi-B and PU.1 ChIPseq data Spi-B and PU.1 ChIPseq data in the OCILY3 DLBCL cell line (Care et al. 2014) was downloaded from the NCBI GEO database (Edgar, Domrachev, and Lash 2002), accession GEO : GSE56857, IDs : GSM1370276, GSM1370275

Proteomics data for CLL PMBCs The proteomics dataset used to investigate gene dosage effects in trisomy 12 (section 5.2.2) was shared by PhD student Sophie Herbst, and published as part of her Dissertation (Herbst 2020).

Availability The datasets described in this thesis, including the drug-stimulus combinatorial screen and associated patient meta data, along with validation experiments (Spi-B and PU.1 shRNA knockdowns, ATACseq of CLL PBMCs and IHC data of patient lymph nodes) are all available as part of the online repository, which can be found here.

2.3 Data processing

2.3.1 Screening data

Data normalisation

Section 3.2. Raw luminescence measurements from the experiments were read in using custom-made R scripts and functions. Raw values represent the luminescence readout of the CellTiter-Glo Luminescent Cell Viability Assay. Each raw count was normalised to internal DMSO values of the same plate. Specifically, the mean of each well corresponding to each stimulus, drug or drug-stimulus treatment was divided by the median of the 48 DMSO negative control wells present on each plate, resulting in viability scores. Control-normalised viability scores were \log_e transformed, to generate log-transformed control-normalised viability scores used for the majority of the downstream analysis (Bruch and Giles et al. 2021). *Initial data read in, normalisation and quality control performed by Peter-Martin Bruch.*

Data from PACE

Whole-exome sequencing, DNA-methylation, RNA-sequencing and copy number variant data accessed from PACE (Oles et al. 2021) was pre-processed, see Dietrich et al. (2017). To see processing steps see description in Dietrich et al. (2017).

2.3.2 Follow - up investigations

ATACseq processing for internal ATACseq of CLL PMBCs treated with DMSO, ibrutinib, IBET-762 and IL4

Section 5.2.4 and ???. The internal CLL dataset contained 32 ATAC-seq samples from 4 patients, treated with DMSO, IL4, ibrutinib, IBET-762 and all combinations. The ATACseq processing pipeline outlined in Berest et al. (2019) was followed to generate GC-biased corrected bam and peak files mapped to the hg38 and the hg19 annotation genome. hg19 mapped files were used in downstream analysis. More specifically, this involved a Snakemake (Kö Ster and Rahmann 2012) pipeline, written by Berest et al. (2019) which accepts raw fastq files, and performs steps quality control, adaptor trimming, alignment, post-alignment filtering and processing steps to generate bam files. The steps are as follows: first FastQC determined sequence quality. Trimmomatic (Bolger, Lohse, and Usadel 2014) was used to remove sequences derived from the Nextera Transposase agent. Next Bowtie2 (Langmead and Salzberg 2012) was used for the alignment step (against hg19), followed by numerous clean-up processes involving Picard tools, CleanSam, FixMateInformation, AddOrReplaceReadGroups, and ReorderSam. Base quality recalibration was performed using GATK (McKenna et al.

2010), allowing the detection and correction of systematic errors in quality score estimated for each base call, thereby increasing data quality.

Data was then filtered, first to remove mitochondrial reads and reads from non-assembled contigs or alternative haplotypes, then to remove reads with a mapping quality below the threshold. Duplicate reads were marked and removed with Picard tools, and read start sites were adjusted as described in Buenrostro et al. (2013) i.e. 4 bp on the forward and 5 bp on the reverse strand. Reads with insertions or deletions were removed using SAMtools (H. Li et al. 2009).

GC bias correction was performed using deepTools (Ramírez et al. 2014). Benjamini's method (Benjamini and Speed 2012) was then performed for each sample to quantify level of GC bias. Peak calling was then performed using MACS2 (Y. Zhang et al. 2008), to generate peak files. The pipeline generated summary statistics and additional files and plots (coverage files for visualisation, transcription start site enrichment, sample-specific fragment length distributions, library complexity measures and PCA sample correlations) that were assessed to determine data quality and any batch effects (Bruch and Giles et al. 2021). *Text adapted from original extract published in Berest et al. (2019). Alignment to hg38 performed by Ivan Berest. [CHECK]*

RNAseq processing for RNAseq of CLL PMBCs treated with DMSO, ibrutinib, IBET-762 and IL4

Section ???. Transcript quantification was performed using Salmon version 0.8.2 (Patro et al. 2017) and the reference genome (GRCh38 version 90), with default parameters and $k = 31$ for the generation of the index file. Gene-level count matrices were generated by importing the quantification data using the `tximport` R package (Love et al. 2021). Downstream library size normalisation and variance stabilising transformation were performed using the R package `DESeq2` (Love, Anders, and Huber 2021).

ATACseq processing for external ATACseq dataset

Section 5.2.4. The Rendeiro et al. (2016) CLL dataset contained 88 ATACseq samples from 55 patients. For the analysis one sample per patient was used passing quality checks, resulting in 52 samples. The ATACseq processing pipeline outlined in Berest et al. (2019) and above was followed to generate GC-biased corrected bam and peak files mapped to the hg19 annotation genome (Bruch and Giles et al. 2021). *Performed by Ivan Berest.*

2.4 Statistical Analysis

The following analysis was performed using R version 4 (R Core Team 2021) with the RStudio interface (RStudio Team 2020), and packages from Bioconductor (Huber et al. 2015). Plots were generated with the R package `ggplot2` (Wickham et al. 2021) and arranged with the R package `patchwork` (T. L. Pedersen 2020).

2.4.1 Analysis of Screening Data

Drug-drug and stimulus - stimulus correlations

Section 3.3.2 and 4.1.1. Pearson correlation coefficients were calculated for each drug - drug and stimulus - stimulus pair, using the `cor` functions in R (R Core Team 2021) with log transformed viability values which were normalised to untreated controls (Bruch and Giles et al. 2021). *Performed with Peter-Martin Bruch for the manuscript Bruch and Giles et al. 2021.*

Correlation of RNA-Receptor Expression with viability scores

Section 3.4.2. RNA count data for matched samples was available for 49 patients and was transformed using the variance stabilising transformation. Stimulus - receptor pairs were defined using the available literature, see Appendix Table 7.4. For each stimulus, a Pearson correlation coefficient was calculated between the log-transformed control-normalised viability values and the expression of the corresponding stimulus receptor for matching samples. Correlation coefficients were visualised in a volcano plot, to determine if any cytokine-receptor pairs showed $R>0.4$ (Bruch and Giles et al. 2021). *Performed with Peter-Martin Bruch for the manuscript Bruch and Giles et al. 2021.*

Consensus clustering and visualisation of stimulus responses

Section 4.1.2. For the heatmap in figure 4.4, the log transformed control-normalised viability scores were scaled for optimal visualisation. For each stimulus, viability values were row-scaled according to the Median Absolute Deviance, and limits were then applied to this row scaling factor for the purposes of visualisation, such that all resulting z scores were between -3 and +3.

The columns (patient samples) of the resulting matrix were then clustered using the `ConsensusClusterPlus` function, from the (Wilkerson and Waltman 2021) package.

The function generated robust clusters for k (number of clusters) = 2 - 7, performing hierarchical clustering based on Euclidean distances, with 10,000 repeats.

To quantify the degree of confidence in the clusters for each k, plots representing the cumulative distribution functions (CDFs) of the consensus matrices for k = 2 - 7, the relative change in area under the CDF curves, and cluster stability were assessed.

The z scores were then visualised for k = 4, using the pheatmap package (Kolde 2019), whereby the columns were clustered according to the dendrogram resulting from the above, and the rows (stimuli) were ordered using the dendrogram order produced by hclust with default branch arrangement (Bruch and Giles et al. 2021). *Performed with Peter-Martin Bruch for the manuscript Bruch and Giles et al. 2021.*

Univariate analysis of gene - stimulus and gene - drug response associations

Section 5.1.1 and 6.2.1. Two-sided Student's t-tests, with equal variance were performed for IGHV status and somatic mutations and copy number aberrations with at least three patient samples in each group (n = 54). Mutations in KRAS, NRAS and BRAF were tested in a single group. p values were adjusted using the BH-adjustment procedure, and a 10% FDR cut off was used to determine significance (Bruch and Giles et al. 2021). *Performed with Peter-Martin Bruch for the manuscript Bruch and Giles et al. 2021.*

Penalised multivariate regression of gene - stimulus associations

Section 5.1.2. To identify gene-stimulus associations, a Gaussian linear model with L1-penalty with mixing parameter alpha = 1 was fitted for each stimulus using the cv.glmnet function from the R package glmnet (Friedman et al. 2021). The feature matrix consisted of genetic features (p=39), IGHV status (input as M = 1 and U = 0), and Methylation Cluster (input as 0, 0.5, 1). All features were thus encoded on a similar scale to ensure equal treatment by lasso constraint in model fitting. Where genetic features showed more than 20% missing values, these were excluded from the feature matrix. Samples without complete annotation for remaining features were removed, resulting in n = 129 samples. The matrix of control-normalised log-transformed viability values for these 129 samples was provided as the response matrix. Using three-fold cross-validation, the optimal penalty parameter λ was selected so as to minimise the cross-validated R2. The reduction in cross-validated mean squared error compared to the null model was used as loss. The model was fitted for 30 bootstrapped repeats, and

the resulting coefficients are the mean of those coefficients that were selected in >75% model fits (Bruch and Giles et al. 2021).

Linear modelling of drug - stimulus interactions

Section 6.1.1. Linear models were fitted for each drug - stimulus combination, to extract a β_{int} term and associated p value for each combinatorial treatment. Linear model was fitted using equation (6.1), using the `lm` function of R (R Core Team 2021).

To fit model, the matrix of log-transformed viability values, for control, single and combinatorial treatments was used. Interactions were filtered according to whether p value for $\beta_{int} < 0.05$. To generate the map of drug - stimulus interactions, the matrix of resulting β_{int} was plotted as a heatmap, with the package `pheatmap`(Kolde 2019) where the rows (stimuli) and columns (drugs) were ordered according to the dendrogram order produced by `hclust` (R Core Team 2021) using default branch arrangement.

Categorising drug - stimulus interactions

Section 6.1.2. To define the four interaction categories, drug - stimulus combinations were first divided with respect to the sign of β_{int} , whereby a positive β_{int} indicates that the viability with combinatorial treatment is higher than would be expected based on additive effects alone and vice versa. The groups were further divided into synergies and antagonisms according to the values of the model coefficients (β_{drug} , $\beta_{stimulus}$ and β_{int}). Synergisms were assigned when coefficients for single treatments (β_{drug} and $\beta_{stimulus}$) were both greater than, or both less than, the observed coefficient for the combinatorial treatment (i.e. $\beta_{drug} + \beta_{stimulus} + \beta_{int}$). For positive antagonisms, $\beta_{drug} + \beta_{stimulus} + \beta_{int}$ was less than either β_{drug} or $\beta_{stimulus}$. For negative antagonisms, $\beta_{drug} + \beta_{stimulus} + \beta_{int}$ was greater than either β_{drug} or $\beta_{stimulus}$. All drug - stimulus interactions for which p value for $\beta_{int} < 0.05$ fit into one of these groups (Bruch and Giles et al. 2021). *Performed with Peter-Martin Bruch for the manuscript Bruch and Giles et al. 2021.*

Modelling of drug - stimulus - gene interactions

Section 6.3. Identification of drug - stimulus interactions that were modulated by genetic features was performed in two steps.

First the linear model in equation (6.1) was fitted in a patient sample specific manner

i.e. equation (6.2) was fit to the matrix of log-transformed, control-normalised viability scores, for each drug - stimulus combination.

This resulted in a higher order interaction term for each drug - stimulus - patient combination, named $\beta_{int}X_{drug}X_{stimulus}X_{patient}$. This term represents a *patient sample-specific* β_{int} for each drug - stimulus combination, quantifying the size of an interaction between a drug and stimulus in each patient genetic background.

In the second step, multivariate regression with L1 (lasso) regularisation was used to identify associations between the size of the patient sample-specific β_{int} terms and genetic features. As input to the model, the response matrix was composed of the sample - specific β_{int} values for each drug-stimulus combination. The feature matrix consisted of genetic features ($p = 39$), IGHV status (input as $M = 1$ and $U = 0$), and Methylation Cluster (input as 0, 0.5, 1). All features were thus encoded on a similar scale to ensure equal treatment by lasso constraint in model fitting. Where genetic features showed more than 20% missing values, these were excluded from the feature matrix. Samples without complete annotation for remaining features were removed, resulting in $n = 129$ samples.

Using three-fold cross-validation, the optimal penalty parameter λ was selected so as to minimise the cross-validated R². The misclassification error was used as loss. The resulting predictors are the mean of those coefficients that were selected in at least 90% of 30 bootstrapped repeats (Bruch and Giles et al. 2021).

2.4.2 Analysis of follow-up data

Assosciation of clusters and lymphocyte doubling times

Section 4.2.2. Data on lymphocyte growth rates were curated from clinical records. To calculate growth rates, a linear model was fit to log10 transformed lymphocyte counts for a series of time points starting with the sample collection date and ending with the time of the next treatment. Where less than four time points were recorded, these patients were excluded, resulting in LDT measurements for 115 patient samples. Associations between LDT measurements and patient clusters were assessed using two-sided Student's t-tests (Bruch and Giles et al. 2021). *Performed with Peter-Martin Bruch for the manuscript Bruch and Giles et al. 2021.*

Assosciation of clusters and patient outcomes

Section 4.2.2. Differential disease progression between patient clusters was measured using TTT as metric. 188 of 192 CLL patients were annotated for treatment information after sample collection. TTT represents the period between the date of sample collection and the date of treatment initiation. TTT was plotted using the Kaplan-Meier method, in which patient samples were stratified by cluster. To calculate significance, univariate Cox proportional hazards regression models were fitted using the `coxph` function of the R package `survival` (Therneau 2021), using C1 as reference for the comparison C1 versus C2 and C4 as reference for C3 versus C4. To determine whether the prognostic value of cluster assignment between C3 and C4 was independent of other prognostic markers, a multivariate Cox proportional hazards regression models was fit, with the design formula `~Cluster + IGHV.status + trisomy12 + TP53`, with Cluster 3 as reference (Bruch and Giles et al. 2021). *Performed with Peter-Martin Bruch for the manuscript Bruch and Giles et al. 2021.*

Penalised multivariate regression to identify genetic predictors of cluster membership

Section 4.2.4. Differential enrichment of genetic features amongst the four patient clusters was quantified using a multinomial linear model with L1-penalty, via the `cv.glmnet` function of the `glmnet` package (Friedman et al. 2021). As input to the model, the discrete response matrix represented the vector of cluster assignments (1-4) for each patient sample. The feature matrix consisted of genetic features ($p = 39$) and IGHV status (input as $M = 1$ and $U = 0$). All features were thus encoded on a similar scale to ensure equal treatment by lasso constraint in model fitting. Where genetic features showed more than 20% missing values, these were excluded from the feature matrix. Samples without complete annotation for remaining features were removed, resulting in $n = 129$ samples. Using three-fold cross-validation, the optimal penalty parameter λ was selected so as to minimise the cross-validated R^2 . The misclassification error was used as loss. The resulting coefficients are the mean of 50 bootstrapped repeats, where coefficients were filtered if they were selected in <60% of cases or were <0.35. Standard deviations were calculated for each coefficient based on the bootstrapped repeats (Bruch and Giles et al. 2021).

Gene expression and Gene Set Enrichment Analysis (GSEA) between clusters

Section 4.2.5. To look for associations between stimulus response data and RNA expression data the R package DESeq2 (Love, Anders, and Huber 2021) was used. RNAseq data was available for 49 matched PBMC samples, 21 of which belonged to C3 and C4 (Bruch and Giles et al. 2021).

To quantify differential gene expression between C3 and C4, genes encoding components of the BCR were first filtered, including genes at the heavy, light and kappa immunoglobulin loci. Differential expression was quantified using DESeq2 protocol (Love, Anders, and Huber 2021) with the design formula ~IGHV.status + Cluster. Genes were then ranked according to the resulting Wald statistics and GSEA was performed using the clusterProfiler package (G. Yu 2021), with the fgsea algorithm and using KEGG pathway gene sets from the MSigDB database (Dolgalev 2021) (Bruch and Giles et al. 2021).

Analysis of differential gene dosage in trisomy 12 CLL

Section 5.2.2. For all RNA samples available in PACE that matched the samples in the screen, differential expression was called using the DESeq2 package (Love, Anders, and Huber 2021), with the design formula ~trisomy12. Raw RNA counts were visualised if the gene had BH-adjusted $p < 0.1$ and belonged to TGF β , JAK-STAT or TLR pathways genesets, as defined in the KEGG database (Kanehisa et al. 2010) downloaded using the msigdbr package (Dolgalev 2021). Proteomic abundance data was also plotted. Samples in proteomics data partially overlap with those in RNAseq data.

Identification of trisomy 12 phenocopies

Section 5.2.3. Trisomy 12 phenocopies were identified using a classification approach. The classifier was built in two steps: First, coefficients were selected that predict trisomy 12 status based on stimulus response, using a binomial linear model with L1-penalty implemented in the R package glmnet (Friedman et al. 2021). The feature matrix consisted of z scores of the viability values after treatment with each stimulus, and was used to predict the response, a vector of the trisomy 12 statuses for each sample. Using three-fold cross-validation, the optimal penalty parameter λ was selected so as to minimise the cross-validated R2. The mean absolute error was used as loss. The model fitting was performed for 50 bootstrapped repeats.

Second, the function `predict` was used with each of the 50 model fits, to assign trisomy 12 status for each sample, based on the matrix of z scores. Non-trisomy 12 samples were determined to be misclassified i.e. phenocopies if they were wrongly annotated as trisomy 12 in >25 of repeats.

diffTF analysis of TF activity in trisomy 12 CLL

Section 5.2.4. For the external ATACseq data set from Rendeiro et al. (2016) ($n = 52$), trisomy 12 status was not included in the published metadata. Trisomy 12 status was annotated based on the mean number of reads in the chromatin accessible peaks for each sample. All samples containing 1.4 times more reads in the peaks located on chromosome 12, compared to the peaks on all other chromosomes, were classified as trisomy 12 ($n = 9$).

Following the `diffTF` Berest et al. (2019) protocol, a consensus peak set was first generated using the function `dba.peakset` from the package `DiffBind` (Stark and Brown 2021) and with `minOverlap = 3`, which defines the minimum number of samples in which a peak should be present to be included in the consensus set. Sex chromosomes, non-assembled contigs and alternative haplotypes were then filtered. Transcription factor binding sites were defined based on the HOCOMOCO v10 database (Kulakovskiy et al. 2016) which summarises TF binding sites as Position Weight Matrices (PWMs) from a range of ChIPseq experiments, resulting in 638 human TFs. `diffTF` was run in permutation mode with design formula: `sample_processing_batch + sex + IGHV status + trisomy 12`. For more detail see Berest et al. (2019).

For the in-house generated ATACseq dataset ($n = 4$), trisomy 12 status was already annotated (Oles et al. 2021). The consensus peak set was defined using `minOverlap = 1` and TF binding sites were defined using the HOCOMOCO v10 database (Kulakovskiy et al. 2016). `diffTF` was run twice (with and without chromosome 12 data) in analytical mode (due to the smaller sample size) with the following parameters design formula ~ `patient + trisomy 12` (Bruch and Giles et al. 2021). *Performed with Ivan Berest for the manuscript Bruch and Giles et al. 2021.*

Functional enrichment analysis of SPIB ChIPseq data

Section 5.2.5. Spi-B and PU.1 ChIPseq data in the OCILY3 DLBCL cell line (Care et al. 2014) was downloaded from the NCBI GEO database (Edgar, Domrachev, and Lash 2002), accession GEO : GSE56857, IDs : GSM1370276, GSM1370275. Spi-B ChIP

peaks were filtered for significance (q value < 0.05). The `annotatePeaks` function from the package `clusterProfiler` (G. Yu 2021) was used to annotate the nearest gene for each ChIP peak. The resulting gene list was filtered to only include genes where the transcription start site (TSS) was within 1kb of its associated ChIP peak, in either direction. The `enricher` function of the `clusterProfiler` package was used to perform over-representation of KEGG (Kanehisa et al. 2010) and Reactome (Jassal et al. 2020) pathways amongst this list of genes (Bruch and Giles et al. 2021).

diffTF analysis of TF activity of CLL samples after treatment with IBET-762 CLL

[SECTION 7 METHOD] Section 6.2.1

Survival analysis of IHC data

Section ???. The levels of STAT6, pSTAT6 and pIRAK4 were obtained from IHC data. First patient samples were split into two groups (low / high) based on their staining levels for each protein. The cut off for each group was calculated using R package `maxstat` (Hothorn 2017) to compute maximally selected rank statistics. 64 of 100 patients were annotated for treatment information after sample collection. TTT represents the period between the date of sample collection and the date of treatment initiation. TTT was plotted using the Kaplan-Meier method with the R package `survminer` (Kassambara, Kosinski, and Biecek 2021), in which patient samples were stratified by staining level (low / high) (Bruch and Giles et al. 2021). *Performed with Peter-Martin Bruch for the manuscript Bruch and Giles et al. 2021.*

Synergy analysis

[Section 7 method]

Analysis of gene expression changes after ibrutinib, IBET-762 and IL4 treatment

[Section 7 method]

Analysis of TF activity changes after ibrutinib, IBET-762 and IL4 treatment

[Section 7 method]

Generation of Gene Regulatory Network

[Section 7 method]

Chapter 3

Data

This chapter provides an overview of the datasets that are central to this thesis. It also covers the generation of resources to make the data and associated analysis publicly-available.

The screening dataset discussed here was produced and published as part of the manuscript Giles and Bruch et al. 2021. Some analysis and figures outlined in this chapter have also been published in Bruch and Giles et al. 2021, and this is clearly stated where this is the case.

3.1 Experimental overview

3.1.1 Drug-stimulus combinatorial perturbation assay and patient sample multi-omic profiling

This thesis centres on a dataset of 192 CLL patient samples subjected to functional and molecular profiling. A drug-stimulus combinatorial perturbation assay (referred to below as the screen) measured the effects of 17 cytokines and microenvironmental stimuli alone and in combination with 12 drugs, to investigate the influence on spontaneous and drug-induced apoptosis (Bruch and Giles et al. 2021).

The screen was primarily designed and performed by Peter-Martin Bruch in the Department of Medicine, University of Heidelberg, and published in the manuscript by Bruch and Giles et al. 2021. Drugs and stimuli were deposited first and patient samples second, using two 384-well plates per patient sample. Each plate contained stimulus, drug

and drug - stimulus wells along with DMSO control wells (Appendix Figures 7.1, 7.2 and 7.3). After 48 hours of incubation at 37°C, cell viability was assessed using the CellTiter-Glo Luminescent Cell Viability Assay. This method estimates the number of viable cells in a culture by determining the quantity of ATP present, which indicates the number of metabolically active cells. The drugs and stimuli tested in the screens are outlined in sections 3.3 and 3.4.

Multi-omics profiles for the patient samples were also available from the PACE repository (Oles et al. 2021), consisting of whole-exome sequencing, DNA-methylation, RNA-sequencing and copy number variant data. In addition, clinical follow-up data was also available for some patients, including LDT, TTT, TTFT and OS.

Collectively, these data enabled (i) characterisation of responses to microenvironmental stimuli, (ii) definition of functional patient subgroups, (iii) profiling of molecular determinants of drug and stimulus responses (iv) mapping of drug - stimulus and drug - stimulus - gene interactions, thus shedding light on the heterogeneity of CLL biology and drug response (Figure 3.1).

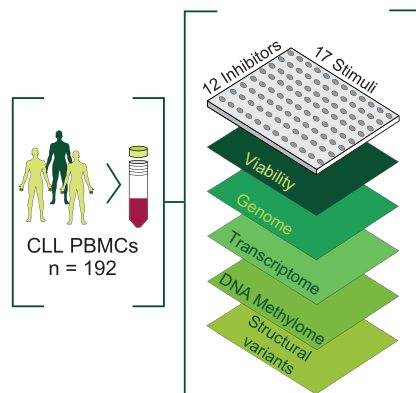


Figure 3.1: Schematic of experimental protocol. By combining 12 drugs and 17 stimuli, we systematically queried the effects of simultaneous stimulation and inhibition of critical pathways in CLL ($n = 192$). Integrating functional drug-stimulus response profiling with four additional omic layers, we identified pro-survival pathways, underlying molecular modulators of drug and microenvironment responses, and drug-stimulus interactions in CLL. *Figure and caption from Bruch and Giles et al. 2021.*

3.1.2 Additional datasets

A number of key findings emerged from the above data which warranted further investigation. In addition to the screen, this thesis makes use of a number of validation datasets, from within our lab and from external sources. These are outlined in the Methods (Chapter 2) and in the relevant results chapters.

3.2 Data Processing

3.2.1 Processing the raw values obtained from the screen

This section describes the process of generating viability scores used in downstream analyses (following the same process as published in Bruch and Giles et al. 2021). Initially, raw luminescence measurements from the experiments were read in using custom-made R scripts and functions. Raw values represent the luminescence read-out of the CellTiter-Glo Luminescent Cell Viability Assay, which is proportional to the amount of ATP present. The ATP levels are directly proportional to the number of viable cells in the well.

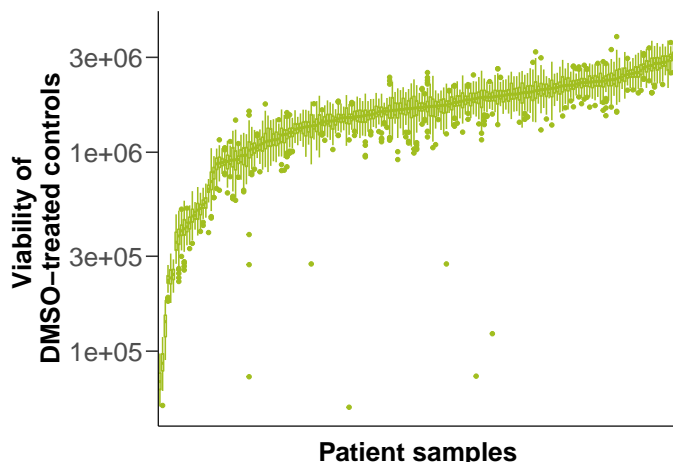


Figure 3.2: Boxplots of raw viability count data prior to normalisation and log transformation. For each of the 192 patient samples, there were 50 DMSO-treated wells. *Raw data read in and initial processing performed by Peter-Martin Bruch, figure adapted from Bruch and Giles et al. 2021.*

Figure 3.2 shows the raw viability values from the DMSO-treated wells for each patient sample. The absolute values vary between patient samples, and between measuring dates, and thus the viability values required additional normalisation.

Each viability value was normalised to internal DMSO values of the same plate. Specifically, the well for each stimulus, drug or drug-stimulus treatment was divided by the median of the 48 DMSO negative control wells present on each plate, resulting in viability scores. A value of 0 indicated that all cells were killed by the treatment, and a value of 1 indicated the cells survived as well as in the negative control.

Given the downstream analysis involved the use of linear modelling, I thus applied a natural logarithm transformation to the viability scores. This generated log-transformed control-normalised viability scores which are used for the majority of the downstream analysis. Here 0 indicates that cells survived as well as negative control.

3.2.2 Quality control and data reproducibility

Next, several additional quality control steps were considered, with the aim of a) adjusting for any spatial effects on each screening plate, b) accounting for any batch effects between screening batches, c) testing data reproducibility.

First, the screening data for each well on each plate was plotted in a grid corresponding to the plate layout, to visualise whether viability values were affected by their position on the plate. We discussed adjusting for any position effect by fitting a surface to the negative control wells, to generate correction factors for each well for each plate. The resulting correction factor was then subtracted from each of the treatment wells. We decided that the position effect was not sufficient to warrant this adjustment, and continued the analysis with the unadjusted values. [CHECK/remove]

With regards to batch effects, screening was performed on 16 separate days. We concluded that normalising data to the DMSO-treated wells on each plate sufficiently accounted for this. [CHECK]. Finally, with respect to data reproducibility, each plate was tested twice, such that the resulting viability scores are the mean of two duplicates [CHECK, add correlation figure].

Thus, the data processing steps generated robust, log-transformed control-normalised viability scores that aim to capture the biological impact of the concomitant application of drugs and stimuli, outlined below.

3.3 Characteristics of drugs used in the screen

3.3.1 The panel of drugs

This study aims to generate a systematic investigation of the impact of soluble factors on therapies and critical pathways in CLL (Bruch and Giles et al. 2021). To that end, a panel of 17 drugs was constructed, encompassing FDA-approved therapies for CLL, along with a number of drugs in clinical trial or laboratory compounds targeting pathways of interest (Figure 3.3). These included fludarabine (a frontline chemotherapeutic) and ibrutinib and idelalisib (newer BCR inhibitors).

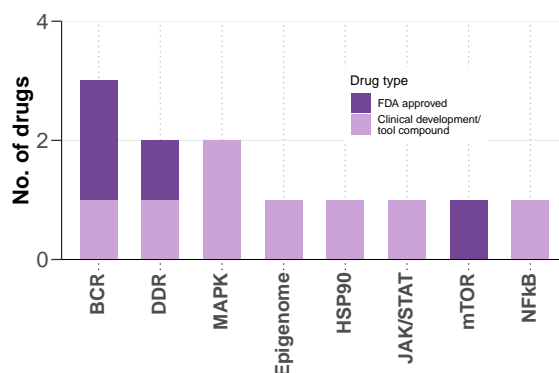


Figure 3.3: Bar plot of the drugs used in screen, indicating targets and licencing status. *Figure from Bruch and Giles et al. 2021.*

The number and concentration of drugs included was limited by the size of the plate. Thus there is minimal overlap between drug targets, and two concentrations were used for each drug. The choice of concentration was guided by the results of a previous drug screen in CLL patients, performed in our lab (Dietrich et al. 2017). The concentrations used were expected to reduce CLL viability without eliminating all cells. Drug concentrations are shown in Appendix Table 7.2.

3.3.2 Assessing drug response

To assess the quality of the drug response data, we quantified correlation coefficients for every drug pair (Bruch and Giles et al. 2021). Drugs were highly correlated if they shared identical target pathways, suggesting that the screen captures inter-individual differences in pathway dependencies, both sensitively and specifically. For example, BCR inhibitors ibrutinib, idelalisib, PRT062607 and selumetinib were all highly correlated (Figure 3.4A).

In addition, the individual drug response profiles (Figure 3.4B) indicated that each of the drugs decreased CLL viability as expected, and in line with previous CLL drug screens

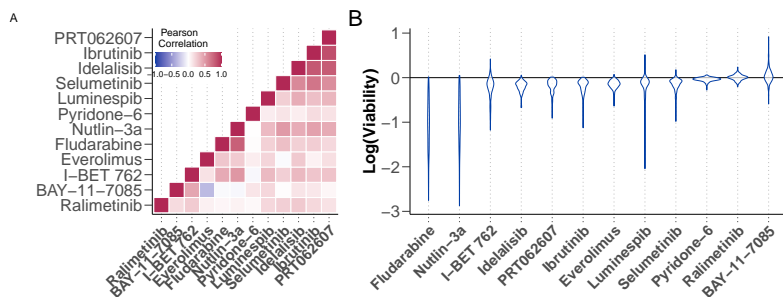


Figure 3.4: (A) Heatmap of Pearson correlation coefficients of each pair of drugs, based on log transformed viability values. See Methods section 2.4.1. (B) Log transformed control-normalised viability values for all drugs that were included in the screen after quality control. p values from Student's t-test. *Figure (A) adapted from original generated with Peter-Martin Bruch for the manuscript Bruch and Giles et al. 2021.*

performed in our lab (Dietrich et al. 2017).

3.4 Characteristics of stimuli used in the screen

3.4.1 The panel of stimuli

The stimuli selected for the screen, their associated targets and concentrations used are described in Appendix Table 7.3. They include 16 individual stimuli, plus HS-5 Culture Medium which encompasses the range of soluble factors secreted by the stromal cell line HS-5 (Bruch and Giles et al. 2021.)

A number of studies have demonstrated the ability of various soluble factors to increase CLL viability or induce drug resistance *ex vivo* (see section 1.3.3). Guided by these observations, the panel of stimuli was selected so as to cover a range of key survival signals in CLL, aiming to minimise redundancy amongst the targeted pathways. The stimuli encompass a cross-section of the complex communication network between CLL cells and non-neoplastic cells, mediated by soluble factors within the tumour microenvironment. 3.5.

The stimuli activate a number of critical pathways in CLL, including BCR, TLR, JAK-STAT, NF κ B and TGF β . For more information on the importance of these pathways see section 1.1.4 and 1.3.3. Amongst these, the roles of BCR, IL4, sCD40L and TLR stimulation were of particular interest.

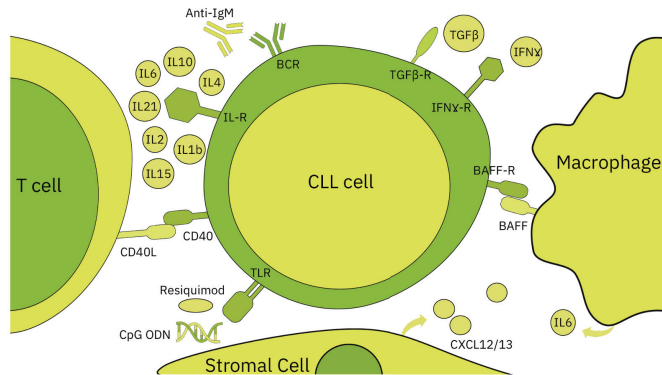


Figure 3.5: A selection of interactions between CLL cells and components of the microenvironment, covered by the screen. See section 1.3.3 for more details on these signals. *Figure adapted from an original published in Wiestner (2015)*.

3.4.2 Assessing stimulus response

Before beginning the downstream analysis, it was first important to determine whether heterogeneity of response to the stimuli could be caused by differences receptor expression, rather than some other cell-intrinsic feature (Bruch and Giles et al. 2021). This would guide our interpretation of the stimulus responses.

To determine this, we calculated Pearson correlation coefficients to compare log-transformed control - normalised viability values for each stimulus, with vst-transformed RNA counts of the matching receptor(s). All Pearson coefficients were less than 0.4, indicating that heterogeneity of response was not related to differential receptor expression.

3.5 Characteristics of patient samples used in the screen

3.5.1 Overview of the molecular profiles of the patient samples

Multi-omics profiles were available for the patient samples in the screen, taken from the Primary Cancer Cell Encyclopedia (PACE) (Oles et al. 2021). The PACE repository represents an initiative by our lab to characterise the multi-omic characteristics of primary tumour samples from leukemia and lymphoma patients. Patient multi-omic profiles included whole-exome sequencing, DNA-methylation, RNA-sequencing and copy number variant data. In addition, clinical information and follow-up data was also available for some patients, including their sex, IGHV status and LDT, TTT, TTFT and OS. Figure ?? summarises the molecular characteristics of the patient samples. For a summary of

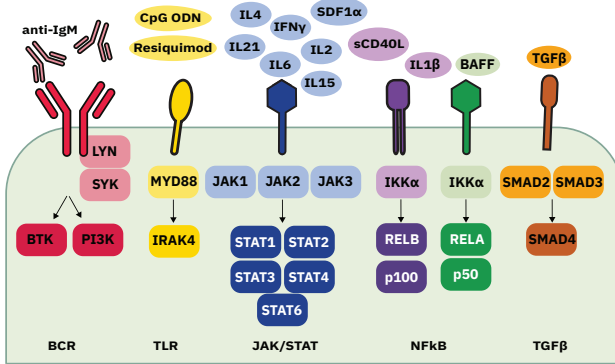


Figure 3.6: Overview of stimuli included in the screen and summary of their associated targets. HS-5 Culture Medium is omitted, as no specific target can be shown. *Figure and caption from Bruch and Giles et al. 2021.*

the number of samples with each mutation, see Appendix Table 7.5.

The findings from this study have potential relevance in a clinical setting. Thus it was important to ensure that the distribution of genetic features amongst the cohort was representative of those observed in clinical practice. Other studies have determined the expected frequency of many recurrent genetic features in CLL (H. Döhner et al. 2000; Puente et al. 2015; Landau et al. 2015) : the distribution of molecular lesions in our cohort is comparable to these (Bruch and Giles et al. 2021).

3.6 Making the data and associated analysis available

Collectively, this dataset represents a valuable resource providing the ability to explore genetic, epigenetic and microenvironmental modulators of survival and drug response in a heterogeneous cohort, and how these relate to clinical outcomes. With CLL samples relatively simple to obtain compared to other cancers, this project (in collaboration with the PACE initiative (Oles et al. 2021)) represents a considerable dataset containing joint functional and molecular profiling of primary cancer samples.

An important goal of my work was thus to ensure that this dataset was both publicly available and accessible for a range of users. I aimed to ensure that our analysis was transparent and reproducible, and that others could explore the dataset for the purposes of their own research. To that end, I developed a shiny app to explore the

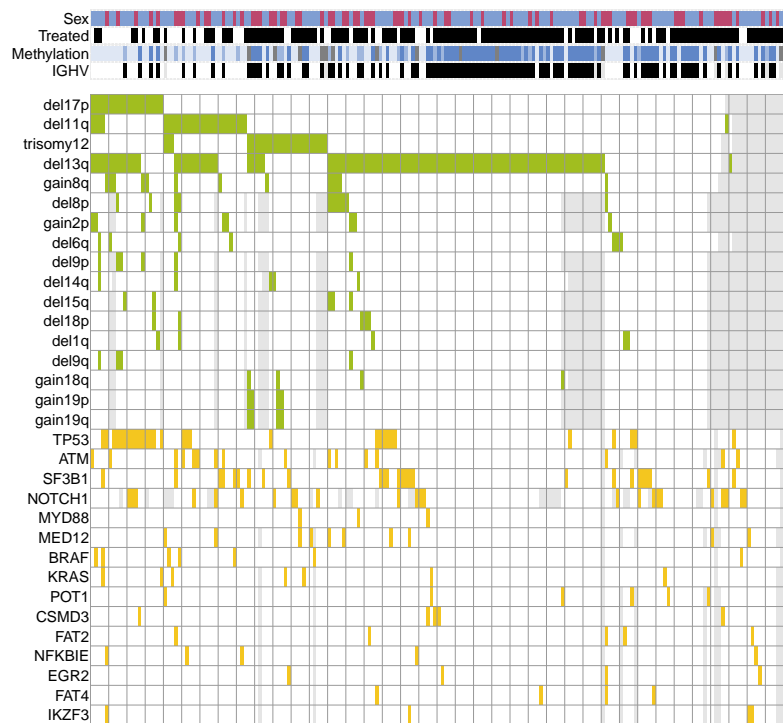


Figure 3.7: Summary of the genetic characteristics of the patient samples in the screen. Annotations: Grey shows when patient sample is not annotated. Black indicates treated / IGHV-M, Green indicates occurrence of CNV, Yellow indicates gene is Mutated.

screening dataset, and published all code and data from the manuscript Bruch and Giles et al. 2021 to an online git repository.

3.6.1 Shiny app

The shiny app can be found here. Figure 3.9 shows the home page. It consists of four tabs, covering the following:

- **Drug and stimulus responses** Explore drug - stimulus interactions and view log-transformed viabilities with single and combinatorial treatments (Figure 3.10).
- **Effects of mutations on drug and stimulus responses** Explore how drug and stimulus responses are modulated by genetic features and view log-transformed viability data stratified by mutations
- **Genetic predictors of drug and stimulus responses** Explore how drug and

Figure 3.8: Summary of the genetic characteristics of the patient samples in the screen. Annotations: Grey shows when patient sample is not annotated. Black indicates treated / IGHV-M, Green indicates occurrence of CNV, Yellow indicates gene is Mutated.

stimulus responses are modulated by genetic features with predictor profiles from section 5.1.2

- **Genetic predictors of drug and stimulus interactions** Explore how drug - stimulus interactions are further modulated by mutations, and view predictor profiles from section 6.3.2

To generate the app, I first curated the individual datasets and ran each of the individual analyses required to generate the plots outline above. I then set up the four tab structure, and adapted the code required to generate plots in a dynamic manner. Finally, I worked on the aesthetics and interface of the app, to ensure that it was both professional and understandable. I then tested the app with number of colleagues, to ensure it was accessible and understandable by a range of users both familiar and unfamiliar with the project. I maintain the app on the university server.

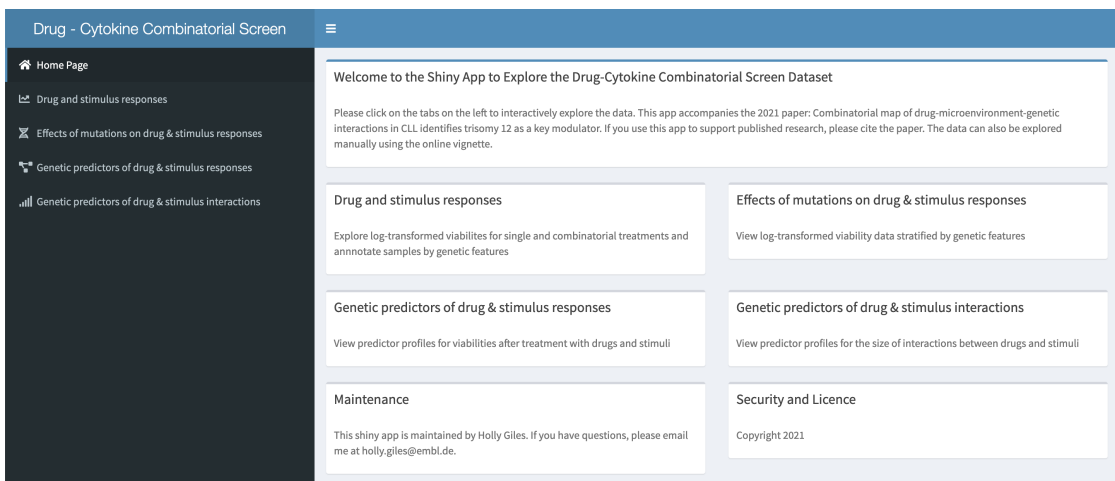


Figure 3.9: Home page of the shiny app accompanying this project. The app was published alongside Bruch and Giles et al. 2021.

3.6.2 Online code repository

The online repository can be found [here](#). The repository consists of the data and executable transcripts to completely reproduce the analysis described in Bruch and Giles et al. 2021 (Figure 3.11).

To generate the repository, I first curated each of the individual datasets, including various objects containing the screening data, patient genetic meta data, ATACseq processed data, RNAseq counts, clinical data include LDT, TTT and OS data, plus the follow up data including lymph node IHV experiments, shRNA knockdown experiments, and additional stimulation and inhibition assays. As many of these data contain sensitive information on patients, I anonymised each object by updating the patient IDs and removing potential identifying features such as age.

I next arranged the analysis into seven separate scripts, one for each figure, such that all individual sections can be rendered into a single html vignette outlining the entire analysis. I ensured that the code in each script was well-annotated and relatively simple to understand and to follow. I shared the code with several colleagues to receive feedback on coding style, and ensured that the analysis could be reproduced by others, and on different operating systems. I published the repository with the along with the preprint (Bruch and Giles et al. 2021).

These online resources are already beginning to serve as a community resource (e.g. J. Lu et al. (2021), *Nature Cancer*), as querying them enables researchers to test new

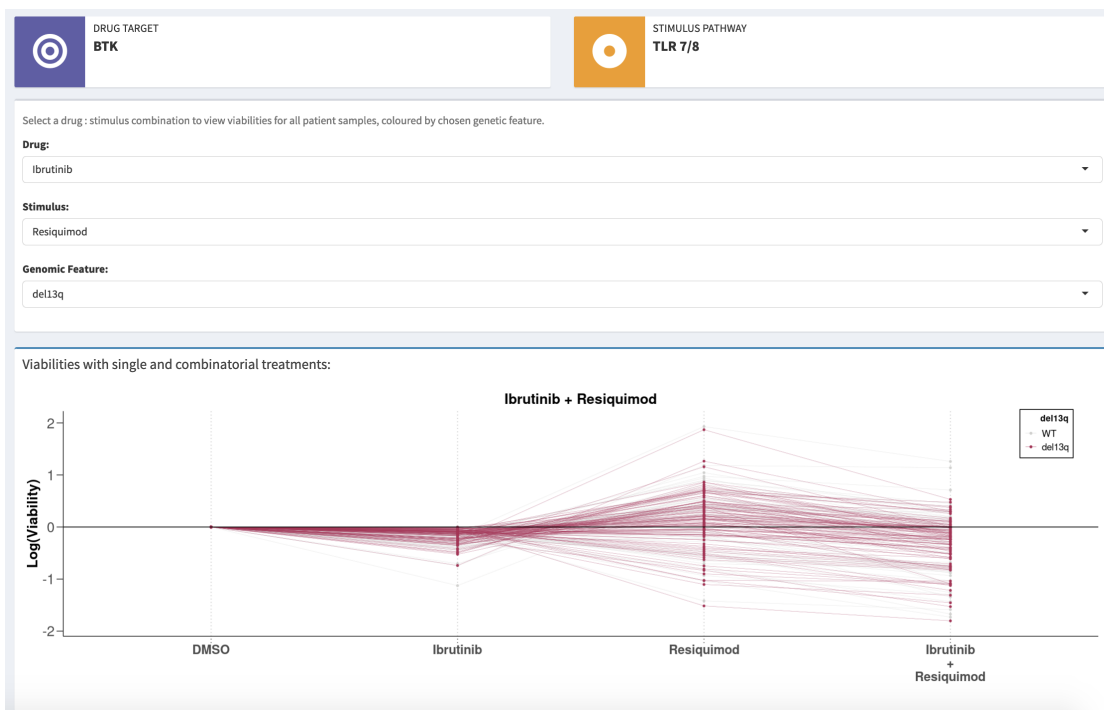


Figure 3.10: Image of one of the shiny tabs, in which the user can explore log-transformed viability values for different drug and stimulus treatments, stratified by genetic features.

hypotheses within minutes and may obviate the need for certain small-scale experiments.

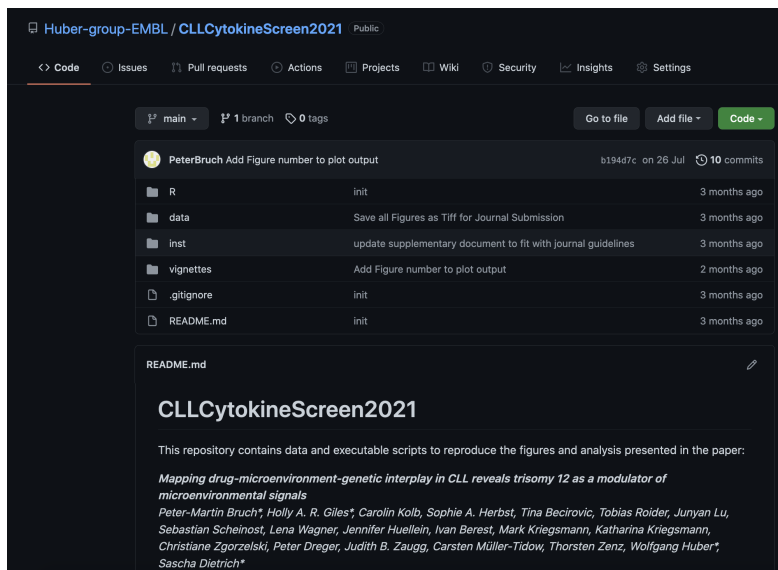


Figure 3.11: Interface of the online code repository

Chapter 4

Ex-vivo sensitivity to microenvironmental stimulation in primary CLL cells

The assay quantified the effects of 17 cytokines and microenvironmental stimuli on cell viability in 192 primary CLL samples. The 17 stimuli were selected based on evidence in the literature that each stimulus had been shown to impact on CLL viability *in vitro*, aiming to minimise redundancy between them (see also Section 3.4.1, Bruch and Giles et al. 2021). Many studies have applied various methods to model the impact of microenvironmental signalling on CLL, and each method has its strengths (see also Section 1.3.5). The assay represents a reductionist model of microenvironmental signalling, making it possible to dissect the effect of individual soluble factors within the protective niche on baseline viability.

This chapter details the analysis of the phenotypic effects of stimuli on CLL viability, leading to the identification of four patient subgroups that differ in their stimulus response profiles. This chapter also covers the clinical and molecular characterisation of these four subgroups (Bruch and Giles et al. 2021).

The results presented in this chapter centre on viability values of CLL PMBCs samples treated with our panel of stimuli. CLL cells do not proliferate *in vitro*, but rather undergo spontaneous apoptosis (Collins et al. 1989). Treatment with various stimuli, or co-culture with NLCs or BMSCs can extend survival of CLL PBMCs *ex vivo* (Collins et al. 1989; Jan A. Burger et al. 2000; Kurtova et al. 2009; Deaglio and Malavasi 2009;

Purroy et al. 2015). To measure the individual phenotypes generated by each of our stimuli, viability was quantified by comparing ATP counts in treated samples, with those in DMSO wells, after 48 hours. A positive viability value indicates that the sample viability was increased relative to control. Values shown have additionally been log-transformed.

Some findings and figures outlines in this chapter have been published in Bruch and Giles et al. 2021, and this is clearly stated where this is the case.

4.1 Proliferating responses to the panel of stimuli

4.1.1 *ex vivo* assay demonstrates functional diversity of cytokines and microenvironmental stimuli

To begin the analysis, I started by investigating heterogeneity amongst responses to the stimuli. I calculated Pearson correlation coefficients for each stimulus pair, using the log-transformed normalised viabilities. The resulting coefficients were ordered using hierarchical clustering and visualised in a symmetrical heatmap (Figure 4.1, Bruch and Giles et al. 2021).

In the resulting heatmap, several clusters of stimuli could be identified, including a larger group corresponding to agonists of TLR and Nf κ B pathways (CpG ODN, Resiquimod, BAFF, sCD40L, IL-1/ β , soluble anti-IgM) and a smaller group encompassing IL4 and TLR stimuli (IL4, sCD40L + IL4, CpG ODN and Resiquimod).

However, whilst certain stimuli clustered into groups, very few stimulus pairs showed any significant correlation. Almost all stimulus pairs showed little correlation ($R < 0.6$), including those that targeted similar downstream pathways, indicating a high degree of functional diversity amongst soluble factors in the CLL microenvironment. For example, JAK-STAT agonists such as IL4 and IL6 showed little correlation (Figure 4.2A).

Only two stimulus pairs showed correlations where $R > 0.6$, and in both cases these targeted near identical receptors or downstream pathways. These included CpG ODN (CpG oligodeoxynucleotides, TLR 9) and Resiquimod (TLR 7 and 8) (Figure 4.2B), and IL4 and IL4 + CD40L which primarily target JAK3 - STAT6 (Bruch and Giles et al. 2021).

Having observed that microenvironmental stimulation induced diverse phenotypes between patient samples, I next aimed to visualise a global overview of these phenotypes.

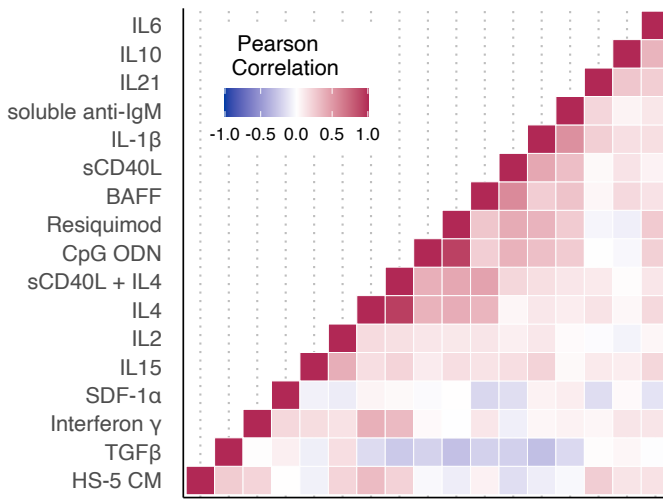


Figure 4.1: Heatmap of Pearson correlation coefficients of each pair of stimuli, based on log transformed viability values. See Methods section 2.4.1. *Figure adapted from original generated with Peter-Martin Bruch for the manuscript Bruch and Giles et al. 2021.*

I plotted log-transformed viability values normalised to DMSO controls for all patient samples and all stimuli (Figure 4.3, Bruch and Giles et al. 2021).

Figure 4.3 shows that the majority of the stimuli increased viability, underlining the supportive nature of the microenvironment in CLL. However, four out of 17 reduced CLL viability relative to control, namely IL6, TGF β and TLR 7/8/9 agonists CpG ODN and Resiquimod in some IGHV-mutated (IGHV-M) samples (Bruch and Giles et al. 2021).

IL4 and TLR7/8/9 agonists Resiquimod and CpG ODN induced the strongest responses, an indication of their potency in modulating CLL cell survival. Notably, TLR agonists increased viability in certain samples, in most cases IGHV-U, and decreased viability in others, mostly IGHV-M. The assay identified IL4 and TLR7/8/9 as key players in CLL-microenvironment cross-talk, and thus remain central throughout the results of this thesis.

4.1.2 Microenvironmental response profiling identifies discrete patient subgroups

To further investigate the variability in responses across the cohort, we next generated a heatmap of all stimuli responses across all samples, using z-scores for optimal visualisation. We performed consensus clustering on the resulting heatmap to group patients

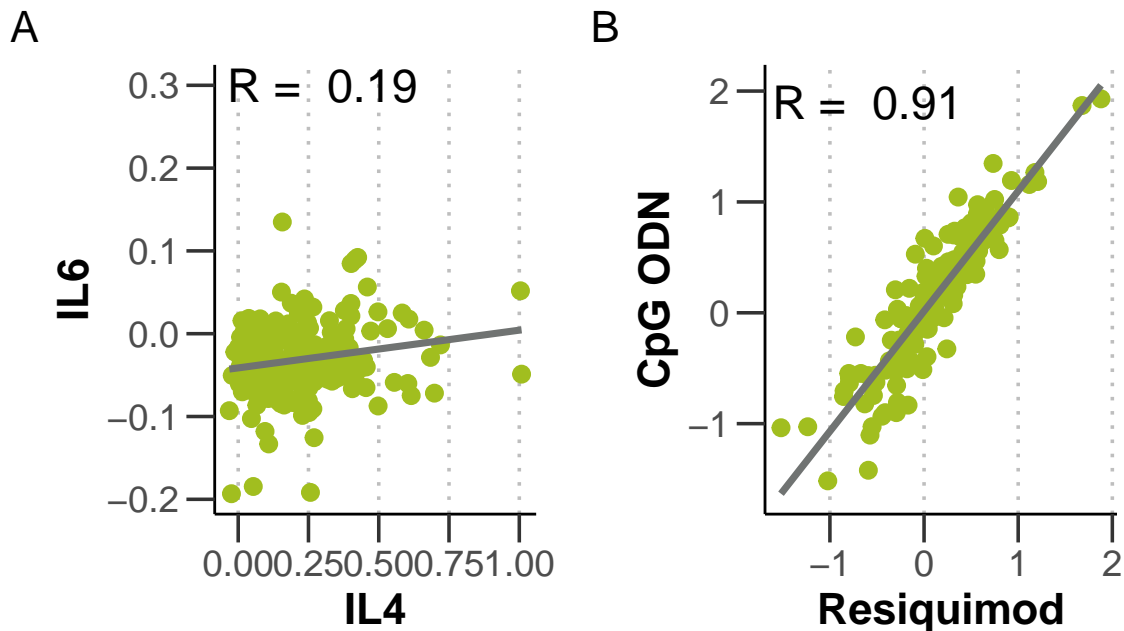


Figure 4.2: Scatter plot of log-transformed viability values, normalised to DMSO controls, for (A) treatment with JAK-STAT agonists IL4 and IL6 and (B) treatment with TLR agonists CpG ODN (TLR9) and Resiquimod (TLR7/8).

according to their response profiles (Figure 4.4, Bruch and Giles et al. 2021).

The consensus clustering method generates robust hierarchical clustering by subsampling from the matrix of values (in this case, the viability z-scores). Using subsampling, it is possible to calculate a “consensus matrix” which indicates the proportion of times each pair of values occupy the same cluster when subsampled together. This is repeated for different numbers of clusters, denoted by k , allowing the user to select the optimal number of clusters for a given dataset.

We ran consensus clustering on the matrix of z-scores for different values of k , and arranged the corresponding heatmaps accordingly. Figure 4.4 shows the arrangement for $k = 4$. Comparing the heatmaps, I concluded on the existence of four robust clusters within the cohort. Each cluster shows a unique response profile to the panel of stimuli.

To support the choice of four clusters, I additionally visualised summaries of the consensus matrices for each value of k , to quantify the degree of confidence in the clusters for each k (Figure 4.5).

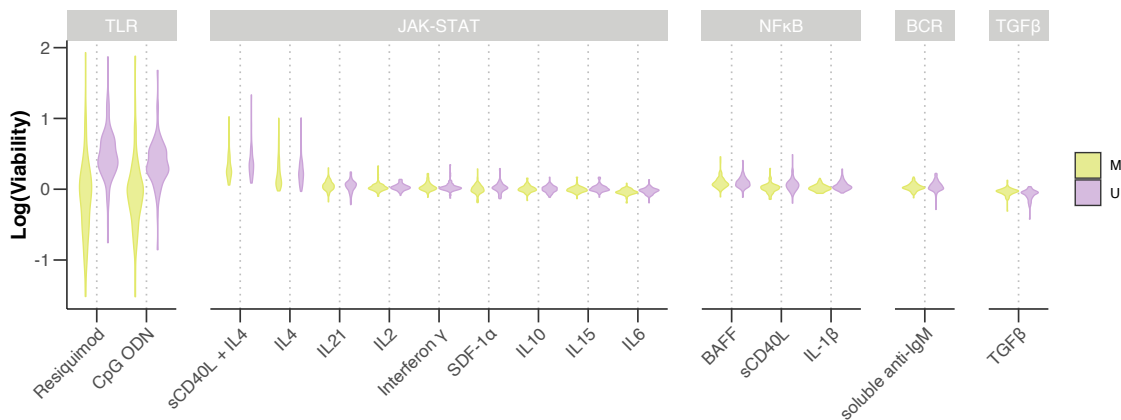


Figure 4.3: Log transformed viabilities after treatment with each stimulus. Stimuli are grouped by corresponding pathway, and responses are stratified by IGHV status. *Figure adapted from Bruch and Giles et al. 2021 .*

The graph of the Cumulative Distribution Functions (CDFs) of the consensus matrix for each k indicated that the CDF reaches a maximum and cluster confidence is maximised at $k = 7$, though above $k = 4$ there is little appreciable increase (Figure 4.5). This is confirmed in the graph showing relative change in the area under the CDF curve, showing there is only a small increase in consensus between $k = 4$ and $k = 5$, supporting the choice of $k = 4$. The cluster tracking plot depicts how each patient sample is assigned for each value of k . For $k = 4$, the plot indicates that C3 and 4 in particular are highly stable (Figure 4.6).

4.2 Functional characterisation of patient clusters

4.2.1 C1 - C4 show distinct response profiles with the panel of stimuli

Consensus clustering identified four patient subgroups, which each responded differently to the panel of stimuli (Bruch and Giles et al. 2021). This raised the possibility that responses to microenvironmental stimulation are linked to cell-intrinsic features, and could be prognostic. Thus, we next aimed to characterise the phenotypic and molecular differences between these four clusters.

I began by investigating the differences between the response profiles of each cluster. I refer to the four clusters as C1 to C4: C1 and C2 were enriched for IGHV-U whilst the samples in C3 and C4 were mostly IGHV-M. Amongst the IGHV-U enriched C1

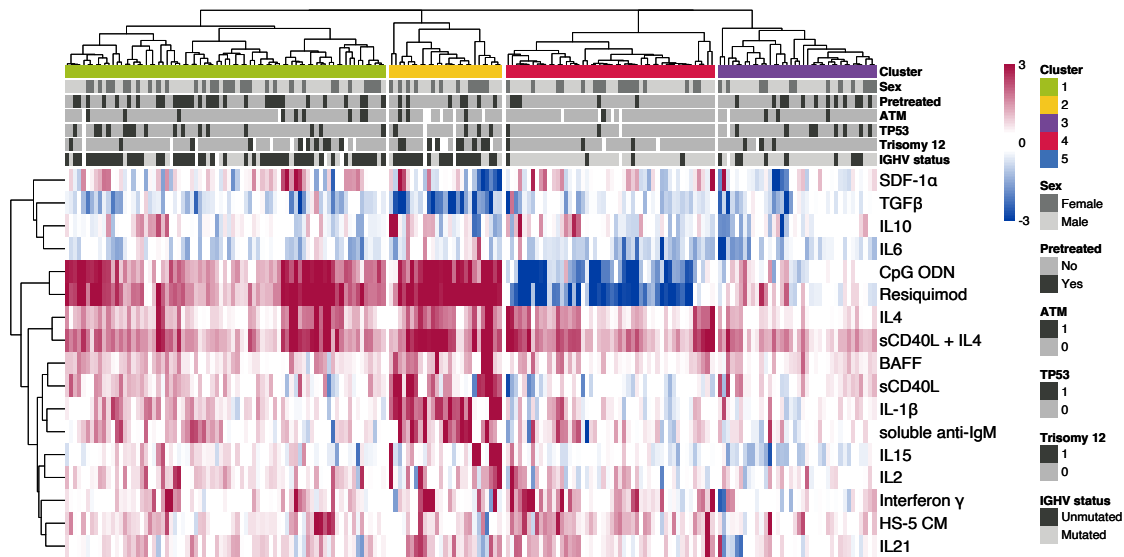


Figure 4.4: The heatmap matrix shows viability measurements for 192 samples (columns) and 17 stimuli (rows). The data are shown z-scores of log-transformed, control-normalised viability values. The colour bars to the right show sample annotations. Consensus clustering was used to define column tree layout, using hierarchical clustering with the Euclidean metric. See Methods section 2.4.1. *Figure generated with Peter-Martin Bruch for the manuscript Bruch and Giles et al. 2021.*

and C2, both showed strong, positive responses to IL4 and TLR7/8/9 stimulation. C2 could be distinguished by stronger responses to the stimuli overall, in particular to NF κ B agonists IL1 β , anti-IgM, BAFF and sCD40L. Amongst the IGHV-M enriched clusters, C3 showed weaker responses to the majority of stimuli, and C4 was defined by a negative response to TLR7/8/9 stimulation (Bruch & Giles et al. 2021). Figure 4.7 summarises these findings in more detail, showing responses stratified by cluster for a subset of the stimuli.

4.2.2 The clusters show differences in disease dynamics

To validate the potential biological significance of these four clusters, we investigated whether the groups showed differential *in vivo* disease progression (Bruch & Giles et al. 2021). Lymphocyte doubling time (LDT)¹ and time to next treatment (TTT)² were

¹ LDT represents rate at which malignant B cells accumulate, and is an independent biomarker that correlates with overall survival (OS) (Baumann et al. 2021).

² TTT reflects time between initiation of one therapy and start of next (Campbell et al. 2020; Delgado and Guddati 2021), accounting for treatment period plus period in which disease / symptoms are controlled.

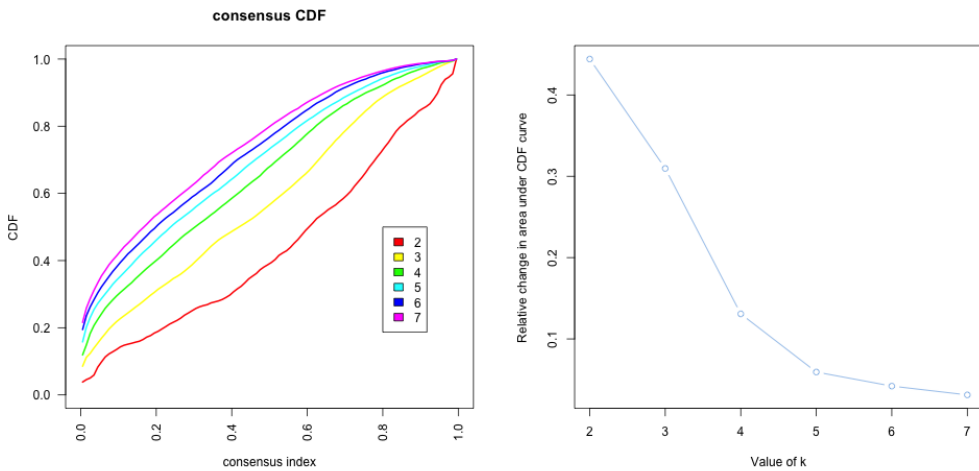


Figure 4.5: (left) CDFs of the consensus matrices for $k = 2 - 7$, as indicated in the legend, estimated using 100 bin histogram. (right) Relative change in area under the CDF curve, for $k = 2 - 7$, to compare k with $k - 1$. In the case of $k = 2$, there is no $k - 1$, so the total area is plotted. Line shows relative increase in consensus between each value of k . See Methods section 2.4.1.

used to quantify CLL proliferative capacity.

C1 and C2 showed a shorter LDT than C3 and C4, which is expected due to the differential proportions of IGHV-U and M patient samples in these groups (Figure 4.8A). Notably, within the IGHV-M enriched clusters C3 and C4, samples in C3 showed a significantly shorter LDT (Student's t-test, p-value = 0.025, Bruch and Giles et al. 2021).

To further validate this, we observed that TTT in the IGHV-M enriched C3 was significantly shorter than C4 (Cox proportional hazards model p value = 0.005) and comparable to the progression dynamics of IGHV-U enriched C1 and 2 (Figure 4.8B, Bruch and Giles et al. 2021).

The difference in disease progression between the clusters indicated that microenvironmental response represents an additional biological layer, holding information relevant to disease dynamics. To validate that these clusters were not simply an indication of any underlying genetic features, we checked whether the observed differences in progression dynamics could be explained by other prognostic markers (Bruch and Giles et al. 2021).

A multivariate Cox proportional hazard model accounting for IGHV status, trisomy 12 and TP53 in addition to the cluster assignment indicated an independent prognostic

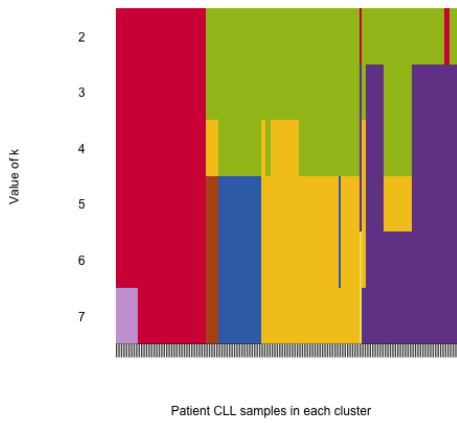


Figure 4.6: Assignment of patient samples (columns), to each cluster, for $k = 1 - 7$ (rows) to demonstrate stability of cluster membership. Cluster colour for $k = 4$ match those in heatmap in 4.4. See Methods section 2.4.1.

value for cluster assignment between C3 and C4 ($p = 0.039$, Table 4.1).

Table 4.1: Table depicting results of multivariate Cox proportional hazard model to test prognostic value of key genetic features and clusters using TTT and C3 as reference. HR indicates Hazard Ratio, CI low and CI high indicate 95 percent confidence intervals. Analysis performed with Peter-Martin Bruch and published in Bruch and Giles et al. 2021.

Factor	HR	p value	CI Low	CI High
Cluster 3 vs Cluster 1	0.96	0.89	0.54	1.72
Cluster 3 vs Cluster 2	1.68	0.17	0.80	3.51
Cluster 3 vs Cluster 4	0.44	0.04	0.20	0.96
IGHV.status	1.74	0.04	1.02	2.96
trisomy 12	0.87	0.71	0.44	1.76
TP53	4.01	<0.0001	2.41	6.69

4.2.3 The clusters show differential responses to drugs *in vitro*

The combinatorial nature of the screen made it possible to investigate drug responses, as well as stimulus responses, for matching samples. The potential clinical relevance of the clusters was underlined by my observation that the samples within each group showed differential responses to drugs *in vitro* (Figure 4.9).

As expected, the IGHV-U enriched clusters C1 and 2 were more sensitive to BCR

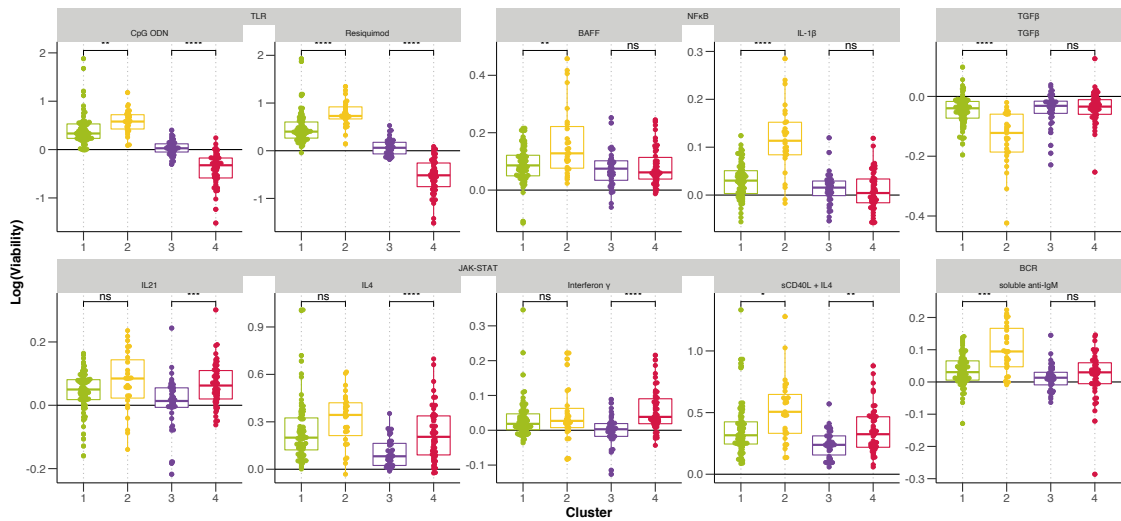


Figure 4.7: Log-transformed normalised viability values stratified by cluster, for each stimulus. Stimuli activating the same pathway are grouped together. P-values from Student's t-test. *Figure adapted from Bruch and Giles et al. 2021.*

inhibition by ibrutinib, idelalisib and PRT062607, than C3 and 4. Between C1 and C2, C2 was more sensitive to a number of the drugs, including idelalisib (SYK) ($p = 0.012$), everolimus (mTOR) ($p = 0.02$) and the chemotherapeutics fludarabine ($p = 0.031$) and nutlin-3a ($p = 0.042$). Amongst C3 and C4, C3 showed lower sensitivity to everolimus ($p = 0.051$) and to fludarabine ($p < 0.001$) and nutlin-3a ($p = 0.01$). This aligns with the observation that patients in C3 have a poorer prognosis, despite the fact most of these samples were annotated as IGHV-M. C4 also showed a positive response to Nf κ B inhibition by BAY-11-7085, and p38 MAPK inhibition by ralimetinib.

Such differential drug response patterns suggests that microenvironmental response may reflect disease-specific CLL biology.

4.2.4 The clusters are enriched for different genetic features

Next I assessed differences in the molecular profiles of samples within each cluster. Visually, it appeared that certain clusters were enriched or depleted for various genetic features recurrent in CLL (Figure 4.10).

To quantify whether each cluster was enriched or depleted for certain genetic features, I used a multinomial modelling approach, with lasso penalisation (for more background on generalised linear models, see section 1.5.3 (Bruch and Giles et al. 2021)).

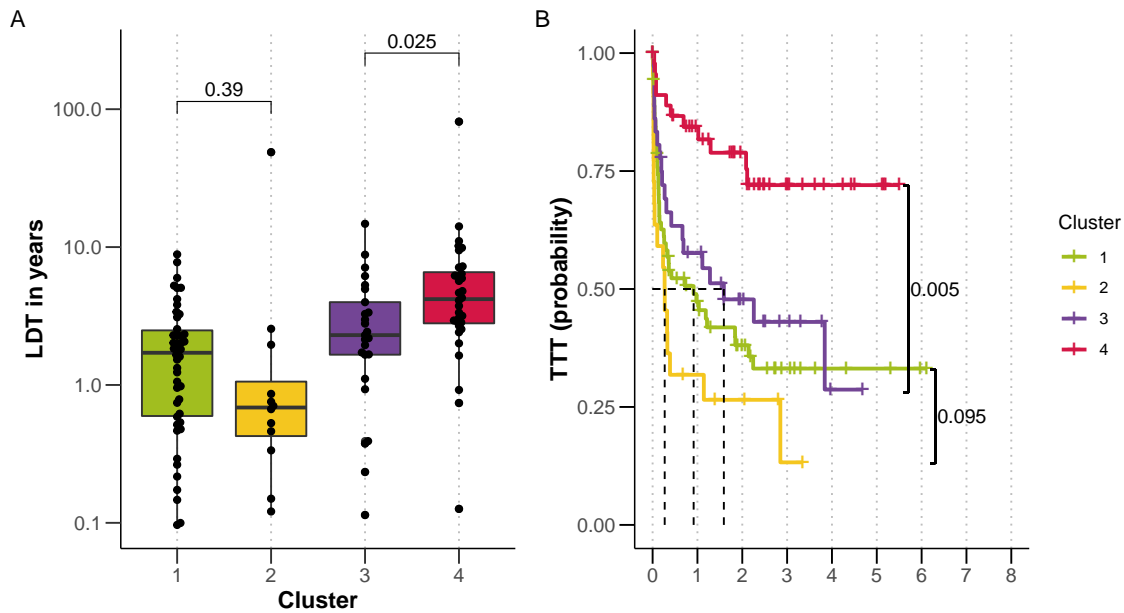


Figure 4.8: (A) LDT stratified by cluster, p-values from Student's t-test. (B) Kaplan-Meier curves to show TTT for each cluster. p-values from univariate Cox proportional hazard models comparing IGHV-U enriched C1 with C2, and IGHV-M enriched C3 with C4. See Methods sections 2.4.2 and 2.4.2. *Figure generated with Peter-Martin Bruch for the manuscript Bruch and Giles et al. 2021 .*

I ran the multinomial model to assign coefficients to genetic features that were associated with each cluster, C1 to C4. Running the regression with lasso regularisation meant that the majority of the coefficients were shrunk towards 0. Genetic features that were assigned a coefficient were thus assumed to be either enriched or depleted within a cluster.

To run the model, I generated a feature matrix, consisting of the genetic data for patient samples and a discrete response matrix, which included the cluster assigned to each patient. Genetic features with >20% missing values were excluded ($n = 39$), and only patients with complete annotation were included in the feature matrix ($n = 137$). I used the function `cv.glmnet` from the R package `glmnet` (Friedman et al. 2021) to generate the model, using 3-fold cross validation, and selecting the optimal model using λ_{min} .

Each cluster was thus assigned a set of genetic coefficients. To ensure that these were robust, I applied certain cut-offs. I ran 50 bootstrapped repeats, and removed features if they were not selected in at least 60% of cases. Additionally, coefficients <0.35 were

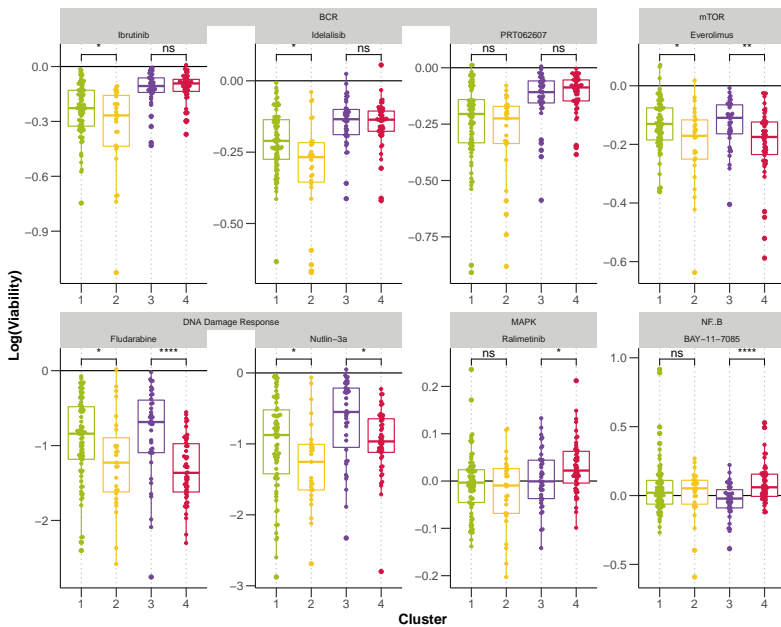


Figure 4.9: Log-transformed normalised viability values, stratified by cluster, for each drug. Drugs targeting the same pathway are grouped together. P-values from Student's t-test.

eliminated.

Figure 4.11 shows the resulting mean coefficients. A positive coefficient indicated that this feature was enriched in the cluster, and a negative coefficient indicated it was depleted. The associated standard deviations are also indicated.

As expected, IGHV status was the main feature that predicted cluster membership. Beyond IGHV status, trisomy 12 and *SF3B1* mutations were enriched in C2, which showed enhanced responses to many stimuli. C4, which was associated with slow in-vivo progression, showed depletion of *TP53*, *ATM*, mutations in *RAS* and *RAF* and gain(8q) (Bruch and Giles et al. 2021).

4.2.5 GSEA of DE genes between subgroups

In addition to genetic features, I investigated differential expression of genes within each cluster. For n = 49 samples, RNAseq data was available for matched PBMC samples. I focused on the difference between C3 and C4, for which 21 RNAseq samples were available (Bruch and Giles et al. 2021). C3 and C4 were of most interest, as they distinguished between two sets of mostly IGHV-M cases that showed distinct disease

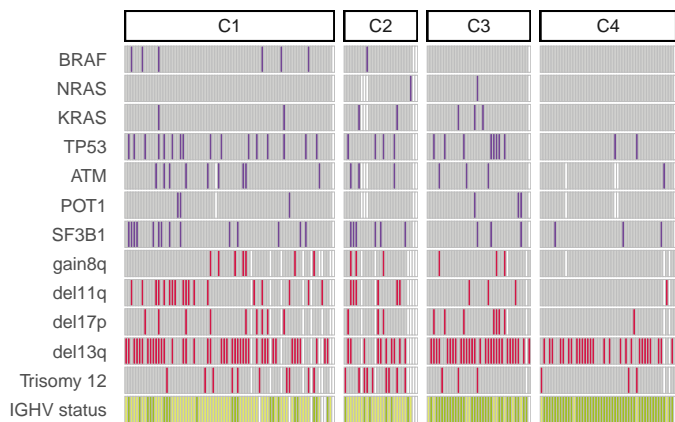


Figure 4.10: Distribution of selected genetic features (rows) within each cluster for all patient samples (columns). White indicates patient sample is not annotated.

dynamics.

To quantify differential gene expression, I began by filtering out immunoglobulin genes, including genes at the heavy, light and kappa loci that encode the antigen receptor of B cells. The clusters each show differential enrichment of IGHV-M and U samples, and thus the differential expression analysis would otherwise be dominated by immunoglobulin genes that are affected by this biomarker.

I followed the DESeq2 protocol (Love, Anders, and Huber 2021) using a design formula to quantify the difference between clusters, and accounting for the confounding effect of IGHV status. 87 genes were differentially expressed (adjusted $p < 0.05$) between C3 and 4 (Figure 4.12).

To assign biological meaning to the differentially expressed genes, I quantified the enrichment of Hallmark pathways amongst the genes. I ranked the genes based on the Wald statistic, and then ran GSEA using the fgsea algorithm (Figure 4.13) (Bruch and Giles et al. 2021).

Several pathways were upregulated amongst samples in C3, compared to C4, indicating that these pathways may relate to the shorter TTT and LDT of patients within this cluster. Pathways associated with higher disease aggression were regulated in C3 including genesets relating to stress response (Unfolded Protein Response, UV Response Up, P53 Pathway), metabolism (Oxidative Phosphorylation) and proliferation (G2M Checkpoint, MYC Targets V1, MTORC1 Signaling, E2F Targets) (Figure 4.14).

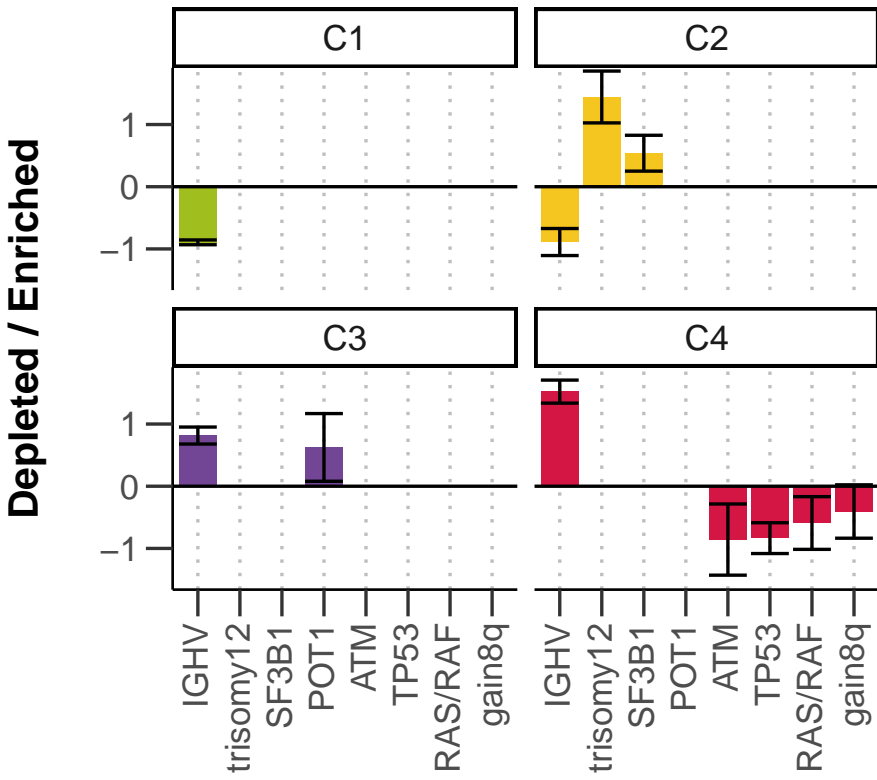


Figure 4.11: Enrichment and depletion of genetic features within each cluster, quantified using lasso-penalised regression. x axis shows genetic features, y axis indicates value and sign of coefficient assigned to feature, for each cluster (positive coefficients are enriched in the cluster, negative coefficients are depleted). Coefficients shown are mean coefficients from 50 bootstrapped repeats and error bars represent the mean plus and minus standard deviation. See Methods section 2.4.2. *Figure from Bruch and Giles et al. 2021.*

In addition, C3 showed upregulation of microenvironmental signalling pathways relative to C4, including TNFa Signalling via NFKB and Interferon Gamma Response (Figure 4.14) (Bruch and Giles et al. 2021). This finding underlines our hypothesis that differential activity of microenvironmental signalling, both *in vivo* and *ex vivo* may be relevant to disease prognosis (Bruch and Giles et al. 2021).

4.3 Summary

The screen enabled a systematic study of the impact of individual microenvironmental pathways on CLL viability. The assay highlighted potent pro-survival signals that are

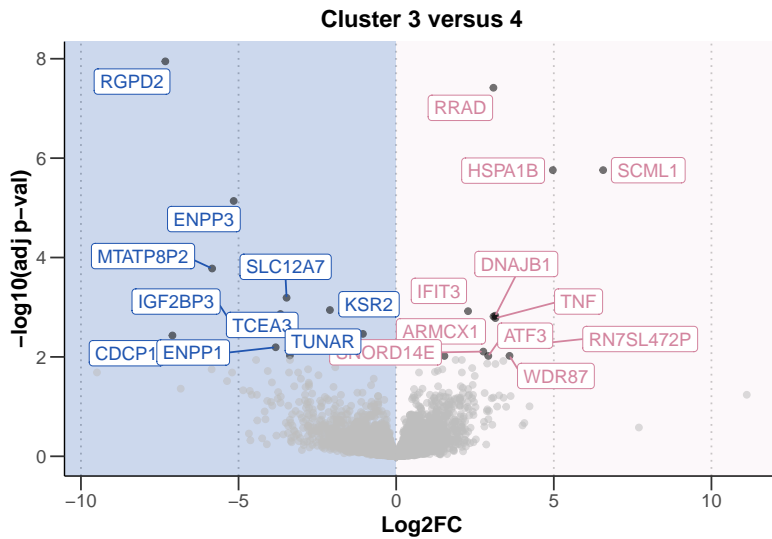


Figure 4.12: Volcano plot of differentially expressed genes between C3 and C4. x axis indicates log₂ fold change values, calculated using the DESeq2 package (Love, Anders, and Huber 2021), y axis gives corresponding -log₁₀(BH-adjusted p value). Darker grey points are labelled where adjusted p < 0.01. See Methods section 2.4.2. *Figure from Bruch and Giles et al. 2021.*

active across heterogeneous genetic backgrounds, such as IL4, and others that operate in subsets of patients, such as TLR. IL4 and TLR represent the key pathways that we focus on throughout the rest of this thesis.

In addition, this screen demonstrates the ability of microenvironmental response profiling, to distinguish disease subgroups. The assay revealed four subgroups with distinct response profiles and molecular properties and clinical outcomes, suggesting that microenvironmental response holds biologically significant information that may be relevant to prognosis and treatment decision making.

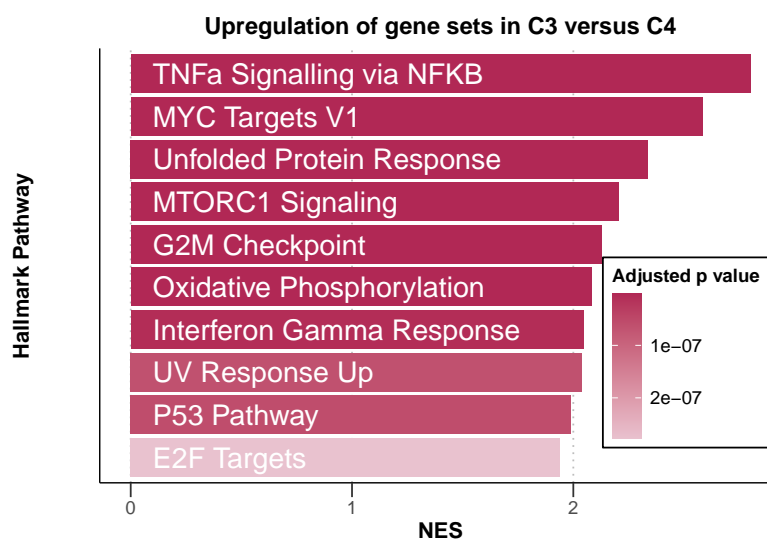


Figure 4.13: Bar plot showing gene set enrichment to compare gene expression of samples in C3 and C4. Normalised enrichment scores (NES) are shown for top ten pathways with smallest adjusted p-value. Gene ranking performed based on Wald statistic, calculated using the DESeq2 package. See Methods section 2.4.2. *Figure from Bruch and Giles et al. 2021.*

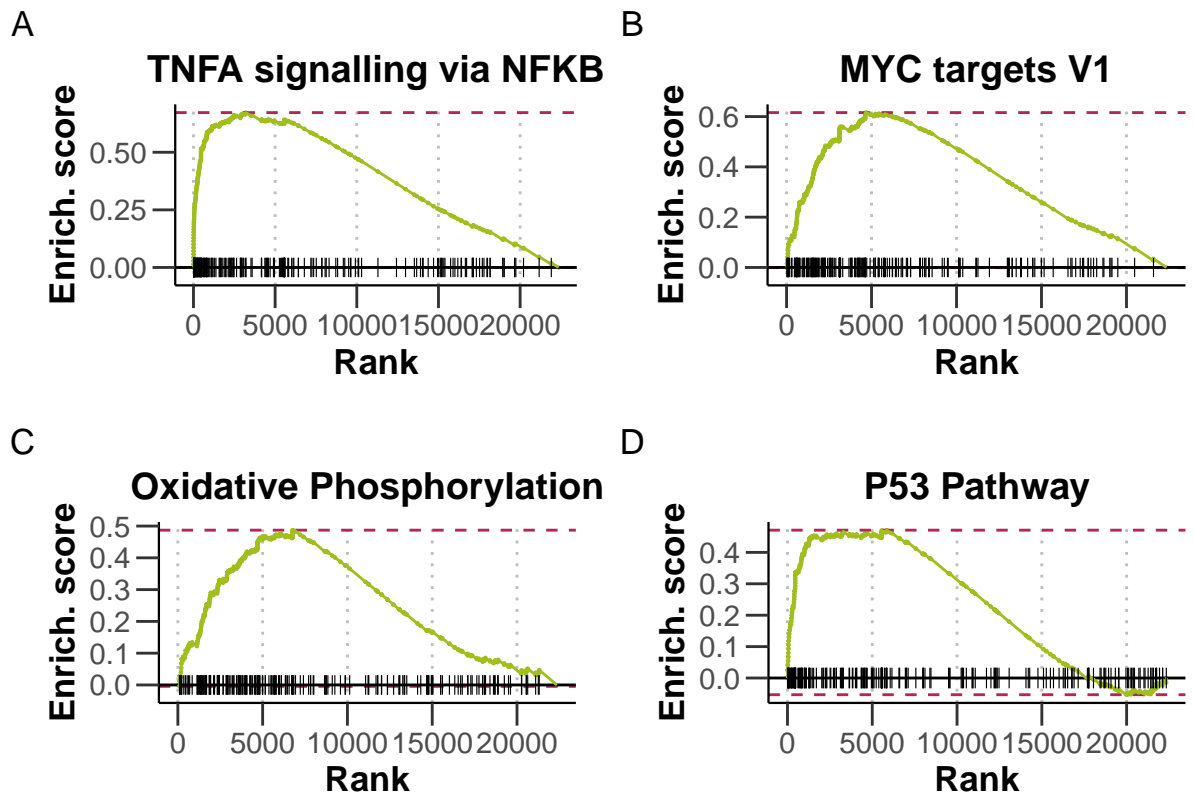


Figure 4.14: Enrichment plot of selected pathways. Gene set enrichment analysis (GSEA) was performed with the Hallmark gene sets from the GSEA Molecular Signatures Database. Wald statistic was used to rank the genes. The green curve corresponds to the Enrichment Score curve, which is the running sum of the weighted enrichment score obtained from GSEA software. See Methods section 2.4.2. *Figure and caption from Bruch and Giles et al. 2021.*

Chapter 5

Genetic modulators of responses to microenvironmental stimulation

Profiling the effects of microenvironmental stimulation of CLL samples revealed the heterogenous nature of responses to external signals. Next I asked to what extent this heterogeneity relates to the molecular profiles of the tumours. I sought to understand which underlying genetic features might modulate responses to external signals, and how these interactions may occur. I combined the screening dataset with multi-omics profiles of the patient samples taken from the PACE repository (Dietrich et al. 2017; Oles et al. 2021) and performed a systematic survey of molecular determinants of stimulus response, using whole-exome sequencing, DNA-methylation, RNA-sequencing and copy number variant data. In addition, ATAC sequencing and Mass Spectrometry data was available for a small subset of patients.

Collectively, these data facilitated an investigation into genetic and epigenetic modulators of microenvironmental signalling, in a heterogeneous cohort that encompasses the clinical and molecular diversity of CLL. In the first part of this chapter, I apply a broad systematic approach to identify important genetic modulators, and in the second, I outline my follow-up investigations into the impact of trisomy 12 on stimulus response.

Some findings and figures outlines in this chapter have been published in Bruch and Giles et al. 2021, and this is clearly stated where this is the case.

5.1 Systematic analysis of the effect of genetic features on responses to stimuli

5.1.1 Univariate analysis identifies IGHV status and trisomy 12 as key modulators of microenvironmental response

To begin, I ran a univariate analysis to compare viability values post-stimulation for patient samples with and without each genetic feature. In total 54 genetic features were surveyed, including IGHV status, somatic gene mutations and structural variants, where there were at least three patient samples in each group (Figure 5.1).

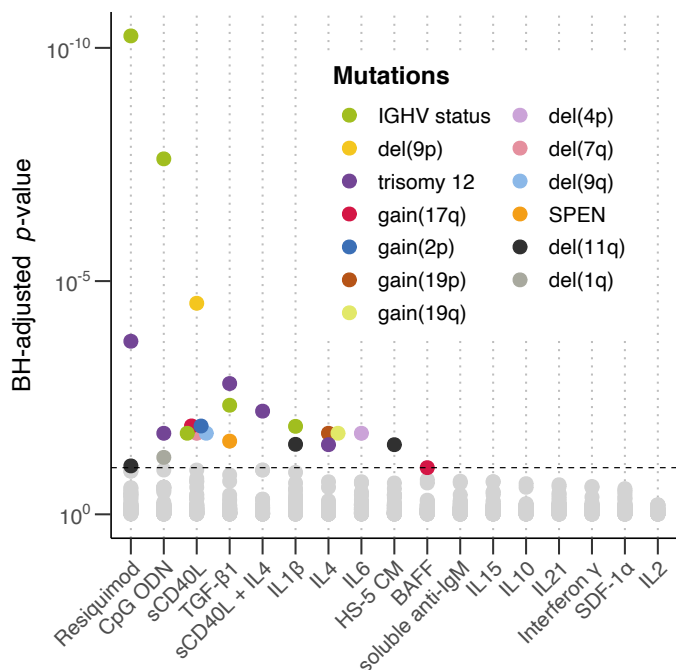


Figure 5.1: Plot showing BH-adjusted p values from Student's t-tests (two-sided, with equal variance), for all tested gene-stimulus associations. Each circle represents a gene-stimulus association. Associations that meet 10% FDR cut off are indicated in colour, where the colour denotes the genetic feature. See Methods section 2.4.1. *Figure generated with Peter-Martin Bruch for the manuscript Bruch & Giles et al. 2021, and caption adapted from manuscript.*

This analysis revealed the extent to which genetic features modulate microenvironmental response: for 10/17 stimuli, at least one genetic feature determined response and for 6/17 stimuli, two or more genetic features significantly altered the response (Student's t-tests, FDR = 10%, Bruch & Giles et al. 2021). The most common features were IGHV

status and trisomy 12. Del(11q) also affected response to several stimuli. Notably, del(13q) and del(17p), which like trisomy 12 and del(11q) are the most common aberrations in CLL and act as prognostic markers (H. Döhner et al. 2000), had no impact on the responses to the panel of stimuli.

5.1.2 Multivariate analysis of gene - stimulus associations confirms IGHV status and trisomy 12 as key modulators of stimulus response

It was possible that there may be interplay between genetic factors in determining responses to external signals. To address this, I applied multivariate modelling to integrate the influence of genetic features, IGHV status and DNA methylation on the size of response (Bruch & Giles et al. 2021). I used a Gaussian linear model with L1-penalty (i.e., lasso regression), to derive a predictor for each stimulus, comprised of these covariates. For background on this approach, see section 1.5.3.

As input to the model, the response matrix was composed of the log transformed viability values for each stimulus. To generate the feature matrix (137 samples versus 41 features), I excluded genetic features for which >20% of the values were missing, and patient samples with incomplete annotation. As predictors, I included genetic mutations and CNVs ($p=39$), IGHV status and Methylation Cluster. I ran lasso regression, as implemented in the R package `glmnet`(Friedman et al. 2021) and the resulting predictors are the mean of those coefficients that were selected in at least 75% of 30 bootstrapped repeats.

Using the output of the regression, I generated predictor profiles for each stimulus. For 5/17 stimuli, there was at least one genetic predictor that met the cut-offs (a selection are shown in Figure 5.2).

The multivariate analysis demonstrated that responses to IL4 and sCD40L + IL4, TLR stimuli and $TGF\beta$ were all affected by multiple genetic features (Bruch & Giles et al. 2021). For example, higher viability in response to IL4 stimulation was associated with trisomy 12 and unmutated IGHV. In contrast, IL4 generated little or no increase in viability in samples with a mutation in *KRAS*, *NRAS* or *BRAF*. These tumours benefited less from the anti-apoptotic effects of IL4, indicating that signalling via Ras-Raf-MEK-ERK may have an inhibitory effect of the pro-survival effects of IL4. To validate this, I visualised data from the screen for IL4 and IL4 + Ralimetinib (a p38 MAPK inhibitor) treated samples. Inhibition of signalling via Ras-Raf-MEK-ERK increased the pro-survival effect of IL4 (paired t-test, $p < 0.0001$, Figure @ref(fig:ral_il4)) [CHECK].

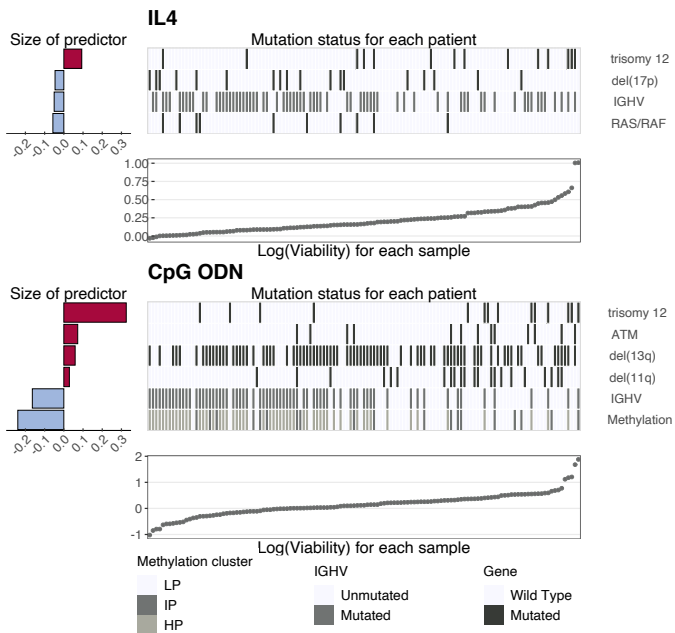


Figure 5.2: Predictor profiles for IL4 and CpG ODN (TLR9) depicting gene - stimulus associations. Bar plots (left) show size and sign of assigned coefficients from Gaussian linear modelling. A positive coefficient indicates that stimulated increase in viability is larger when genetic feature is present. Scatter plots (bottom) and corresponding heatmaps above show how presence of selected genetic feature relates to sample viabilities. Scatter plots show ranked log-transformed viability values for each sample and heatmaps show mutation status for each predictor, for corresponding sample in scatter plot. See Methods section 2.4.1. *Figure and caption adapted from Bruch & Giles et al. 2021.*

(ref:ral_il4) Beeswarm-boxplots of log-transformed control-normalised viability values for IL4 and IL4 + Ralimetinib treated samples.

5.1.3 Response to TLR stimulation is dependent on IGHV status, trisomy 12 and mutations in DNA Damage Response genes

The multivariate analysis highlighted that TLR stimulation by CpG ODN (TLR9) and Resiquimod (TLR 7/8) both showed the largest number of predictors, so I next decided to look into this in more detail. The predictors included del(11q) and *ATM*, del(17p) and *TP53*, IGHV status, trisomy 12 and *SF3B1* (Bruch & Giles et al. 2021), reflecting the multiple layers of biology involved here. Further, the survival differences between the clusters identified in section 4.2.1 indicated that TLR response may relate to disease

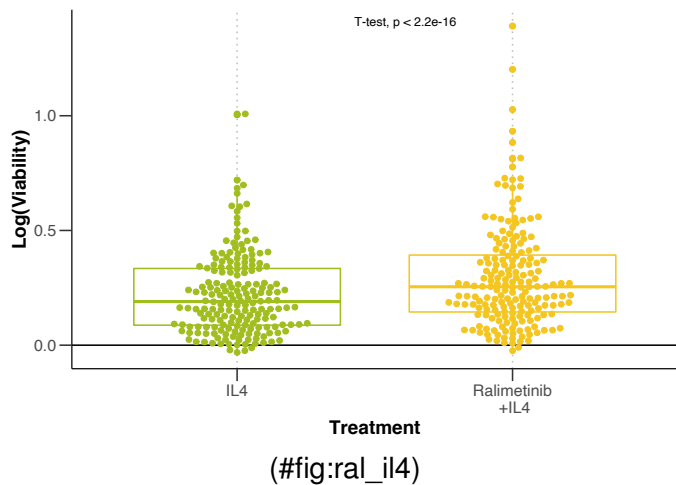


Figure 5.3: (#fig:ral_il4)

progression, thus warranting a more detailed look at the underlying features modulating TLR signalling (Figure 5.4).

The features with the strongest impact on TLR response were IGHV status and trisomy 12. Chatzouli et al. (2014) have previously shown that TLR responses is dependent on IGHV status (see also, section 1.3.3 and these results highlight trisomy 12 as an additional, novel determinant (Bruch & Giles et al. 2021). In samples without trisomy 12, TLR stimulation increases the viability of IGHV-U samples, whilst it decreases viability in IGHV-M samples, as expected. In contrast, in samples with trisomy 12, TLR stimulation increases viability regardless of IGHV status (Student's t-test, $p<0.001$ and $p = 0.018$, Figure 5.5).

Chatzouli et al. (2014)'s observations point to the existence of specific types of BCR/TLR collaboration in CLL depending on the IGHV status of the tumour, either activating pro-survival pathways, or inducing apoptosis. The results here suggest that synergy between the BCR and TLR pathways may also be modulated by trisomy 12. [CHECK]

TLR stimulation also increased viability in samples with mutations in the DNA damage response pathway, namely del(11q), del(17p), and *ATM* and *TP53* (Del(17p) is associated with loss of TP53 (Zenz et al. 2010) and Del(11q) is associated with loss of ATM (Kipps et al. 2017)). This suggests that there may also be cross-talk between the TLR and DNA damage response pathway, and that this affects the outcome of TLR stimulation. [CHECK]

The effect of TLR stimulation on CLL viability is thus dependent on the molecular make-

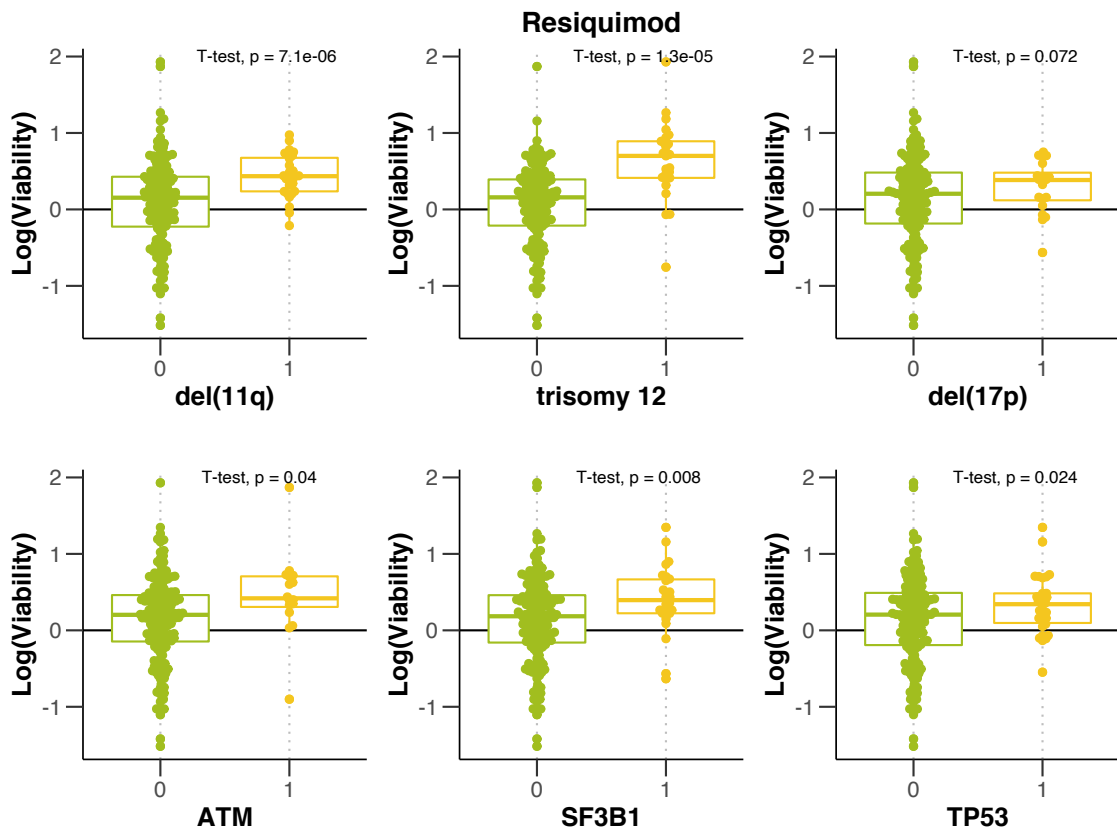


Figure 5.4: Control-normalised log transformed viability values after treatment with Resiquimod (TLR 7/8), stratified by named genetic features.

up of the tumour. The observations in section 4.2.1 also indicate that pro-survival versus pro-apoptotic responses to TLR stimulation may relate to disease progression i.e. the subgroup of patients (C3) that showed slower disease progression was the sole subgroup in which TLR stimulation induced apoptosis. BCR signalling is viewed as central to CLL pathogenesis and prognosis; the role of TLR signalling may be under appreciated. [CHECK]

Collectively, this work represents a large-scale attempt to profile the integrative effects of cell-extrinsic signals and cell-intrinsic features in lymphoma (Bruch and Giles et al. 2021). In CLL, this systematic approach highlighted trisomy 12 as the most common feature to modulate responses (Bruch and Giles et al. 2021). The rest of this chapter outlines my work to investigate the role of trisomy 12 in microenvironmental response.

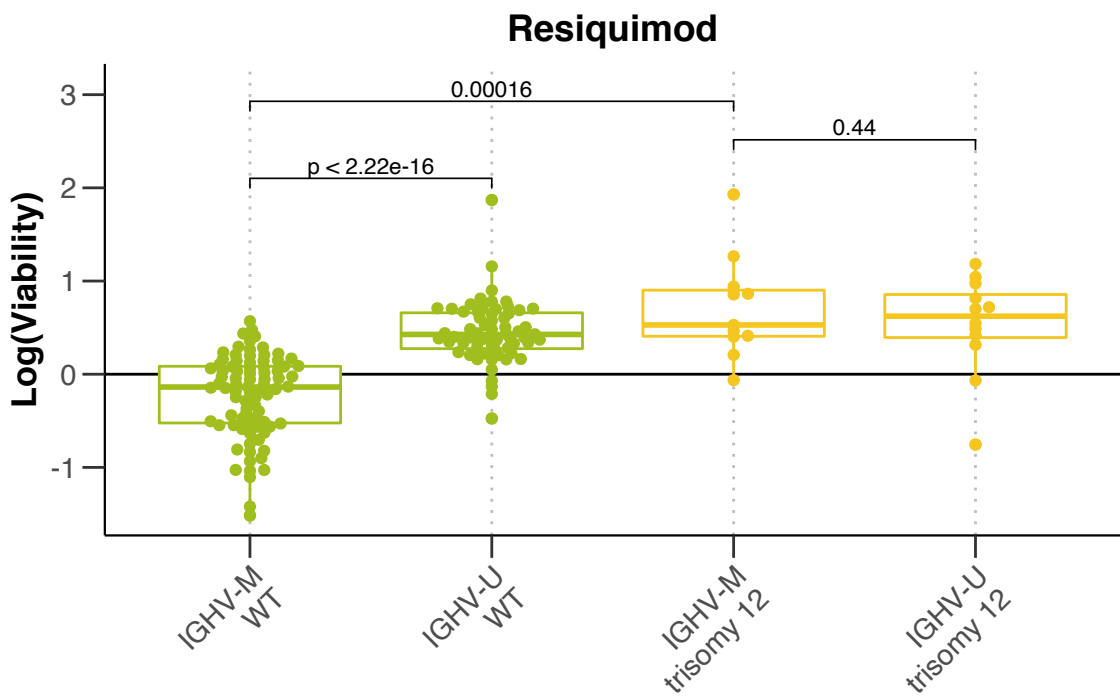


Figure 5.5: Beeswarm-boxplot showing control-normalised log transformed viability values, after treatment with Resiquimod (TLR 7/8), stratified by trisomy 12 and IGHV status. p-values from Student's t-tests. *Figure generated with Peter-Martin Bruch for the manuscript Bruch & Giles et al. 2021, and caption adapted from manuscript.*

5.2 Investigating trisomy 12 as a modulator of microenvironmental response

5.2.1 Trisomy 12 is a modulator of microenvironmental response

Trisomy 12 modulated responses to IL4, TGF β , soluble CD40L + IL4 and TLR stimuli (Bruch & Giles et al. 2021, Figure 5.6). For example, the increase in viability induced by IL4 was enhanced in trisomy 12 samples, as was the decrease in viability in response to TGF β stimulation.

Trisomy 12 is commonly mutated in CLL (15% of cases) (H. Döhner et al. 2000). Until recently, this genetic lesion was regarded as conferring intermediate risk, though novel therapies have improved outcomes for trisomy 12 cases (Bosch and Dalla-Favera 2019). However, the functional explanation for its recurrence is incompletely understood. Previous work has shown a role for gene dosage effects in the pathogenic

mechanism: Kienle et al. (2005) show that overexpression of genes including CDK4 and E2F1 leads to increased cell cycling and higher proliferative capacity. Likewise, Herbst (2020) showed that BCR signalling proteins are also upregulated, which may also contribute to the increased proliferative capacity. Correspondingly trisomy 12 cases show increased susceptibility to BCR inhibition (Dietrich et al. 2017) (see also, section 1.1.5).

In the following, I outline my work to investigate the incompletely understood role of trisomy 12 in CLL.

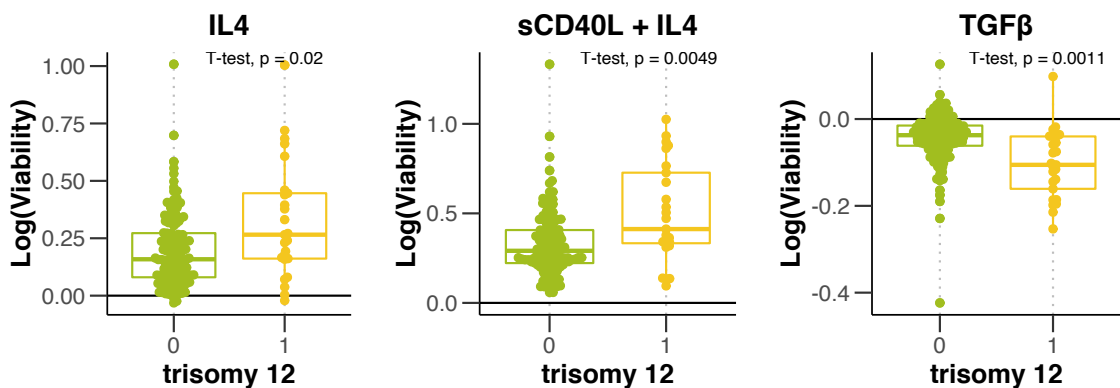


Figure 5.6: Control-normalised log transformed viability values after treatment with IL4, sCD40L + IL4 and TGF β , stratified by trisomy 12.

5.2.2 **STAT6, IRAK4 and SMAD3 are more highly expressed in trisomy 12 CLL**

Trisomy 12 samples contain a third copy of chromosome 12: transcriptomic and proteomic profiling of CLL samples with this lesion have demonstrated that this has a major impact on gene expression and protein abundances (Abruzzo et al. 2018; Herbst 2020; Meier-Abt et al. 2021).

Guided by this observation, I began by investigating RNA and protein expression levels amongst genes involved in the TGF β , IL4 and TLR pathways, to which trisomy 12 samples respond more strongly. The aim was to determine whether proteins in these pathways are more abundant in trisomy 12 CLL, thus contributing to the enhanced response.

I ran differential expression analysis to compare CLL samples from the screen with and without trisomy 12. Next, I filtered the differentially expressed genes (adjusted $p <$

0.1) for those belonging to the TGF β , JAK-STAT and TLR pathways genesets, from the KEGG database. I visualised the RNA counts and protein abundances (Herbst 2020) for those genes.

Only a small proportion of the differentially expressed genes belonged to the TGF β , JAK-STAT and TLR pathways genesets. However of those that were, several genes were key downstream mediators of these pathways (Figure 5.7). Amongst TGF β signalling genes, 7/95 were upregulated in trisomy 12, including SMAD3. 12/160 IL4 signalling genes were differentially expressed, including STAT2. 2/116 genes in the TLR geneset were differentially expressed, including IRAK4 on chromosome 12. Amongst these key mediators SMAD3, STAT2, and IRAK4, all showed higher protein abundance in addition to increased RNA expression. Notably, STAT6, the key downstream mediator of IL4 signalling, was not differentially expressed, but also showed differential protein abundance. Many of the over-expressed genes are not located on chromosome 12, indicating the extent to which the differential dosage of this chromosome has on the expression of the entire genome. [CHECK]

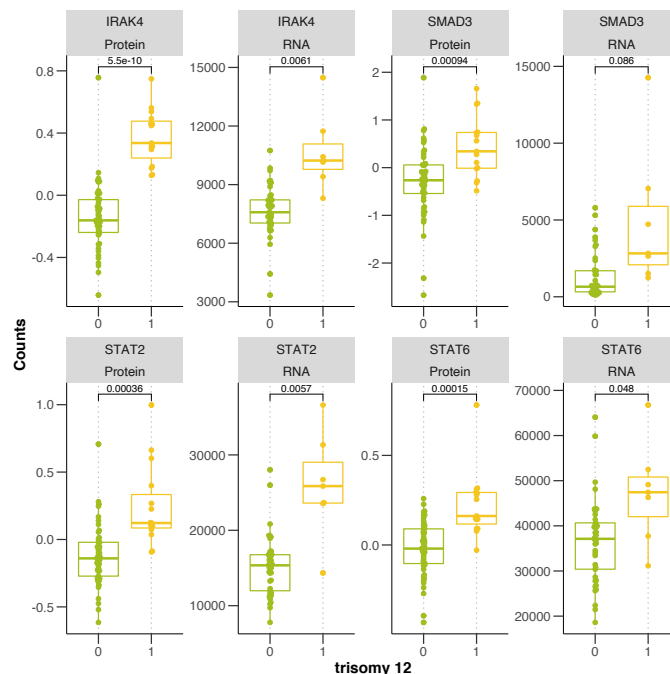


Figure 5.7: Beeswarm-boxplots showing RNA counts and protein abundances stratified by trisomy 12 status. P values from Student's t-test. See Methods section 2.4.2. *Proteomics dataset from Herbst (2020)*

Next I looked for further evidence to directly link the higher gene dosage of cytokine

signalling genes, to enhanced responses to cytokine signals.

5.2.3 Classification analysis identifies trisomy 12 phenocopies that show increased expression of *IRAK4* and *SMAD3*

I next investigated whether any non-trisomy 12 samples might display a trisomy 12-like phenotype (referred to as a phenocopy), in that they respond in a similar way to the panel of stimuli. The aim was to identify trisomy 12 phenocopies and to isolate the feature of these samples that might explain the underlying cause of enhanced response to external signals in trisomy 12 CLL. In particular, I was interested to see if these phenocopies showed higher expression, or even gene amplification, of the signalling genes identified in section 5.2.2.

To identify trisomy 12 phenocopies, I began by generating a classifier to predict the trisomy 12 status of a sample from the stimulus response matrix. I aimed to find non-trisomy 12 samples that were consistently misclassified as trisomy 12.

The classifier was built using binomial regression, with lasso penalisation, as implemented in the R package `glmnet` (Friedman et al. 2021). The feature matrix consisted of z scores of the viability values after treatment with each stimulus, and was used to predict the response (trisomy 12 status). I ran the model for 50 bootstrapped repeats. Resiquimod (TLR 7/8), sCD40L+IL4 and TGF β were selected as coefficients that predict trisomy 12 status (Figure 5.8), as would be expected based on the observations in section 5.2.1.

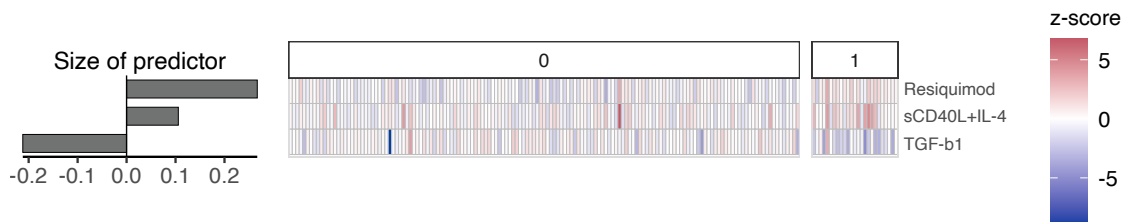


Figure 5.8: Predictor profile showing coefficients selected as predictors of trisomy 12 status. Here, binomial modelling with L1-penalty was used to identify associations between responses to stimuli and trisomy 12 status. Bar plots (left) show size and sign of assigned coefficients named on the right. A positive coefficient indicates that trisomy 12 samples show larger increase in viability when stimulated. Facet labels (top) and corresponding heatmap below show how the viability with each named stimulus relates to trisomy 12 status. The model shown was selected from 50 bootstrapped repeats, based on maximal AUC. See Methods section 2.4.2.

I then predicted trisomy 12 status with the same viability matrix, using each of the 50 bootstrapped model fits. I compared the results of the classification with the true trisomy 12 status. I identified two trisomy 12 phenocopies i.e. patient samples that were misclassified as trisomy 12 in more than 50% of repeats, referred to as Phenocopy A and B in the below.

I aimed to determine what features these phenocopies shared with trisomy 12 samples. Phenocopy A showed the lowest viability with $\text{TGF}\beta$ (Figure 5.9), and Phenocopy B showed the highest viability with IL4, and the second highest with Resiquimod (TLR 7/8).

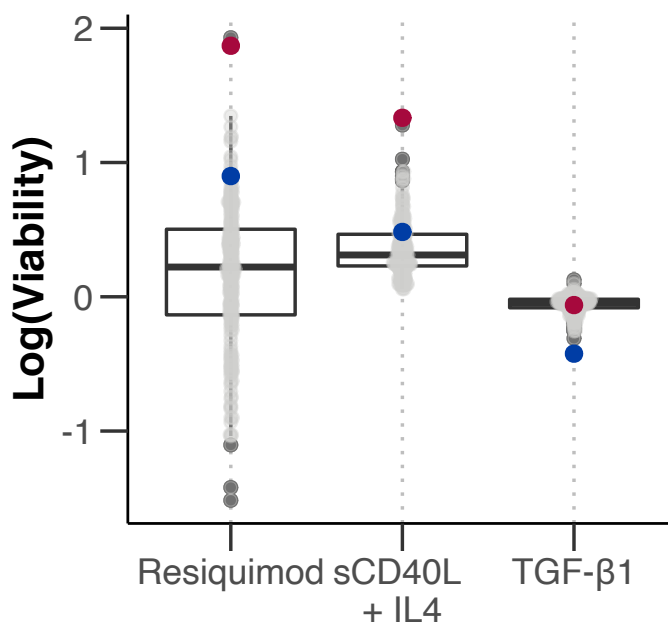


Figure 5.9: Control-normalised log-transformed viability values, for all samples after treatment with Resiquimod (TLR 7/8), sCD40L + IL4 and $\text{TGF}\beta$. Phenocopies A and B are indicated in blue and red, respectively. See Methods section 2.4.2.

I investigated whether either of these non-trisomy 12 samples contained any regional amplifications on chromosome 12, which may help to isolate the gene(s) causing the tumour to respond more strongly to these signals. The whole exome sequencing data (Dietrich et al. 2017) for both patient samples indicated that Phenocopy A had several amplified regions at 12p13.31 (42 copies), 12q24.13 (10 copies) and 12q24.33 (21 copies). An examination of the genes in these regions indicated that none of the signalling genes identified in 5.2.2 could be found in these regions, and no clear candidate gene(s) emerged that may be involved in responses to external signals.

In the absence of gene amplification, I checked if patient samples A and B might show higher expression of the signalling genes identified in 5.2.2 by visualising the RNA expression levels for *SMAD3*, *IRAK4* and *STAT6* for these patients (Figure 5.10). Phenocopy A, which responded most strongly to Resiquimod (TLR 7/8), showed high levels of *IRAK4* compared to the other non-trisomy 12 samples. Phenocopy B, which responded strongly to TGF β showed the highest level of *SMAD3* expression amongst the non-trisomy 12 samples. Thus, whilst neither patient sample contained an amplicon of *SMAD3* or *IRAK4*, its possible that increased expression of these proteins enables a stronger response to the corresponding pathway.

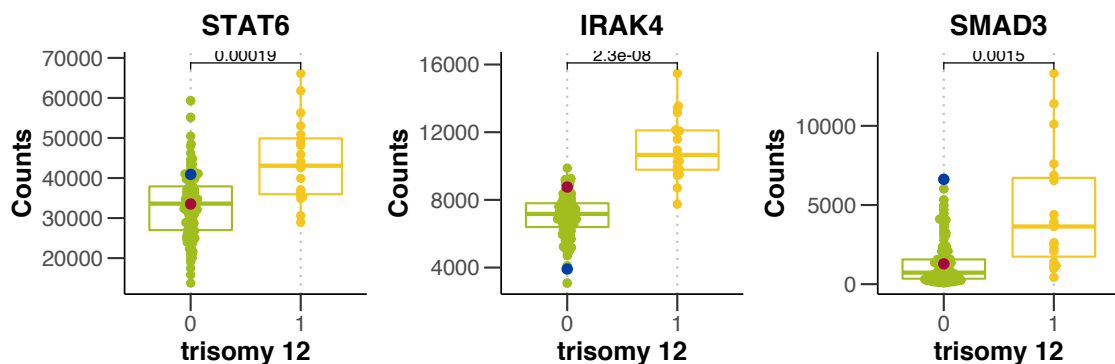


Figure 5.10: Raw RNA counts for *SMAD3*, *IRAK4* and *STAT6*, stratified by trisomy 12 status. Phenocopies A and B are indicated in blue and red, respectively. P values from Student's t-test.

These results collectively suggest that increased gene dosage of key genes in the IL4, TLR and TGF β pathways may underlie the increased response of trisomy 12 samples to these pathways. This is also reflected in the patient samples A and B, which responded more strongly to the TGF β and TLR pathways, respectively, and correspondingly higher levels of SMAD3 and STAT6 proteins. However, computational techniques can only go so far in providing biological proof, and more work is needed here to confirm this finding. In addition to gene dosage effects, I also investigated differences in transcription factor binding site accessibility in trisomy 12. The results of this warranted further follow up, and this forms the focus of rest of this chapter. [CHECK]

5.2.4 Spi-B and PU.1 TFs show higher binding site accessibility in trisomy 12 CLL

Trisomy 12 has been well-studied at both the transcriptomic and proteomic level, and yet the cause of its recurrence in CLL is not fully understood. Thus, I next decided

to investigate the impact of trisomy 12 on the epigenetic landscape of CLL, which is less well studied. In particular, I wanted to investigate differential transcription factor binding site accessibility in CLL, which would give an indicator of which pathways are differentially active (Bruch and Giles et al. 2021).

This investigation involved two independent ATAC sequencing datasets. The first, generated internally, consisted of two WT and two trisomy 12 samples (Bruch & Giles et al. 2021). The second, taken from Rendeiro et al. (2016) comprised 43 WT and nine trisomy 12 samples.

In the external dataset, trisomy 12 status was not annotated. To do this, we used the ATACseq reads to call trisomy 12 in samples that contained > 1.4 times more reads per peak (i.e. genomic region) on average in chromosome 12, compared to peaks on other chromosomes.

Next, we used the `diffTF` software (Berest et al. 2019) to identify TFs that showed differential binding site accessibility between the WT and trisomy 12 samples (Figure 5.11). `diffTF` enables comparison of TF activity between two conditions, using chromatin accessibility data. In this cases, `diffTF` compared binding site accessibility for 638 TFs, from the HOCOMOCO v10 database (Kulakovskiy et al. 2016), between trisomy 12 and WT samples (Bruch & Giles et al. 2021).

Running this analysis on both ATACseq datasets indicated that the binding sites of nine TFs were more accessible ($p<0.05$) in the trisomy 12 samples of the larger, external dataset (Figure 5.12). In the smaller in-house dataset, the binding sites of 92 TFs were likewise more accessible (Supp. Figure 7.4). RNA and proteomics data show different abundances of transcripts and proteins in trisomy 12 CLL: ATACseq data here shows that this also corresponds to a specific signalling signature in trisomy 12 CLL (Bruch and Giles et al. 2021).

We confirmed that the results were not affected by the additional copy of chromosome 12. Rerunning the `diffTF` analysis without the ATACseq reads from chromosome 12 had minor impact on the significant TFs.

In both datasets, the TFs with the largest increase in binding site accessibility in trisomy 12 were Spi-B and/or PU.1 (Bruch & Giles et al. 2021). Both TFs share similar binding motifs and exhibit functional redundancy (Garrett-Sinha et al. 2001), which makes it difficult to distinguish from ATACseq data alone whether either or both are more active.

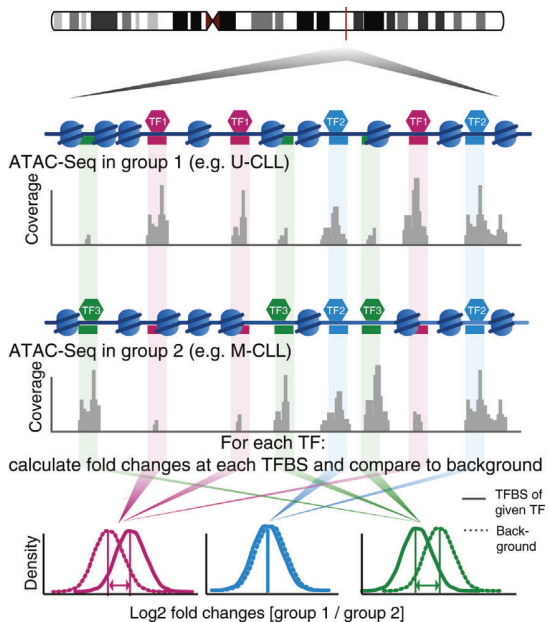


Figure 5.11: diffTF workflow from Berest et al. (2019). diffTF accepts a list of TFs along with the genomic locations of their binding sites. For each TF, the software computes the distribution of fold changes between the trisomy 12 and WT samples, using the ATACseq peaks at each TF binding site in each condition. The software compares this distribution to a background set of fold changes generated using GC content-matched loci that do not contain the same TF binding site motif. Each TF is thus assigned assigned a weighted mean difference value, which quantifies the change in binding site accessibility, and a p value. *Figure from original published in Berest et al. (2019), and adapted with permission.*

Spi-B and PU.1 are haematopoietic regulators that are known to be key regulators of healthy B-cell function (Turkistany and Dekoter 2011), controlling B-cell responses to environmental cues including CD40L, TLR ligands and IL4 (Willis et al. 2017).

Spi-B and PU.1 appeared to be upregulated in trisomy 12 CLL, and evidence in the literature indicated that these may regulate environmental sensing genes, providing a link between trisomy 12, and enhanced responses to external signals (Bruch and Giles et al. 2021).

To provide further evidence of this, I next aimed to profile the downstream effects of Spi-B and PU.1 in lymphoma.

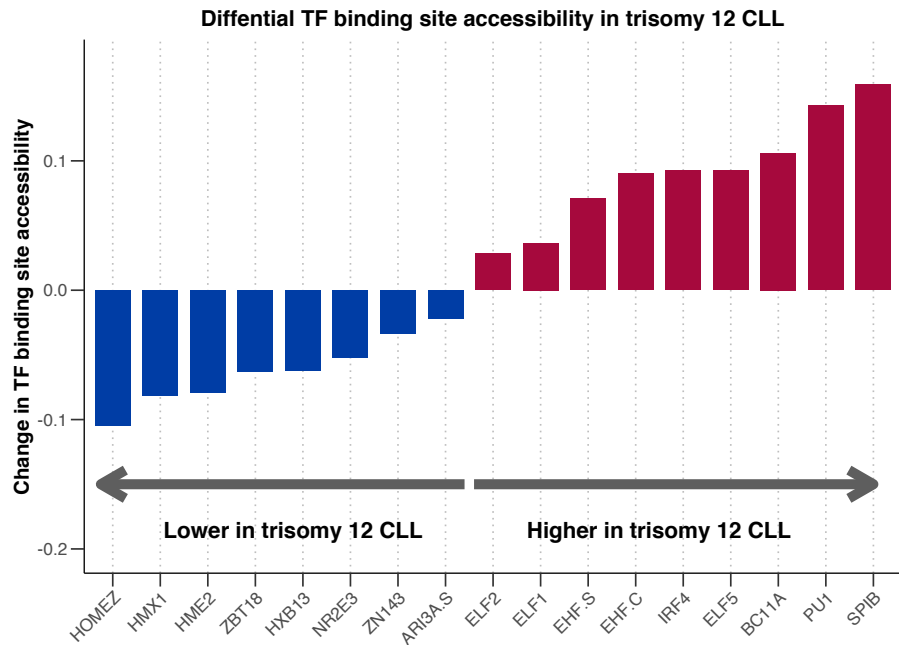


Figure 5.12: Bar plot showing the results of the diffTF analysis for the external dataset (Rendeiro et al. 2016). y axis shows change in TF binding site accessibility (weighted mean difference) between trisomy 12 ($n = 9$) and non-trisomy 12 samples ($n = 43$), x axis indicates TF names. 17 / 638 TFs, with BH adjusted $p < 0.05$ are shown. p values generated by diffTF in permutation mode. TF binding sites defined in HOCOMOCO v10 (Kulakovskiy et al. 2016). See Methods section 2.4.2 ATACseq data from Rendeiro et al. (2016). Trisomy 12 annotation performed together with PhD student Ivan Berest. ATACseq processing and diffTF run by Ivan Berest. Figure and caption adapted from Bruch and Giles et al. 2021.

5.2.5 Spi-B and PU.1 targets are enriched for immune signalling pathways

The above observations suggested Spi-B and PU.1 might coordinate transcriptional response to external signals, thus modulating CLL proliferation in response to the microenvironment. To identify Spi-B and PU.1 target genes specifically in lymphoma, I acquired a ChIPseq dataset (Care et al. 2014) containing data on Spi-B and PU.1 binding in lymphoma cell lines. I used this dataset to test for functional enrichment of immune signalling pathways amongst the TF targets (Bruch and Giles et al. 2021).

To define TF targets, I took the closest gene to each significant ChIP peak (q value < 0.05), and within $\pm 1\text{kb}$ of the TSS. I then tested for over-representation of these TF targets amongst selected KEGG (Kanehisa et al. 2010) and Reactome (Jassal et al.

2020) genesets, using the R package `clusterProfiler` (G. Yu 2021). This method corresponded to a one-sided version of Fisher's exact test. This analysis showed TLR, BCR and TGF β signalling genes to be enriched ($p < 0.01$) amongst Spi-B targets (Figure 5.13, (Bruch and Giles et al. 2021)).

Pathway	Geneset Database	Geneset Size	Spi-B targets (/3253)	SPIB p-value	PU.1 targets (/250)	PU1 p-value
BCR Signaling Pathway	KEGG	75	36	0.000	4	0.056
TLR Signaling Pathway	KEGG	102	40	0.000	5	0.046
Signaling by TGFbeta Receptor Complex	Reactome	73	26	0.007	0	1.000

Figure 5.13: Table shows results from over-representation tests of selected KEGG and Reactome pathways amongst Spi-B and PU.1 targets. Columns show geneset pathways, corresponding database, the number of genes within geneset, the number of Spi-B and PU.1 target genes within geneset (total number of target genes defined also shown). p-values from over-representation test. *ChIPseq data from Care et al. (2014). Figure and caption adapted from Bruch & Giles et al 2021.*

5.2.6 Double knockdown of Spi-B and PU.1 reduces proliferation of trisomy 12 cell lines

To establish the functional impact of Spi-B and PU.1 inhibition in trisomy 12 lymphoma, we investigated the impact of inhibiting these TFs on proliferation of lymphoma cell lines (Figure 5.14). Single and double shRNA knockdowns were generated in lymphoma cell lines, namely SU-DHL4 and SU-DHL5 (trisomy 12) and SU-DHL2 (no trisomy 12) and then measured cell counts at 24 hour intervals (Bruch & Giles et al. 2021).

The single knockdowns had a small impact on proliferation: Spi-B inhibition reduced proliferation in SU-DHL5, as did PU.1 to a lesser extent. Double knockdown of both TFs markedly reduced proliferation in SU-DHL2 and SU-DHL4, and was lethal in SU-DHL5. This result suggested that both these TFs play an important role in the proliferative capacity of the tumour cells, and that there is functional redundancy between Spi-B and PU.1 in this context.

Collectively, these observations demonstrate that trisomy 12 modulates responses to microenvironmental signals. Trisomy 12 appears to increase Spi-B and PU.1 activity, which regulate genes relating to environmental sensing, and reduce proliferation of cell lines when inhibited (Bruch and Giles et al. 2021).

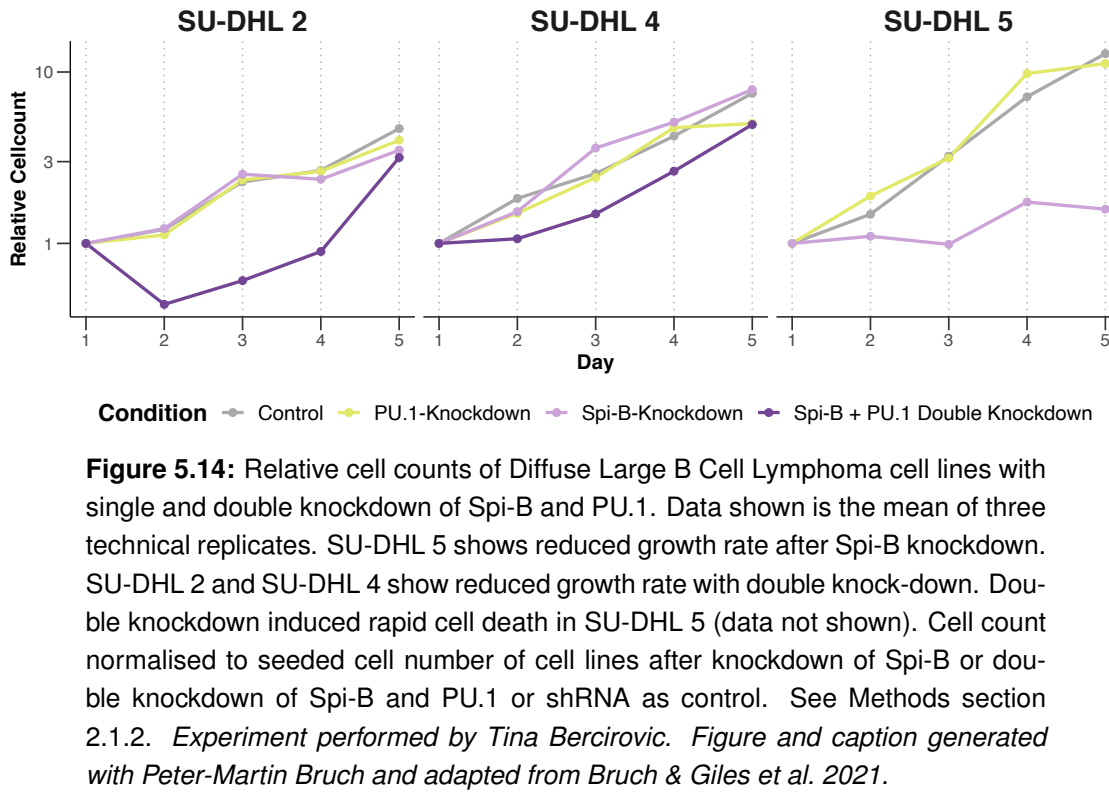


Figure 5.14: Relative cell counts of Diffuse Large B Cell Lymphoma cell lines with single and double knockdown of Spi-B and PU.1. Data shown is the mean of three technical replicates. SU-DHL 5 shows reduced growth rate after Spi-B knockdown. SU-DHL 2 and SU-DHL 4 show reduced growth rate with double knock-down. Double knockdown induced rapid cell death in SU-DHL 5 (data not shown). Cell count normalised to seeded cell number of cell lines after knockdown of Spi-B or double knockdown of Spi-B and PU.1 or shRNA as control. See Methods section 2.1.2. *Experiment performed by Tina Bercirovic. Figure and caption generated with Peter-Martin Bruch and adapted from Bruch & Giles et al. 2021.*

5.3 Summary

This chapter outlines a systematic survey of genetic determinants of microenvironmental response, leading to two key findings. Firstly, TLR signalling has a range of effects on CLL viability, and this is determined by many genetic features, including IGHV status, trisomy 12 and mutation in the DNA Damage Response pathway. Secondly, I identify trisomy 12 as a modulator of microenvironmental response, and show that higher activity of Spi-B and PU.1 may mediate this effect (Bruch and Giles et al. 2021).

Chapter 6

Molecular and microenvironmental modulators of drug response in CLL

Chapters 4 and 5 provide a systematic exploration of the effect of microenvironmental stimulation on *ex vivo* CLL biology, and how these pathways can be modulated by genetic features. Collectively, these results underline the fact that cancer biology is determined by an integrated network of cell-intrinsic molecular aberrations and cell-extrinsic signals generated by cell-cell contacts and soluble factors. In this chapter, I present my investigations into the impact of each of these on **drug response**.

The effect of genetic features on *in vitro* drug response in CLL has been well-characterised, including as part of recent work produced by our lab (Dietrich et al. 2017). Many studies have also demonstrated the impact of individual microenvironmental signals on drug response *ex vivo*, including a number of studies demonstrating that soluble factors can induce resistance to clinical drugs (Fonte et al. 2013; Aguilar-Hernandez et al., n.d.; Kallesh D. Jayappa et al. 2017; McWilliams et al. 2019).

Evidence of microenvironmental signals inducing resistance to therapies *in vivo* is less prevalent, although there is widespread consensus that the microenvironment, in particular the lymph node, plays an important role in patient outcomes. A number of studies have shown enlarged lymph nodes are associated with MRD (Moreton et al. 2005), in particular, incomplete response to ibrutinib is associated with persistently enlarged lymph nodes (Ahn et al. 2018). For more information see Introduction section

1.3.4.

Guided by these observations, this chapter explores the impact of genetic features, and microenvironmental stimulation on drug response, both individually and in combination. In section 6.1, the impact of the panel of stimuli on drug response is quantified by identifying drug - stimulus interactions. In section 6.2, the impact of genetic features on drug response is explored. In section 6.3, multivariate modelling is applied to investigate how drug - microenvironment interactions can be further modulated by genetic features. Finally, in section ??, I outline my work to investigate the interaction between IL4 and ibrutinib, identified in the above analysis.

The analyses described here benefit from linear regression and generalised linear modelling approaches, described in more detail in section 1.5.3.

Some findings and figures outlined in this chapter have been published in Bruch and Giles et al. 2021, and this is clearly stated where this is the case.

6.1 The impact of microenvironmental stimuli on drug response

6.1.1 Linear modelling maps interactions between drugs and stimuli

To begin the analysis, I first aimed to screen for cases where stimulus pathways specifically interacted with drug target pathways (Bruch and Giles et al. 2021). I evaluated computational methods for quantifying this, and decided to apply linear modelling based on the following principle:

When a stimulus is individually applied to a CLL sample, the stimulus activates signalling cascades that modulate CLL viability and impact the rate of spontaneous apoptosis. When a stimulus is co-applied with a drug, the stimulus will continue to impact upon baseline viability, at the same time as the drug inhibits baseline viability. Assuming the drug and stimulus do not interact, the viability of the tumour cells with the combinatorial treatment will equate to the additive impact of both the compounds.

In the case that there is some interaction between the stimulus pathway and drug target pathway, the resulting viability will not simply be additive. The difference between the additive, or expected viability, and the true measured viability, can be quantified by an **interaction factor**. Linear modelling aims to quantify this **interaction factor**. [CHECK: is this clear?]

Based on this principle, I fitted linear models to the viability data for each drug - stimulus combination, outlined in Equation (6.1) (Bruch and Giles et al. 2021). I used the `lm` function implemented in the R package `stats`(R Core Team 2021).

Equation (6.1) quantifies how the viability with any combination can be predicted:

$$\log(V) = \beta_{drug}X_{drug} + \beta_{stimulus}X_{stimulus} + \beta_{int}X_{drug}X_{stimulus} + \epsilon \quad (6.1)$$

where V is the predicted viability with a given treatment, β_{drug} , $\beta_{stimulus}$ and β_{int} are coefficients for the drug, stimulus and combinatorial terms and X_{drug} and $X_{stimulus}$ are indicator variables (0 or 1) for the presence or absence of a drug/stimulus. ϵ is the vector of model residuals. See also Methods section 2.4.1. Equation from Bruch and Giles et al. 2021.

Here β_{int} quantifies how the combined treatment effect differs from the sum of the individual treatments. This approach identified 45 drug-stimulus combinations (out of 204), where β_{int} had $p < 0.05$, highlighting the extent to which drug action can be modulated by cell-extrinsic signals *ex vivo* (Bruch and Giles et al. 2021).

6.1.2 Drug - stimulus interactions can be categorised by their mode of action

The interactions identified through linear modelling demonstrated different modes of action. I was most interested to identify stimuli which induce drug resistance, and drugs that may inhibit the pro-survival effects of a stimulus, which represent candidate drugs for targeting the microenvironment in the clinic. To establish which interactions may be of interest within a clinical context, the drug - stimulus interactions were classified into four categories (Bruch and Giles et al. 2021).

The categories were firstly defined based on whether the interaction was antagonistic or synergistic, i.e. the stimulus / drug acted to oppose or reinforce the activity of the other. These were further divided based on the sign of β_{int} i.e. whether the combinatorial viability was higher (positive) or lower (negative) than would be expected based on additive effects (Figure 6.1A).

These categories encompassed the following interaction types. Type I defined positive antagonisms in which stimuli reversed drug action, leading to decreased drug efficacy and increased CLL viability. This group highlights drug - stimulus interactions that could be relevant to treatment resistance pathways *in vivo*. Type II negative antagonisms highlighted cases where the drug inhibited the stimulus, reducing the effect of the stimulus

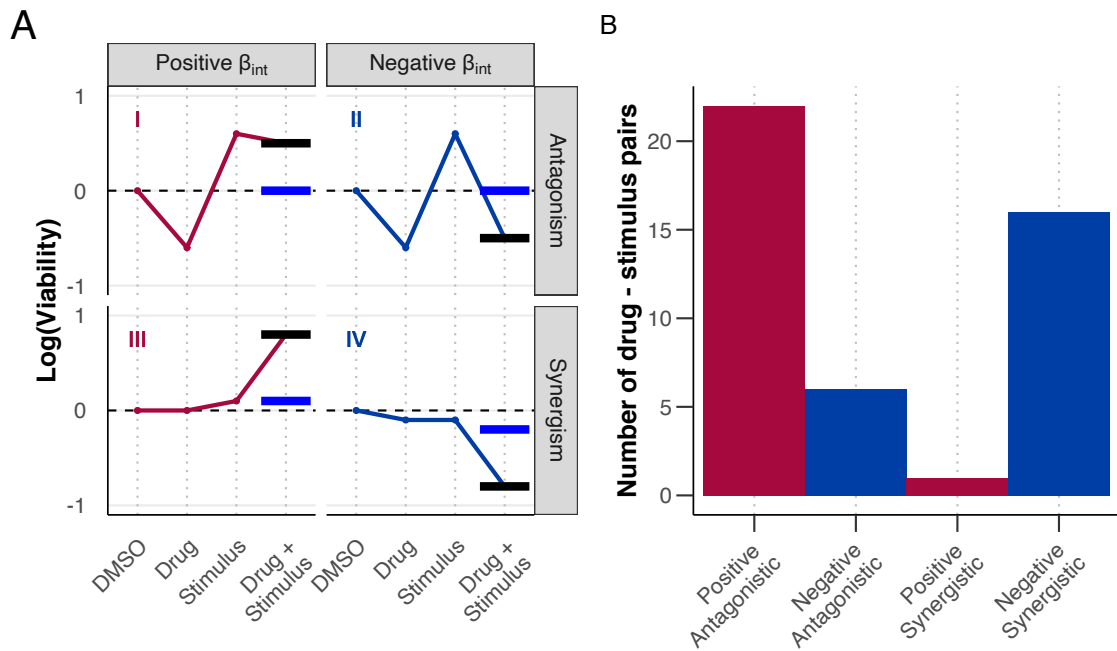


Figure 6.1: (A) Graphical line plots representing typical response patterns for each of the four drug - stimulus interaction categories (types I - IV). x-axis shows treatment, y-axis shows log transformed viability values, facet labels indicate interaction type. Blue and black horizontal lines demonstrate effect of interaction on viability with combinatorial treatment. Blue line shows predicted viability based on additive effects alone and black line shows viability accounting for additive effects and interaction. (B) Histogram showing number of drug-stimulus interactions within each category, where p value for β_{int} is <0.05 . See Methods section 2.4.1 and 2.4.1. *Figure generated with Peter-Martin Bruch for the manuscript Bruch & Giles et al. 2021, and caption adapted from manuscript.*

on baseline viability, and decreasing CLL viability. These interactions include drugs that represent candidates to target microenvironmental signalling pathways *in vivo*. Type III and type IV interactions cover synergies, in which the drug and stimulus increase the effect of the other. Type III positive synergies led to increased CLL viability with the combinatorial treatment, whilst type IV negative synergies led to increased drug efficacy and lower viability. In the latter case, these may highlight cases where drug efficacy is dependent on external pathways, and indicate where co-culture approaches may be more appropriate in laboratory studies of *ex vivo* drug action. Figure 6.1B quantifies the number of interactions in each category.

6.1.3 Investigating specific drug-stimulus interactions indicates that INF γ induces resistance to ibrutinib *in vitro*

The combined approach of fitting linear models and subsequently classifying these interactions represents an attempt to generate a comprehensive map of drug - stimulus interactions in CLL (Bruch and Giles et al. 2021, Figure 6.2). The aim is that this resource may facilitate further work into these drug - stimulus interactions, such as the work outlined in section ??.

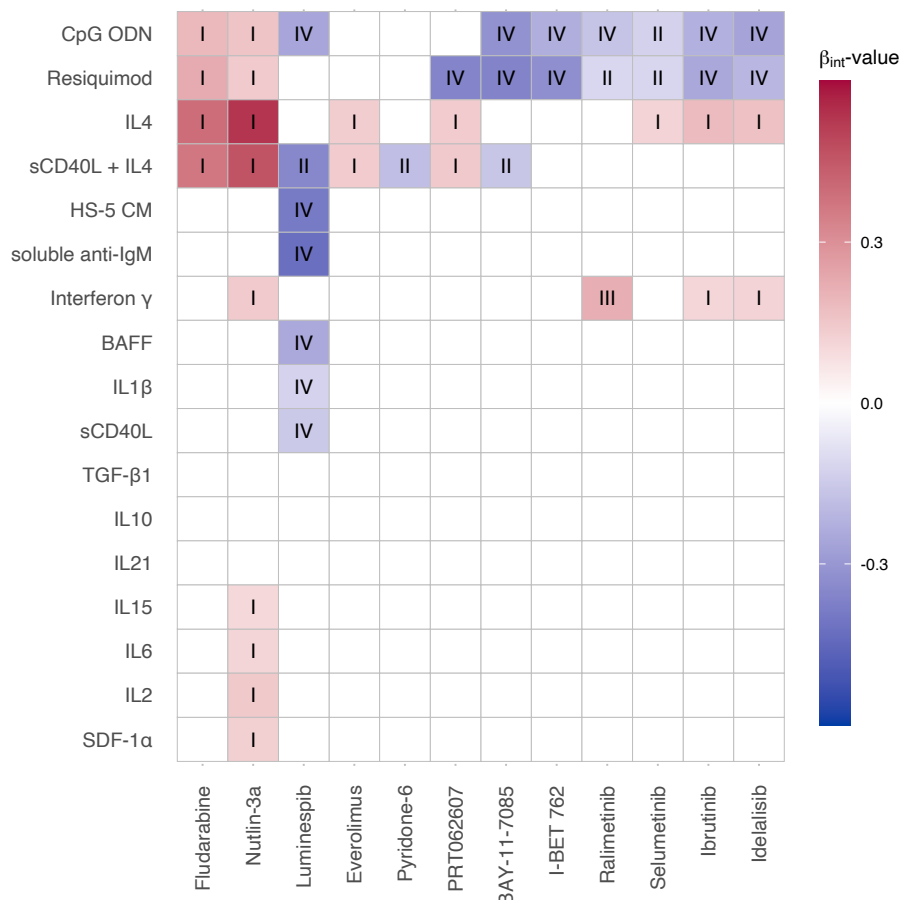


Figure 6.2: “Heatmap of β_{int} values for all drug - stimulus combinations where $p < 0.05$, annotated with interaction type (I - IV). Scale indicates size and sign of β_{int} . Rows and columns clustered according to hierarchical clustering.” See Methods section 2.4.1 and 2.4.1. *Figure generated with Peter-Martin Bruch for the manuscript Bruch & Giles et al. 2021, and caption taken from manuscript.*

Having generated an overview of drug - stimulus interactions, I next examined each interaction within each category with the aim of identifying the most clinically interesting

examples (Figure 6.3, (Bruch and Giles et al. 2021)).

Positive antagonistic Interactions categorised as positive antagonistic were the most common i.e. the stimulus reversed drug action. This group included known resistance mechanisms such as the inactivation of ibrutinib by IL4 stimulation (Figure 6.3A)(Aguilar-Hernandez et al., n.d.), indicating that the modelling and classification approach successfully recapitulated established drug - stimulus interactions (Bruch and Giles et al. 2021).

Additionally, this analysis demonstrated the broader significance of IL4-induced resistance, beyond what previous work has shown. IL4 showed the highest number of positive antagonistic interactions amongst all of the stimuli and inhibited a range of drugs, including BCR inhibitors and chemotherapeutics. This is investigated in more detail in section ?? below.

In addition to IL4, IFN γ showed the second largest number of positive antagonistic interactions. IFN γ stimulation induced resistance to BCR inhibition by ibrutinib and idelalisib, and to the chemotherapeutic Nutlin-3a (MDM2) (Figure 6.3B, Bruch and Giles et al. 2021), and may represent a novel targetable resistance mechanism (Bruch and Giles et al. 2021).

IL4 and IFN γ induced resistance to common pathways and thus I stipulated that both stimuli may share the same mechanism of action. This was supported by the observations in section 5.1.2, in which I demonstrated that IL4 showed a smaller increase in viability in cells that had mutations in Ras-Raf-MEK-ERK, and that inhibition of p38 MAPK activity with ralimetinib increased the pro-survival effect of IL4 stimulation. IFN γ demonstrated similar behaviour whereby p38 MAPK inhibition increased the pro-survival effect of stimulating this pathway (Appendix Figure 7.7). Collectively these observations suggest that IL4 and IFN γ may operate via a common pro-survival mechanism, which is negatively regulated by activity of MAPK signalling. [CHECK]

Negative antagonisms There were six cases of negative antagonisms, whereby drug action inhibited the pro-survival effect of the stimulus. Such cases could potentially be used to target micronenivironmental signals *in vivo*. As IL4 appeared to be the most potent conferrer of drug resistance, it was of greatest interest to identify drugs that may inhibit this pathway. For example, the Pan-JAK inhibitor pyridone-6 inhibited the increase in viability with sCD40L + IL4 stimulation (Figure 6.3C, Bruch and Giles et al. 2021).

Positive synergisms The model identified a single positive synergism, in which IFN γ

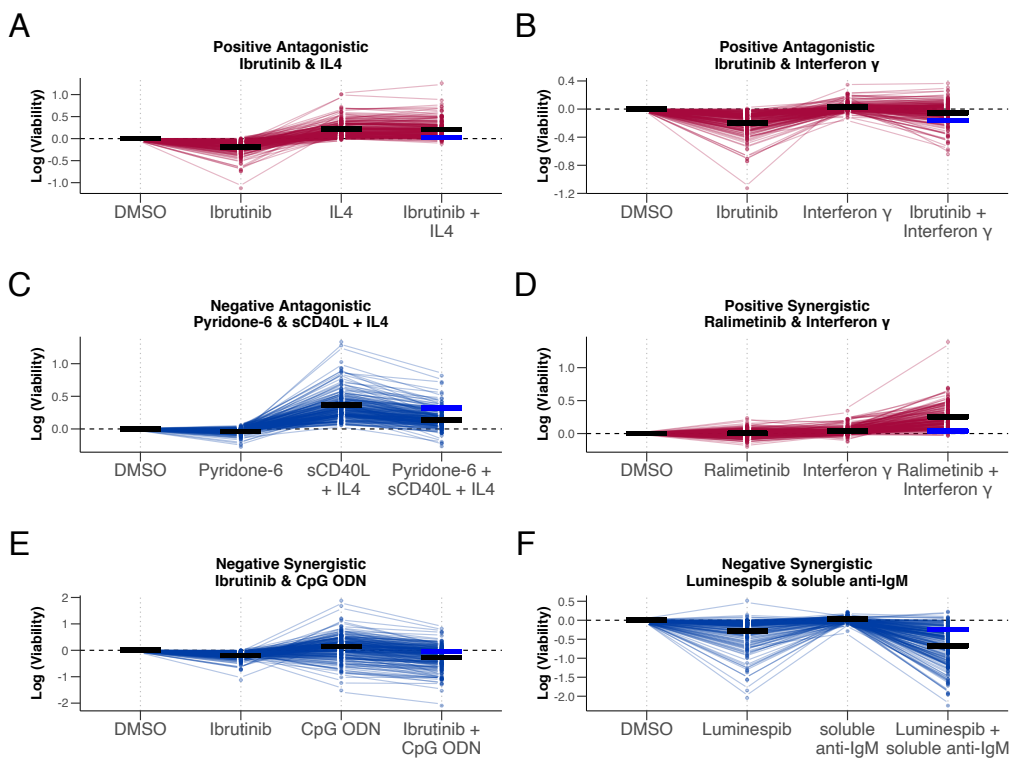


Figure 6.3: Line plots showing examples of drug-stimulus interactions. x-axis indicates treatment, y-axis shows log transformed viability values, with matching samples linked across treatments. Black horizontal lines represent predicted viability for each treatment, using coefficients from linear model fit. For combinatorial treatment, blue line indicates predicted viability based on additive effects alone, and black line indicates predicted viability accounting for additive effects plus interaction. See Methods section 2.4.1. *Figure generated with Peter-Martin Bruch for the manuscript Bruch & Giles et al. 2021, and caption taken from manuscript.*

treatment in combination with ralimetinib, a p38 MAPK inhibitor, stimulated a large increase in viability that was not observed in each of the single treatments (Figure 6.3D, (Bruch et al. 2021)). As discussed above, this finding suggests a potential inhibitory effect of p38 MAPK activity on signalling via IFN γ (Bruch and Giles et al. 2021).

Negative synergisms 16 drug - stimulus combinations demonstrated negative synergistic interactions. This implied that the efficacy of the drug was somehow dependent upon, or increased by, activation of the stimulus pathway. For example, luminespib, a HSP90 inhibitor, showed higher efficacy with a number of stimuli, including soluble anti-IgM, indicating that *ex vivo* measurements of luminespib action are likely to be affected by the presence or absence of microenvironmental signals (Figure 6.3F, Bruch

and Giles et al. 2021).

Collectively, these results represent a comprehensive and systematic study of the influence of the microenvironment on drug efficacy in CLL. This work highlights key resistance pathways, strategies for targeting microenvironmental resistance, and underlines important pathways in *ex vivo* studies of drug efficacy (Bruch and Giles et al. 2021).

This work aims to serve as a resource, to provide a basis for further follow-up studies. All drug - stimulus combinations and interactions can be explored on the online shiny app, and the whole analysis can be replicated, or adapted, from the online code repository, published alongside Bruch and Giles et al. 2021. In this thesis, I have selected IL4-induced resistance to BCR inhibition and ibrutinib to investigate in more detail (see below, section ??.

6.2 Genetic modulators of drug response

6.2.1 Univariate analysis identifies trisomy 12 as a key modulator of drug response

I next aimed to screen for cases where molecular features modulated drug responses. Previous work in our lab (Dietrich et al. 2017) has generated the largest survey of molecular determinants of response in CLL to date. Here I repeat a similar analysis, as it was valuable to establish the effects of mutations independently of stimuli on drug response within my dataset before investigating the impact of mutations on drug - stimulus interactions.

I performed a comprehensive survey of genetic determinants of drug response, to establish the effects of mutations independently of stimuli on drug response. I used the genetic data, including all mutations, copy number variants andIGHV status for which there were greater than three cases in the cohort ($n = 54$), to perform t-tests to identify molecular features that impact on drug response (Figure 6.4).

This analysis recapitulated the findings of previous work (Dietrich et al. 2017). For example IGHV-U CLL samples responded more strongly to BCR inhibition by ibrutinib (BTK) and idelalisib (Pi3K), and TP53 and del(17p) mutations conferred resistance to nutlin-3a (MDM2) and fludarabine (Purine analogue).

In addition, this analysis highlighted the broad impact of trisomy 12 on drug response

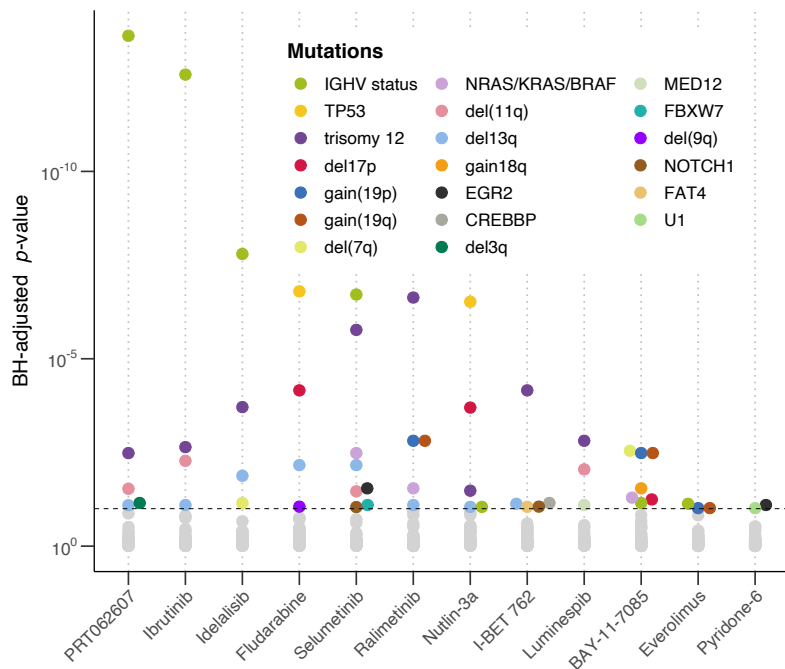


Figure 6.4: Plot showing BH-adjusted p values from Student's t-tests (two-sided, with equal variance), for all tested drug-gene associations. Tests performed for IGHV status, somatic mutations and copy number aberrations ($n = 54$). Each coloured circle represents a gene-stimulus association meeting 10% FDR cut off. See Methods section 2.4.1 *Figure from Bruch and Giles et al. 2021*.

ex vivo (Figure 6.5). While trisomy 12 CLL demonstrates higher proliferative capacity, tumours with trisomy 12 are more treatable due to higher sensitivity to chemotherapeutics and ibrutinib. This was reflected in the *in vitro* data in this study; the presence of trisomy 12 increased sensitivity to 8 / 12 drugs.

These included increased sensitivity to p38 MAPK inhibition by ralimetinib, agreeing with previous work demonstrating higher trisomy 12 sensitivity with a range of MEK and ERK inhibitors and suggesting an essential role for MEK/ERK signalling in trisomy 12 CLL (Dietrich et al. 2017).

I also noted that trisomy 12 CLL showed increased sensitivity to IBET-762, a bromodomain inhibitor that has been shown to suppress transcriptional responses to cytokine signalling via JAK-STAT (Chan et al. 2015). The results in section 5.2.1 indicated that trisomy 12 enhances responses to some cytokines. I was interested to see whether bromodomain inhibition may provide a strategy to target this feature of trisomy 12 samples. I decided to investigate the impact of IBET-762 treatment on the trisomy 12 transcrip-

tion factor signature determined in Figure 5.12. I made use of an additional ATACseq dataset consisting of four CLL PBMC samples each treated with IBET-762 and DMSO as control. I visualised inferred TF activity for trisomy 12 signature TFs, calculated using `diffTF` (Berest et al. 2019). All nine TFs showing higher accessibility in trisomy 12 CLL (Figure 5.12) exhibited decreased accessibility upon treatment with IBET-762 (Appendix Figure ??). This result suggests that bromodomain inhibition may represent a potential target in CLL patients with trisomy 12 (Bruch and Giles et al. 2021). [CHECK: Does it make sense to include this here, or is it a distraction from the main story?]

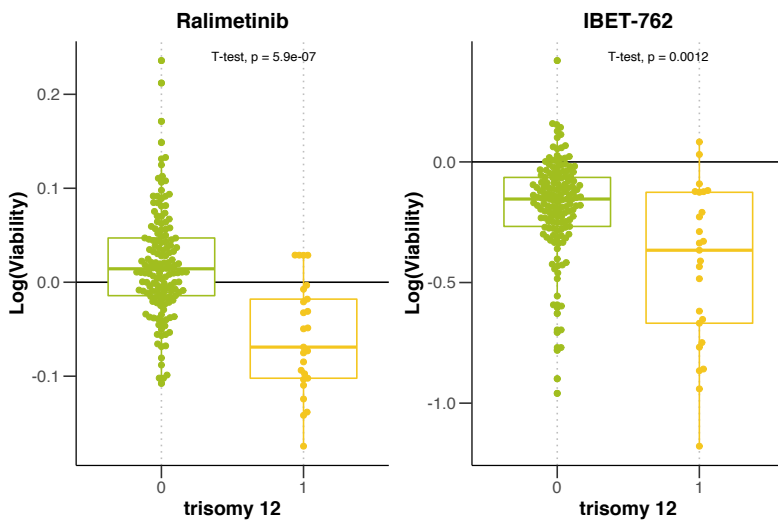


Figure 6.5: Beeswarm-boxplots showing control-normalised log transformed viability values after treatment with (A) Ralimetinib (p38 MAPK) and (B) IBET-762 (BRD2/3/4), stratified by trisomy 12.

6.3 The modulatory effect of mutations on drug - stimuli interactions

6.3.1 Patient - specific linear modelling identifies drug - stimulus - gene interactions

Sections 6.1 & 6.2 explore the effects of microenvironmental signals and molecular features on drug response independently. I next aimed to investigate their collective effect on *in vitro* drug efficacy in CLL, by quantifying the extent to which genetic driver mutations modulated the interactions between stimuli and drugs (Bruch and Giles et al. 2021).

I began by conceptualising methods to quantify the collective effect of the drugs, stimuli and genetic features on CLL viability and biology. I decided to adapt the linear model in Equation (6.1), by fitting this model in a patient sample - specific manner (Bruch and Giles et al. 2021):

$$\begin{aligned} \log(V) = & \beta_{drug} X_{drug} + \beta_{stimulus} X_{stimulus} + \beta_{patient} \\ & \beta_{drug-stimulus} X_{drug} X_{stimulus} \\ & + \beta_{drug-patient} X_{drug} X_{patient} + \beta_{stimulus-patient} X_{stimulus} X_{patient} \\ & \beta_{int} X_{drug} X_{stimulus} X_{patient} + \epsilon \end{aligned} \quad (6.2)$$

where V is the predicted viability of a patient sample with a given treatment, β_{drug} , $\beta_{stimulus}$, $\beta_{patient}$, $\beta_{drug-stimulus}$, $\beta_{drug-patient}$, $\beta_{stimulus-patient}$ and β_{int} are regression coefficients for the drug, stimulus, patient sample and combinatorial terms and X_{drug} , $X_{stimulus}$ and $X_{patient}$ are indicator variables (0 or 1) for the presence or absence of a drug/stimulus/patient sample. ϵ is the vector of model residuals. See also Methods section 2.4.1. Equation from Bruch and Giles et al. 2021.

With these patient sample-specific β_{int} terms, it was possible to search for associations between the size of β_{int} and genetic features. The aim was to screen for molecular features that increased or decreased the size of a drug - stimulus interactions, using multivariate regression with L1 (lasso) regularisation.

To assemble the inputs for the model, first the response matrix was composed of the sample - specific β_{int} values for each drug-stimulus combination. To generate the feature matrix (137 samples versus 40 features), I excluded genetic features for which >20% of the values were missing, and patient samples with incomplete annotation. As predictors, I included genetic mutations and CNVs ($p = 39$) and IGHV status (coded as 0-1). I ran lasso regression, as implemented in the R package `glmnet`(Friedman et al. 2021), using three-fold cross-validation with misclassification error as loss. This approach identified genetic predictors of the size of drug - stimulus interactions, where the predictors represent the mean coefficient values that were selected in at least 90% of 30 bootstrapped repeats.

This analysis revealed that 60/204 drug - stimulus interactions were modulated by at least one genetic feature (Figure 6.6, Appendix Figure 7.5, Bruch and Giles et al. 2021). A positive coefficient here indicates that the presence of the genetic feature is associated with more positive β_{int} , in other words, the viability with the drug and stimulus is higher than expected in the presence of the genetic feature.

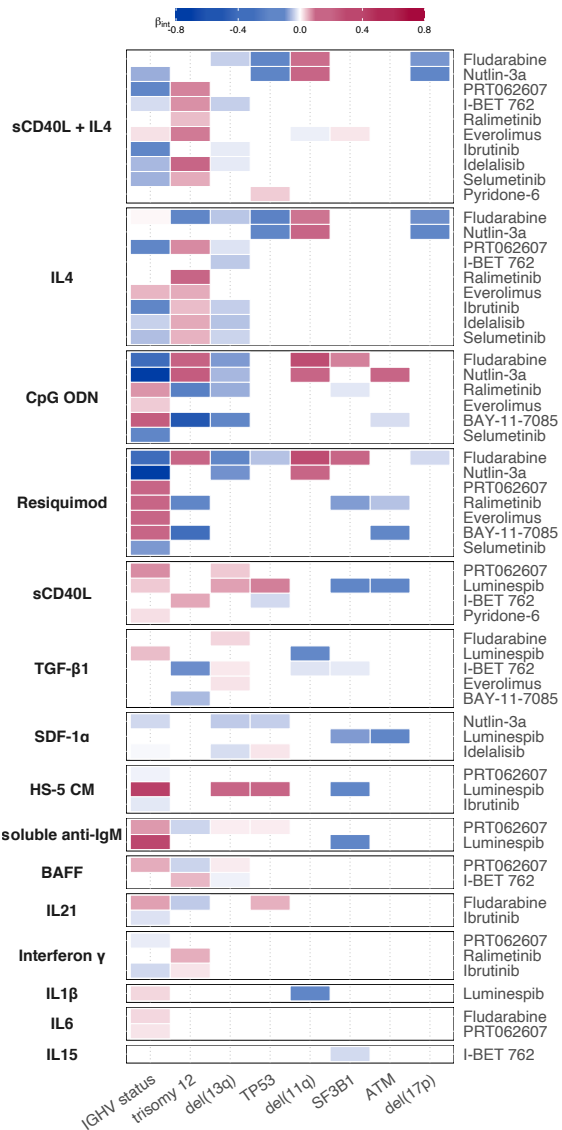


Figure 6.6: Heatmap summarising genetic predictors of drug - stimulus interactions. Each row depicts a single drug - stimulus combination, and each coloured tile indicates that β_{int} for given drug and stimulus combination is modulated by corresponding genetic feature. Thus each row represents the output of a single model fit (as in Figure 6.7). Colour of tile indicates size and sign of coefficient assigned to genetic feature, where a positive coefficient corresponds to a more positive β_{int} if the feature is present. Only top 8 most commonly selected genetic features are shown. Drug - stimulus combinations with no genetic predictors of β_{int} amongst top 8 shown are omitted for clarity. See Methods section 2.4.1. *Figure from Bruch and Giles et al. 2021. Peter-Martin Bruch contributed to figure design.*

Applying this broad scale screening approach established some wider trends. Firstly, trisomy 12 and IGHV status impacted the largest number of drug - stimulus interactions, indicating that their impact on stimulus and drug response individually also extends to drug-stimulus interactions. Secondly, out of all the stimuli, IL4 and sCD40L + IL4-based interactions were modulated by the largest number of features. IL4 alone increased viability uniformly across genetic backgrounds; its interaction with drugs may be more influenced by genetic features. Notably, the presence of trisomy 12 acted to increase IL4-induced drug resistance, in almost all drugs for which $\beta_{int} > 0.05$.

6.3.2 Patient - specific drug - stimulus interactions of clinical interest

The multivariate modelling approach outlined above was a valuable screening tool. Using the results of this screening approach, I next examined each individual hit to establish which drug - stimulus - gene interactions were the most biologically interesting. This analysis highlighted several interactions that may have clinical importance and may warrant further investigation (Bruch and Giles et al. 2021).

The first of these concerned the interaction between fludarabine (purine analogue) and CpG ODN (TLR9). The value of β_{int} for fludarabine and CpG ODN was modulated by six genetic factors; most strongly by IGHV status, del(11q) and trisomy 12 (Figure 6.7, Bruch and Giles et al. 2021).

I visualised sample responses to CpG ODN and fludarabine stratified by two of these features: IGHV status and trisomy 12 (Figure 6.8, Bruch and Giles et al. 2021). In IGHV-M non-trisomy 12 samples, TLR stimulation increased fludarabine efficacy. In samples that were either IGHV-U or trisomy 12, the reverse was true and TLR stimulation induced resistance to fludarabine (Bruch and Giles et al. 2021).

I observed a similar effect with other chemotherapeutic drugs. Nutlin-3a is an MDM2 inhibitor, which in our dataset showed higher efficacy in IGHV-U, trisomy12, and del(11q) CLLs (Figure 6.4, Figure 6.5, Appendix Figure 7.6). TLR stimulation reduced nutlin-3a toxicity in these same genetic backgrounds, i.e nutlin-3a efficacy in the context of CpG ODN stimulation was lower in IGHV-U, trisomy 12 and del(11q) samples (Figure 6.9, Figure 6.10). This observation underlines the need to observe *in vitro* drug activity in the context of microenvironmental signals [CHECK].

The modelling approach also identified interactions where the differential size of β_{int} was driven by the single treatment effect, rather than the combination. For example, if a drug was more efficacious in a certain genetic background, but a stimulus nonetheless

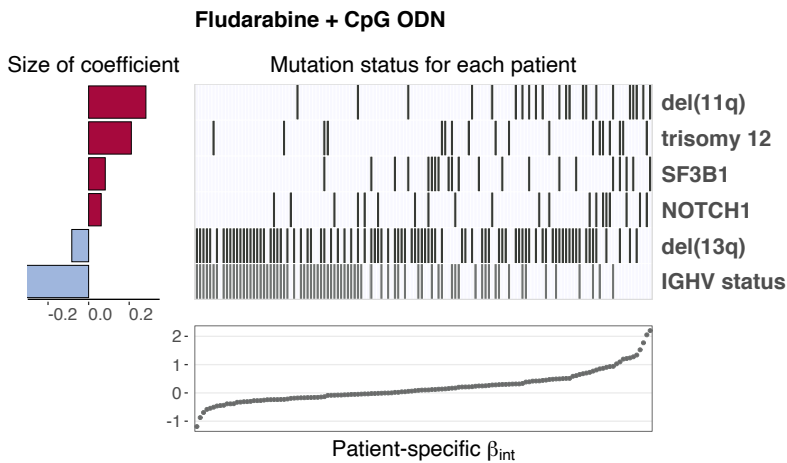


Figure 6.7: “Genetic features that modulate the size of β_{int} between fludarabine (purine analogue) and CpG ODN (TLR9). Scatter plot, heatmap and bar plots indicate inputs and outputs of equation (6.2). Bar plots indicate size and sign of coefficients assigned to genetic features named on right. Scatter plot depicts β_{int} values for each patient sample i.e. response matrix. Heatmap tiles indicate mutation status for the selected genetic features (i.e. feature matrix) corresponding to same sample in scatter plot below, to show how size of β_{int} varies with each feature.” See Methods section 2.4.1. *Figure and caption from Bruch and Giles et al. 2021.*

eradicated drug toxicity, the size of the interaction was larger in this genetic background. This is because the increase in expected viability in these samples (quantified by β_{int}) would be even higher than in other genetic backgrounds.

This was the case with ibrutinib + IL4 for instance (Bruch and Giles et al. 2021). Ibrutinib showed higher efficacy in trisomy 12 and IGHV-U samples and IL4 induced complete resistance to ibrutinib independently of genetic background. Thus in trisomy 12 and IGHV-U samples treated with ibrutinib, the increase in viability in the context of IL4 stimulation was larger than in non-trisomy 12 and IGHV-M samples, and thus these features were assigned positive coefficients.

This result highlights that IL4-induced resistance may be a broad spectrum resistance mechanism, even in tumours with molecular features that are associated with higher ibrutinib efficacy. IL4 signalling may represent a drug resistance mechanism common to many CLLs, in a disease known for its molecular and genetic heterogeneity, though more *in vivo* evidence is required here (Figure 6.11, Figure 6.12, (Bruch and Giles et al. 2021).

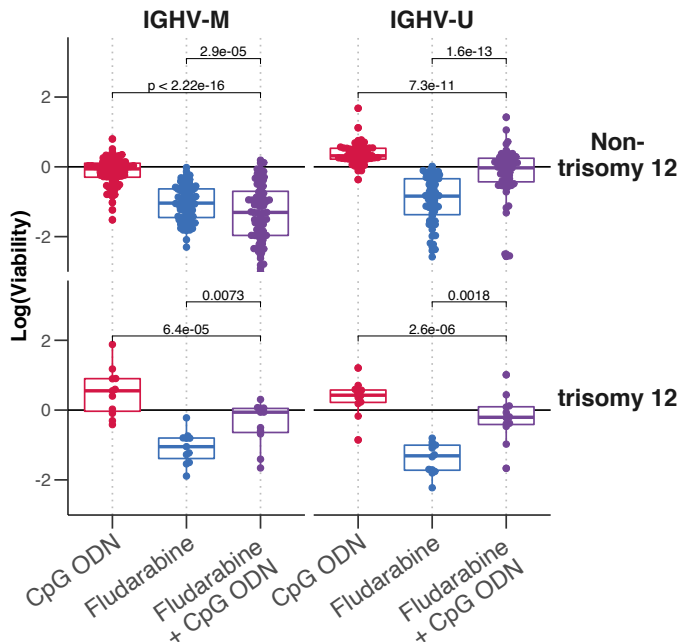


Figure 6.8: “Beeswarm-boxplots of log-transformed viability values for fludarabine (purine analogue) and CpG ODN (TLR9) single and combinatorial treatments, faceted by IGHV status and trisomy 12 status. P-values from paired Student’s t-tests.” *Figure and caption from Bruch and Giles et al. 2021.*

6.4 Summary

This work aims to integrate the effects of mutations and the microenvironment in drug response in CLL, at a large scale. The results demonstrate the value of using multi-omic data (consisting of both observational data on patient samples and perturbation data generated through screening) to generate more complex biological insights that can guide further clinical studies.

More specifically, these results identify a number of novel drug-resistance pathways, including the impact of IFN γ on ibrutinib. Trisomy 12 is identified as an important modulator of drug response. Additionally, these results show that certain resistance pathways are context-dependent. In particular, the ability of TLR stimulation to induce resistance to chemotherapeutics is modulated by IGHV and trisomy 12 status.

Overall these findings illustrate how the presence of known genetic alterations determines how drugs and external stimuli interact with each other.

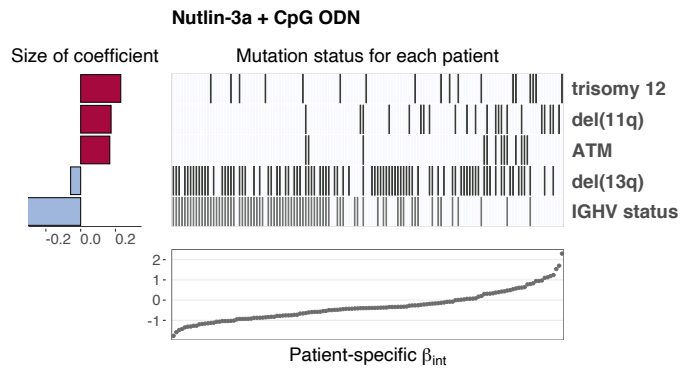


Figure 6.9: Predictor profile depicting genetic features that modulate the size of β_{int} between nutlin-3a (MDM2) and CpG ODN (TLR9). Plot generated as in Figure 6.7. See Methods section 2.4.1.

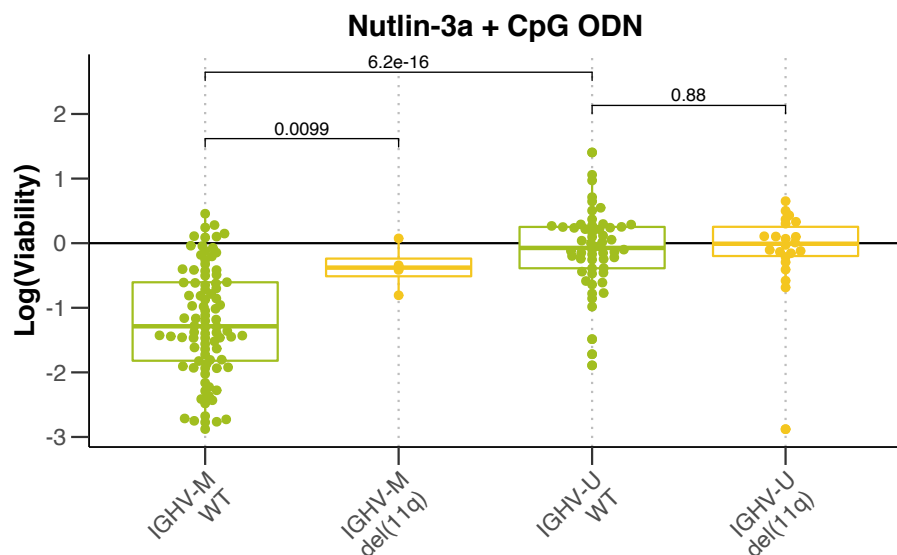


Figure 6.10: Beeswarm-boxplot showing control-normalised log transformed viability values, after treatment with CpG ODN (TLR9) and nutlin-3a (MDM2), stratified by del(11q) and IGHV status. WT indicates sample is not annotated as del(11q). p-values from Student's t-tests.

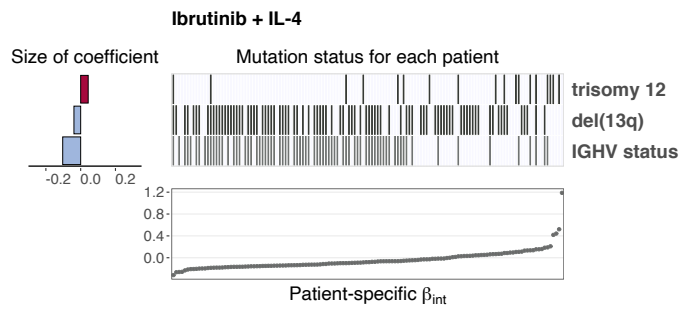


Figure 6.11: Predictor profile depicting genetic features that modulate the size of β_{int} between ibrutinib (BTK) and IL4. Plot generated as in Figure 6.7. See also Methods section 2.4.1. *Figure from Bruch and Giles et al. 2021.*

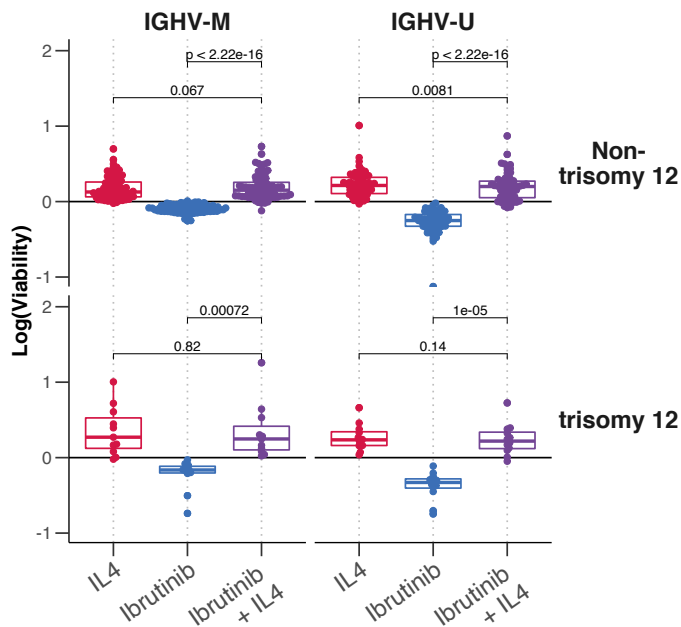


Figure 6.12: “Beeswarm-boxplots of log-transformed viability values for ibrutinib (BTK) and IL4 single and combinatorial treatments, faceted by IGHV status and trisomy 12 status. P-values from paired Student’s t-tests.” *Figure and caption from Bruch and Giles et al. 2021.*

Chapter 7

Discussion

“All models are wrong, but some are useful.”

— George E. P. Box

References

- 10 Abruzzo, Lynne V., Carmen D. Herling, George A. Calin, Christopher Oakes, Lynn L. Barron, Haley E. Banks, Vikram Katju, Michael J. Keating, and Kevin R. Coombes. 2018. “Trisomy 12 chronic lymphocytic leukemia expresses a unique set of activated and targetable pathways.” *Haematologica* 103 (12): 2069–78. <https://doi.org/10.3324/haematol.2018.190132>.
- Agathangelidis, Andreas, Nikos Darzentas, Anastasia Hadzidimitriou, Xavier Brochet, Fiona Murray, Xiao Jie Yan, Zadie Davis, et al. 2012. “Stereotyped B-cell receptors in one-third of chronic lymphocytic leukemia: A molecular classification with implications for targeted therapies.” *Blood* 119 (19): 4467–75. <https://doi.org/10.1182/blood-2011-11-393694>.
- Aguilar-Hernandez, Maria M, Matthew D Blunt, Rachel Dobson, Alison Yeomans, Stephen Thirdborough, Marta Larrayoz, Lindsay D Smith, et al. n.d. “IL-4 enhances expression and function of surface IgM in CLL cells.” <https://doi.org/10.1182/blood-2015-11>.
- Ahn, Inhye E, Mohammed Z H Farooqui, Xin Tian, Janet Valdez, Clare Sun, Susan Soto, Jennifer Lotter, et al. 2018. “Depth and durability of response to ibrutinib in CLL: 5-year follow-up of a phase 2 study.” *Blood* 131 (21): 2357–66. <https://doi.org/10.1182/blood-2017-12-820910>.
- Alexandrov, Ludmil B., Serena Nik-Zainal, David C. Wedge, Samuel A. J. R. Aparicio, Sam Behjati, Andrew V. Biankin, Graham R. Bignell, et al. 2013. “Signatures of mutational processes in human cancer.” *Nature* 500 (7463): 415–21. <https://doi.org/10.1038/nature12477>.
- Allen, Christopher D. C., and Jason G. Cyster. 2008. “Follicular dendritic cell networks of primary follicles and germinal centers: Phenotype and function.” *Seminars in Im-*

munology 20 (1): 14–25. <https://doi.org/10.1016/J.SMIM.2007.12.001>.

Amigo-Jiménez, Irene, Elvira Bailón, Noemí Aguilera-Montilla, María José Terol, José A García-Marco, and Angeles García-Pardo. 2015. “Bone marrow stroma-induced resistance of chronic lymphocytic leukemia cells to arsenic trioxide involves Mcl-1 up-regulation and is overcome by inhibiting the PI3K δ or PKC β signaling pathways.” *Oncotarget* 6 (42): 44832–48. <https://doi.org/10.18632/oncotarget.6265>.

Anda-Jáuregui, Guillermo de, and Enrique Hernández-Lemus. 2020. “Computational Oncology in the Multi-Omics Era: State of the Art.” *Frontiers*. <https://doi.org/10.3389/fonc.2020.00423>.

Argelaguet, Ricard, Britta Velten, Damien Arnol, Sascha Dietrich, Thorsten Zenz, John C Marioni, Florian Buettnner, Wolfgang Huber, and Oliver Stegle. 2018. “MultiOmics Factor Analysis—a framework for unsupervised integration of multiomics data sets.” *Molecular Systems Biology* 14 (6): e8124. <https://doi.org/10.15252/msb.20178124>.

Asslaber, Daniela, Eva M Grössinger, Tamara Girbl, Sebastian W Hofbauer, Alexander Egle, Lukas Weiss, Richard Greil, and Tanja N Hartmann. 2013. “Mimicking the microenvironment in chronic lymphocytic leukaemia - where does the journey go?” *Br J Haematol*. <https://doi.org/10.1111/bjh.12151>.

Austen, Belinda, Judith E Powell, Azra Alvi, Ian Edwards, Laura Hooper, Jane Starczynski, A Malcolm R Taylor, Christopher Fegan, Paul Moss, and Tatjana Stankovic. 2005. “Mutations in the ATM gene lead to impaired overall and treatment-free survival that is independent of IGVH mutation status in patients with B-CLL.” *Blood* 106 (9): 3175–82. <https://doi.org/10.1182/blood-2004-11-4516>.

Axelrod, M, Z Ou, L K Brett, L Zhang, E R Lopez, A T Tamayo, V Gordon, et al. 2014. “Combinatorial drug screening identifies synergistic co-targeting of Bruton’s tyrosine kinase and the proteasome in mantle cell lymphoma.” Nature Publishing Group. <https://doi.org/10.1038/leu.2013.249>.

Bagnara, Davide, Matthew S. Kaufman, Carlo Calissano, Sonia Marsilio, Piers E. M. Patten, Rita Simone, Philip Chum, et al. 2011. “A novel adoptive transfer model of chronic lymphocytic leukemia suggests a key role for T lymphocytes in the disease.” *Blood* 117 (20): 5463–72. <https://doi.org/10.1182/blood-2010-12-324210>.

Balatti, Veronica, Arianna Bottoni, Alexey Palamarchuk, Hansjuerg Alder, Laura Z. Rassenti, Thomas J. Kipps, Yuri Pekarsky, and Carlo M. Croce. 2012. “NOTCH1

mutations in CLL associated with trisomy 12.” *Blood* 119 (2): 329–31. <https://doi.org/10.1182/blood-2011-10-386144>.

Bankhead, Peter, Maurice B. Loughrey, José A. Fernández, Yvonne Dombrowski, Daragh G. McArt, Philip D. Dunne, Stephen McQuaid, et al. 2017. “QuPath: Open source software for digital pathology image analysis.” *Scientific Reports* 7 (1): 16878. <https://doi.org/10.1038/s41598-017-17204-5>.

Barretina, Jordi, Giordano Caponigro, Nicolas Stransky, Kavitha Venkatesan, Adam A. Margolin, Sungjoon Kim, Christopher J. Wilson, et al. 2012. “The Cancer Cell Line Encyclopedia enables predictive modelling of anticancer drug sensitivity.” *Nature* 483 (7391): 603–7. <https://doi.org/10.1038/nature11003>.

Basu, Amrita, Nicole E Bodycombe, Jaime H Cheah, Edmund V Price, Ke Liu, Giannina I Schaefer, Richard Y Ebright, et al. 2013. “XAn interactive resource to identify cancer genetic and lineage dependencies targeted by small molecules.” *Cell* 154 (5): 1151–61. <https://doi.org/10.1016/j.cell.2013.08.003>.

Baumann, Tycho, Riccardo Moia, Gianluca Gaidano, Julio Delgado, Adalgisa Condoluci, Neus Villamor, Anil Babu Payedimarri, et al. 2021. “Lymphocyte doubling time in chronic lymphocytic leukemia modern era: a real-life study in 848 unselected patients.” *Leukemia* 35 (8): 2325–31. <https://doi.org/10.1038/s41375-021-01149-w>.

Beekman, Renée, Vicente Chapaprieta, Núria Russiñol, Roser Vilarrasa-Blasi, Núria Verdaguer-Dot, Joost H. A. Martens, Martí Duran-Ferrer, et al. 2018. “The reference epigenome and regulatory chromatin landscape of chronic lymphocytic leukemia.” *Nature Medicine* 24 (6): 868–80. <https://doi.org/10.1038/s41591-018-0028-4>.

Benjamini, Yuval, and Terence P Speed. 2012. “Summarizing and correcting the GC content bias in high-throughput sequencing.” *Nucleic Acids Research* 40 (10): e72. <https://doi.org/10.1093/nar/gks001>.

Berest, Ivan, Christian Arnold, Armando Reyes-Palomares, Giovanni Palla, Kasper Dindler Rasmussen, Holly Amelia Rebecca Giles, Peter-Martin Bruch, et al. 2019. “Quantification of Differential Transcription Factor Activity and Multiomics-Based Classification into Activators and Repressors: diffTF.” *Cell Reports* 29 (10): 3147–3159.e12. <https://doi.org/10.1016/J.CELREP.2019.10.106>.

Bhattacharya, Nupur, Michaela Reichenzeller, Maiwen Caudron-Herger, Sarah Haebe, Nathan Brady, Susanne Diener, Maria Nothing, et al. 2015. “Loss of cooperativity of

secreted CD40L and increased dose-response to IL4 on CLL cell viability correlates with enhanced activation of NF- κ B and STAT6.” *International Journal of Cancer* 136 (1): 65–73. <https://doi.org/10.1002/ijc.28974>.

Bhoi, Sujata, Viktor Ljungström, Panagiotis Baliakas, Mattias Mattsson, Karin E Smedby, Gunnar Juliusson, Richard Rosenquist, and Larry Mansouri. 2016. *Epigenetics* 11 (6): 449–55. <https://doi.org/10.1080/15592294.2016.1178432>.

Binder, Mascha, Barbara Léchenne, Ramesh Ummanni, Christian Scharf, Stefan Balabanov, Maria Trusch, Hartmut Schlüter, Ingke Braren, Edzard Spillner, and Martin Trepel. 2010. “Stereotypical chronic lymphocytic leukemia B-cell receptors recognize survival promoting antigens on stromal cells.” *PLoS ONE* 5 (12): e15992. <https://doi.org/10.1371/journal.pone.0015992>.

Bolger, Anthony M, Marc Lohse, and Bjoern Usadel. 2014. “Genome analysis Trimmomatic: a flexible trimmer for Illumina sequence data” 30 (15): 2114–20. <https://doi.org/10.1093/bioinformatics/btu170>.

Borche, L, A Lim, JL Binet, and G Dighiero. 1990. “Evidence that chronic lymphocytic leukemia B lymphocytes are frequently committed to production of natural autoantibodies.” *Blood* 76 (3): 562–69. <https://doi.org/10.1182/blood.v76.3.562.562>.

Bosch, Francesc, and Riccardo Dalla-Favera. 2019. “Chronic lymphocytic leukaemia: from genetics to treatment.” *Nature Reviews. Clinical Oncology* 16 (11): 684–701. <https://doi.org/10.1038/s41571-019-0239-8>.

Bröker, Barbara M., Adek Klajman, Pierre Youinou, Jean Jouquan, Colin P. Worman, John Murphy, Lorna Mackenzie, et al. 1988. “Chronic lymphocytic leukemic (CLL) cells secrete multispecific autoantibodies.” *Journal of Autoimmunity* 1 (5): 469–81. [https://doi.org/10.1016/0896-8411\(88\)90068-6](https://doi.org/10.1016/0896-8411(88)90068-6).

Brown, Jennifer R, John C Byrd, Steven E Coutre, Don M Benson, Ian W Flinn, Nina D Wagner-Johnston, Stephen E Spurgeon, et al. 2014. “Idelalisib, an inhibitor of phosphatidylinositol 3-kinase p110 δ , for relapsed/refractory chronic lymphocytic leukemia.” *Blood* 123 (22): 3390–97. <https://doi.org/10.1182/blood-2013-11-535047>.

Bruch, Peter-Martin, Holly A. R. Giles, Carolin Kolb, Sophie A. Herbst, Tina Becirovic, Tobias Roider, Junyan Lu, et al. 2021. “Mapping drug-microenvironment-genetic interplay in CLL reveals trisomy 12 as a modulator of microenvironmental signals.”

bioRxiv Cancer Biology, July, 2021.07.23.453514. <https://doi.org/10.1101/2021.07.23.453514>.

Buenrostro, Jason D, Paul G Giresi, Lisa C Zaba, Howard Y Chang, and William J Greenleaf. 2013. “Transposition of native chromatin for fast and sensitive epigenomic profiling of open chromatin, DNA-binding proteins and nucleosome position.” *Nature Methods* 10 (12): 1213–18. <https://doi.org/10.1038/nmeth.2688>.

Burger, J A, N J Zvaifler, N Tsukada, G S Firestein, and T J Kipps. 2001. “Fibroblast-like synoviocytes support B-cell pseudoemperipoleisis via a stromal cell-derived factor-1- and CD106 (VCAM-1)-dependent mechanism.” *The Journal of Clinical Investigation* 107 (3): 305–15. <https://doi.org/10.1172/JCI11092>.

Burger, Jan A. 2020. “Treatment of Chronic Lymphocytic Leukemia.” Edited by Dan L. Longo. *New England Journal of Medicine* 383 (5): 460–73. <https://doi.org/10.1056/NEJMra1908213>.

Burger, Jan A., Meike Burger, and Thomas J. Kipps. 1999. “Chronic Lymphocytic Leukemia B Cells Express Functional Cxcr4 Chemokine Receptors That Mediate Spontaneous Migration Beneath Bone Marrow Stromal Cells.” *Blood* 94 (11): 3658–67. <https://doi.org/10.1182/BLOOD.V94.11.3658>.

Burger, Jan A, and Nicholas Chiorazzi. 2013. “B cell receptor signaling in chronic lymphocytic leukemia.” *Trends Immunol.* <https://doi.org/10.1016/j.it.2013.07.002>.

Burger, Jan A, and John G Gribben. 2014. “The microenvironment in chronic lymphocytic leukemia (CLL) and other B cell malignancies: insight into disease biology and new targeted therapies.” *Seminars in Cancer Biology* 24 (February): 71–81. <https://doi.org/10.1016/j.semcancer.2013.08.011>.

Burger, Jan A., Nobuhiro Tsukada, Meike Burger, Nathan J. Zvaifler, Marie Dell’Aquila, and Thomas J. Kipps. 2000. “Blood-derived nurse-like cells protect chronic lymphocytic leukemia B cells from spontaneous apoptosis through stromal cell-derived factor-1.” *Blood* 96 (8): 2655–63. <https://doi.org/10.1182/BLOOD.V96.8.2655>.

Burger, Meike, Tanja Hartmann, Myriam Krome, Justyna Rawluk, Hirokazu Tamamura, Nobutaka Fujii, Thomas J. Kipps, and Jan A. Burger. 2005. “Small peptide inhibitors of the CXCR4 chemokine receptor (CD184) antagonize the activation, migration, and antiapoptotic responses of CXCL12 in chronic lymphocytic leukemia B cells.” *Blood*

106 (5): 1824–30. <https://doi.org/10.1182/blood-2004-12-4918>.

Bürkle, Andrea, Matthias Niedermeier, Annette Schmitt-Gräff, William G. Wierda, Michael J. Keating, and Jan A. Burger. 2007. “Overexpression of the CXCR5 chemokine receptor, and its ligand, CXCL13 in B-cell chronic lymphocytic leukemia.” *Blood* 110 (9): 3316–25. <https://doi.org/10.1182/blood-2007-05-089409>.

Buschle, M, D Campana, S R Carding, C Richard, A V Hoffbrand, and M K Brenner. 1993. “Interferon gamma inhibits apoptotic cell death in B cell chronic lymphocytic leukemia.” *The Journal of Experimental Medicine* 177 (1): 213–18. <https://doi.org/10.1084/jem.177.1.213>.

Byrd, John C., Jennifer R. Brown, Susan O’Brien, Jacqueline C. Barrientos, Neil E. Kay, Nishitha M. Reddy, Steven Coutre, et al. 2014. “Ibrutinib versus Ofatumumab in Previously Treated Chronic Lymphoid Leukemia.” *New England Journal of Medicine* 371 (3): 213–23. <https://doi.org/10.1056/nejmoa1400376>.

Byrd, John C, Richard R Furman, Steven E Coutre, Ian W Flinn, Jan A Burger, Kristie A Blum, Barbara Grant, et al. 2013. “Targeting BTK with ibrutinib in relapsed chronic lymphocytic leukemia.” *The New England Journal of Medicine* 369 (1): 32–42. <https://doi.org/10.1056/NEJMoa1215637>.

Cahill, N, A. C. Bergh, M Kanduri, H Göransson-Kultima, L Mansouri, A Isaksson, F Ryan, et al. 2013. “450K-array analysis of chronic lymphocytic leukemia cells reveals global DNA methylation to be relatively stable over time and similar in resting and proliferative compartments.” *Leukemia* 27 (1): 150–58. <https://doi.org/10.1038/leu.2012.245>.

Calin, George Adrian, Calin Dan Dumitru, Masayoshi Shimizu, Roberta Bichi, Simona Zupo, Evan Noch, Hansjuerg Aldler, et al. 2002. “Frequent deletions and down-regulation of micro-RNA genes miR15 and miR16 at 13q14 in chronic lymphocytic leukemia.” *Proceedings of the National Academy of Sciences of the United States of America* 99 (24): 15524–29. <https://doi.org/10.1073/pnas.242606799>.

Campbell, Belinda A, Julia J Scarsbrick, Youn H Kim, Ryan A Wilcox, Christopher McCormack, and H Miles Prince. 2020. “Time to next treatment as a meaningful endpoint for trials of primary cutaneous lymphoma.” *Cancers* 12 (8): 1–11. <https://doi.org/10.3390/cancers12082311>.

Care, Matthew A, Mario Cocco, Jon P Laye, Nicholas Barnes, Yuanxue Huang, Ming

- Wang, Sharon Barrans, et al. 2014. "SPIB and BATF provide alternate determinants of IRF4 occupancy in diffuse large B-cell lymphoma linked to disease heterogeneity." *Nucleic Acids Research* 42 (12): 7591–7610. <https://doi.org/10.1093/nar/gku451>.
- Carey, Alyssa, David K Edwards, Christopher A Eide, Laura Newell, Elie Traer, Bruno C Medeiros, Daniel A Pollyea, et al. 2017. "Identification of Interleukin-1 by Functional Screening as a Key Mediator of Cellular Expansion and Disease Progression in Acute Myeloid Leukemia." *Cell Reports* 18 (13): 3204–18. <https://doi.org/10.1016/j.celrep.2017.03.018>.
- Chan, Chun Hin, Celestia Fang, Anna Yarilina, Rab K Prinjha, Yu Qiao, and Lionel B Ivashkiv. 2015. "BET bromodomain inhibition suppresses transcriptional responses to cytokine-Jak-STAT signaling in a gene-specific manner in human monocytes." *European Journal of Immunology* 45 (1): 287–97. <https://doi.org/10.1002/eji.201444862>.
- Chang, Julie Elizabeth, and Brad Steven Kahl. 2012. "Bendamustine for treatment of chronic lymphocytic leukemia." *Expert Opinion on Pharmacotherapy* 13 (10): 1495–505. <https://doi.org/10.1517/14656566.2012.693163>.
- Chatzouli, Maria, Stavroula Ntoufa, Nikos Papakonstantinou, Elisavet Chartomatsidou, Achilles Anagnostopoulos, Panagoula Kollia, Paolo Ghia, Marta Muzio, Kostas Stamatakopoulos, and Chrysoula Belessi. 2014. "Heterogeneous Functional Effects of Concomitant B Cell Receptor and TLR Stimulation in Chronic Lymphocytic Leukemia with Mutated versus Unmutated Ig Genes." *The Journal of Immunology* 192 (10): 4518–24. <https://doi.org/10.4049/jimmunol.1302102>.
- Cheng, S, J Ma, A Guo, P Lu, J P Leonard, M Coleman, M Liu, J J Buggy, R R Furman, and Y L Wang. 2014. "BTK inhibition targets in vivo CLL proliferation through its effects on B-cell receptor signaling activity." *Leukemia* 28 (3): 649–57. <https://doi.org/10.1038/leu.2013.358>.
- Chiorazzi, Nicholas, and Manlio Ferrarini. 2003. "B cell chronic lymphocytic leukemia: Lessons learned from studies of the B cell antigen receptor." Annual Reviews 4139 El Camino Way, P.O. Box 10139, Palo Alto, CA 94303-0139, USA. <https://doi.org/10.1146/annurev.immunol.21.120601.141018>.
- Chiorazzi, Nicholas, Kanti R Rai, and Manlio Ferrarini. 2005. "Chronic lymphocytic leukemia." *The New England Journal of Medicine* 352 (8): 804–15. <https://doi.org/10.1056/NEJMoa043612>.

org/10.1056/NEJMra041720.

Chu, Charles C., Rosa Catera, Katerina Hatzi, Xiao Jie Yan, Lu Zhang, Xiao Bo Wang, Henry M. Fales, et al. 2008. "Chronic lymphocytic leukemia antibodies with a common stereotypic rearrangement recognize nonmuscle myosin heavy chain IIA." *Blood* 112 (13): 5122–29. <https://doi.org/10.1182/blood-2008-06-162024>.

Chung, James B., Michael Silverman, and John G. Monroe. 2003. "Transitional B cells: step by step towards immune competence." *Trends in Immunology* 24 (6): 342–48. [https://doi.org/10.1016/S1471-4906\(03\)00119-4](https://doi.org/10.1016/S1471-4906(03)00119-4).

Cimmino, Amelia, George Adrian Calin, Muller Fabbri, Marilena V Iorio, Manuela Fer-racin, Masayoshi Shimizu, Sylwia E Wojcik, et al. 2005. "miR-15 and miR-16 induce apoptosis by targeting BCL2." *Proceedings of the National Academy of Sciences of the United States of America* 102 (39): 13944–49. <https://doi.org/10.1073/pnas.0506654102>.

Collins, Russell J., Louise A. Verschuer, Brian V. Harmon, Roger L. Prentice, John H. Pope, and John F. R. Kerr. 1989. "Spontaneous programmed death (apoptosis) of Bchronic lymphocytic leukaemia cells following their culture in vitro." *British Journal of Haematology* 71 (3): 343–50. <https://doi.org/10.1111/j.1365-2141.1989.tb04290.x>.

Crassini, Kyle, Yandong Shen, Stephen Mulligan, and O. Giles Best. 2017. "Modeling the chronic lymphocytic leukemia microenvironment in vitro." Taylor & Francis. <https://doi.org/10.1080/10428194.2016.1204654>.

Crompt, Emerence, Michael Van Damme, Karlien Pieters, Marjorie Vermeersch, David Perez-Morga, Philippe Mineur, Marie Maerevoet, et al. 2017. "Extracellular vesicles of bone marrow stromal cells rescue chronic lymphocytic leukemia B cells from apoptosis, enhance their migration and induce gene expression modifications." *Haematologica* 102 (9): 1594–604. <https://doi.org/10.3324/haematol.2016.163337>.

Damle, Rajendra N., Tarun Wasil, Franco Fais, Fabio Ghiotto, Angelo Valetto, Steven L. Allen, Aby Buchbinder, et al. 1999. "Ig V Gene Mutation Status and CD38 Expression As Novel Prognostic Indicators in Chronic Lymphocytic Leukemia." *Blood* 94 (6): 1840–47. <https://doi.org/10.1182/BLOOD.V94.6.1840>.

Dancescu, M, M Rubio-Trujillo, G Biron, D Bron, G Delespesse, and M Sarfati. 1992. "Interleukin 4 protects chronic lymphocytic leukemic B cells from death by apoptosis

and upregulates Bcl-2 expression.” *The Journal of Experimental Medicine* 176 (5): 1319–26. <https://doi.org/10.1084/jem.176.5.1319>.

De Rooij, Martin F. M., Annemieke Kuil, Christian R Geest, Eric Eldering, Betty Y Chang, Joseph J Buggy, Steven T Pals, and Marcel Spaargaren. 2012. “The clinically active BTK inhibitor PCI-32765 targets B-cell receptor- and chemokine-controlled adhesion and migration in chronic lymphocytic leukemia.” *Blood* 119 (11): 2590–94. <https://doi.org/10.1182/blood-2011-11-390989>.

Deaglio, Silvia, and Fabio Malavasi. 2009. “Chronic lymphocytic leukemia microenvironment: Shifting the balance from apoptosis to proliferation.” <https://doi.org/10.3324/haematol.2009.006676>.

Decker, Thomas, Christian Bogner, Madlen Oelsner, Christian Peschel, and Ingo Ringshausen. 2010. “Antiapoptotic effect of interleukin-2 (IL-2) in B-CLL cells with low and high affinity IL-2 receptors.” *Annals of Hematology* 89 (11): 1125–32. <https://doi.org/10.1007/s00277-010-0994-1>.

Defoiche, Julien, Christophe Debacq, Becca Asquith, Yan Zhang, Arsène Burny, Dominique Bron, Laurence Lagneaux, Derek Macallan, and Luc Willems. 2008. “Reduction of B cell turnover in chronic lymphocytic leukaemia.” *British Journal of Haematology* 143 (2): 240–47. <https://doi.org/10.1111/j.1365-2141.2008.07348.x>.

Del Giudice, Ilaria, Davide Rossi, Sabina Chiaretti, Marilisa Marinelli, Simona Tavolaro, Sara Gabrielli, Luca Laurenti, et al. 2012. “NOTCH1 mutations in +12 chronic lymphocytic leukemia (CLL) confer an unfavorable prognosis, induce a distinctive transcriptional profiling and refine the intermediate prognosis of +12 CLL.” *Haematologica* 97 (3): 437–41. <https://doi.org/10.3324/haematol.2011.060129>.

Delgado, Amanda, and Achuta Kumar Guddati. 2021. “Clinical endpoints in oncology - a primer.” *American Journal of Cancer Research* 11 (4): 1121–31. <http://www.ncbi.nlm.nih.gov/pubmed/33948349%20http://www.ncbi.nlm.nih.gov/pmc/articles/PMC8085844/>.

Dicker, F, H Herholz, S Schnittger, A Nakao, N Patten, L Wu, W Kern, T Haferlach, and C Haferlach. 2009. “The detection of TP53 mutations in chronic lymphocytic leukemia independently predicts rapid disease progression and is highly correlated with a complex aberrant karyotype.” *Leukemia* 23 (1): 117–24. <https://doi.org/10.1038/leu.2008.274>.

- Dietrich, Sascha, Magorzata Ole, Junyan Lu, Leopold Sellner, Simon Anders, Britta Velten, Bian Wu, et al. 2017. “Drug-perturbation-based stratification of blood cancer.” *Journal of Clinical Investigation* 128 (1): 427–45. <https://doi.org/10.1172/JCI93801>.
- Ding, Wei, Grzegorz S. Nowakowski, Traci R. Knox, Justin C. Boysen, Mary L. Maas, Susan M. Schwager, Wenting Wu, et al. 2009. “Bi-directional activation between mesenchymal stem cells and CLL B-cells: implication for CLL disease progression.” *British Journal of Haematology* 147 (4): 471–83. <https://doi.org/10.1111/j.1365-2141.2009.07868.x>.
- Döhner, Hartmut, Konstanze Fischer, Martin Bentz, Katrin Hansen, Axel Benner, Georges Cabot, Daniela Diehl, et al. 1995. “p53 Gene Deletion Predicts for Poor Survival and Non-Response to Therapy With Purine Analogs in Chronic B-Cell Leukemias.” *Blood* 85 (6): 1580–89. <https://doi.org/10.1182/BLOOD.V85.6.1580.BLOODJOURNAL8561580>.
- Döhner, H, Stephan Stilgenbauer, Axel Benner, Elke Leupolt, Alexander Kröber, Lars Bullinger, Konstanze Döhner, Martin Bentz, and Peter Lichter. 2000. “Genomic aberrations and survival in chronic lymphocytic leukemia.” *The New England Journal of Medicine* 343 (26): 1910–16. <https://doi.org/10.1056/NEJM200012283432602>.
- Dolgalev, Igor. 2021. *Msigdbr: MSigDB Gene Sets for Multiple Organisms in a Tidy Data Format*. <https://igordot.github.io/msigdbr/>.
- Du, W, and O Elemento. 2015. “Cancer systems biology: Embracing complexity to develop better anticancer therapeutic strategies.” *Oncogene* 34 (25): 3215–25. <https://doi.org/10.1038/onc.2014.291>.
- Dubois, Nathan, Emerence Cromptot, Nathalie Meuleman, Dominique Bron, Laurence Lagneaux, and Basile Stamatopoulos. 2020. “Importance of Crosstalk Between Chronic Lymphocytic Leukemia Cells and the Stromal Microenvironment: Direct Contact, Soluble Factors, and Extracellular Vesicles.” Frontiers Media SA. <https://doi.org/10.3389/fonc.2020.01422>.
- Edgar, Ron, Michael Domrachev, and Alex E. Lash. 2002. “Gene Expression Omnibus: NCBI gene expression and hybridization array data repository.” *Nucleic Acids Research* 30 (1): 207–10. <https://doi.org/10.1093/nar/30.1.207>.
- Elston, Lauren, Chris Fegan, Robert Hills, Shaikh S Hashimdeen, Elisabeth Walsby, Peter Henley, Chris Pepper, and Stephen Man. 2020. “Increased frequency of CD4+

PD-1+ HLA-DR+ T cells is associated with disease progression in CLL." *British Journal of Haematology* 188 (6): 872–80. <https://doi.org/10.1111/bjh.16260>.

Enzler, Thomas, Arnon P Kater, Weizhou Zhang, George F Widhopf, Han Yu Chuang, Jason Lee, Esther Avery, Carlo M Croce, Michael Karin, and Thomas J Kipps. 2009. "Chronic lymphocytic leukemia of E μ -TCL1 transgenic mice undergoes rapid cell turnover that can be offset by extrinsic CD257 to accelerate disease progression." *Blood* 114 (20): 4469–76. <https://doi.org/10.1182/blood-2009-06-230169>.

Fabbri, Giulia, and Riccardo Dalla-Favera. 2016. "The molecular pathogenesis of chronic lymphocytic leukaemia." *Nat Rev Cancer*. <https://doi.org/10.1038/nrc.2016.8>.

Fabbri, Giulia, Silvia Rasi, Davide Rossi, Vladimir Trifonov, Hossein Khiabanian, Jing Ma, Adina Grunn, et al. 2011. "Analysis of the chronic lymphocytic leukemia coding genome: Role of NOTCH1 mutational activation." *Journal of Experimental Medicine* 208 (7): 1389–1401. <https://doi.org/10.1084/jem.20110921>.

Fais, Franco, Fabio Ghiotto, Shiori Hashimoto, Brian Sellars, Angelo Valetto, Steven L Allen, Philip Schulman, et al. 1998. "Chronic lymphocytic leukemia B cells express restricted sets of mutated and unmutated antigen receptors." *Journal of Clinical Investigation* 102 (8): 1515–25. <https://doi.org/10.1172/JCI3009>.

Farinello, Diego, Monika Woziska, Elisa Lenti, Luca Genovese, Silvia Bianchetti, Edoardo Migliori, Nicolò Sacchetti, et al. 2018. "A retinoic acid-dependent stroma-leukemia crosstalk promotes chronic lymphocytic leukemia progression." *Nature Communications* 9 (1): 1787. <https://doi.org/10.1038/s41467-018-04150-7>.

Fedorchenko, Oleg, Marius Stiefelhagen, Abdul A. Peer-Zada, Romy Barthel, Petra Mayer, Laura Eckei, Alexandra Breuer, et al. 2013. "CD44 regulates the apoptotic response and promotes disease development in chronic lymphocytic leukemia." *Blood* 121 (20): 4126–36. <https://doi.org/10.1182/blood-2012-11-466250>.

Ferreira, Pedro G, Pedro Jares, Daniel Rico, Gonzalo Gómez-López, Alejandra Martínez-Trillo, Neus Villamor, Simone Ecker, et al. 2014. "Transcriptome characterization by RNA sequencing identifies a major molecular and clinical subdivision in chronic lymphocytic leukemia." *Genome Research* 24 (2): 212–26. <https://doi.org/10.1101/gr.152132.112>.

Fischer, Ute, Jun J. Yang, Tomokatsu Ikawa, Daniel Hein, Carolina Vicente-Dueñas,

- Arndt Borkhardt, and Isidro Sánchez-García. 2020. “Cell Fate Decisions: The Role of Transcription Factors in Early B-cell Development and Leukemia.” *Blood Cancer Discovery* 1 (3): 224–33. <https://doi.org/10.1158/2643-3230.bcd-20-0011>.
- Fonte, Eleonora, Benedetta Apollonio, Lydia Scarfò, Pamela Ranghetti, Claudia Fazi, Paolo Ghia, Federico Caligaris-Cappio, and Marta Muzio. 2013. “In vitro sensitivity of CLL cells to fludarabine may be modulated by the stimulation of Toll-like receptors.” *Clinical Cancer Research : An Official Journal of the American Association for Cancer Research* 19 (2): 367–79. <https://doi.org/10.1158/1078-0432.CCR-12-1922>.
- Friedberg, Jonathan W, Jeff Sharman, John Sweetenham, Patrick B Johnston, Julie M Vose, Ann LaCasce, Julia Schaefer-Cutillo, et al. 2010. “Inhibition of Syk with fostamatinib disodium has significant clinical activity in non-Hodgkin lymphoma and chronic lymphocytic leukemia.” *Blood* 115 (13): 2578–85. <https://doi.org/10.1182/blood-2009-08-236471>.
- Friedman, Jerome, Trevor Hastie, Rob Tibshirani, Balasubramanian Narasimhan, Kenneth Tay, and Noah Simon. 2021. *Glmnet: Lasso and Elastic-Net Regularized Generalized Linear Models*. <https://CRAN.R-project.org/package=glmnet>.
- Furman, Richard R, Jeff P Sharman, Steven E Coutre, Bruce D Cheson, John M Pagel, Peter Hillmen, Jacqueline C Barrientos, et al. 2014. “Idelalisib and Rituximab in Relapsed Chronic Lymphocytic Leukemia.” *New England Journal of Medicine* 370 (11): 997–1007. <https://doi.org/10.1056/nejmoa1315226>.
- Gaiti, Federico, Ronan Chaligne, Hongcang Gu, Ryan M Brand, Steven Kothen-Hill, Rafael C Schulman, Kirill Grigorev, et al. 2019. “Epigenetic evolution and lineage histories of chronic lymphocytic leukaemia.” *Nature* 569 (7757): 576–80. <https://doi.org/10.1038/s41586-019-1198-z>.
- Garnett, Mathew J., Elena J. Edelman, Sonja J. Heidorn, Chris D. Greenman, Anahita Dastur, King Wai Lau, Patricia Greninger, et al. 2012. “Systematic identification of genomic markers of drug sensitivity in cancer cells.” *Nature* 483 (7391): 570–75. <https://doi.org/10.1038/nature11005>.
- Garrett-Sinha, Lee Ann, Richard Dahl, Sridhar Rao, Kevin P. Barton, and M. Celeste Simon. 2001. “PU.1 exhibits partial functional redundancy with Spi-B, but not with Ets-1 or Elf-1.” *Blood* 97 (9): 2908–12. <https://doi.org/10.1182/blood.V97.9.2908>.

- Ghia, Paolo, Andrzej Pluta, Małgorzata Wach, Daniel Lysak, Tomas Kozak, Martin Simkovic, Polina Kaplan, et al. 2020. "Ascend: Phase III, randomized trial of acalabrutinib versus idelalisib plus rituximab or bendamustine plus rituximab in relapsed or refractory chronic lymphocytic leukemia." In *Journal of Clinical Oncology*, 38:2849–61. 25. J Clin Oncol. <https://doi.org/10.1200/JCO.19.03355>.
- Gimenez, Neus, Rupal Tripathi, Ariadna Giró, Laia Rosich, Mònica López-Guerra, Irene López-Oreja, Heribert Playa-Albinyana, et al. 2020. "Systems biology drug screening identifies statins as enhancers of current therapies in chronic lymphocytic leukemia." *Scientific Reports* 10 (1): 22153. <https://doi.org/10.1038/s41598-020-78315-0>.
- Goede, Valentin, Kirsten Fischer, Raymonde Busch, Anja Engelke, Barbara Eichhorst, Clemens M. Wendtner, Tatiana Chagorova, et al. 2014. "Obinutuzumab plus Chlorambucil in Patients with CLL and Coexisting Conditions." *New England Journal of Medicine* 370 (12): 1101–10. <https://doi.org/10.1056/nejmoa1313984>.
- Gonzalez, David, Pilar Martinez, Rachel Wade, Sarah Hockley, David Oscier, Estella Matutes, Claire E Dearden, Sue M Richards, Daniel Catovsky, and Gareth J Morgan. 2011. "Mutational status of the TP53 gene as a predictor of response and survival in patients with chronic lymphocytic leukemia: Results from the LRF CLL4 trial." *Journal of Clinical Oncology* 29 (16): 2223–29. <https://doi.org/10.1200/JCO.2010.32.0838>.
- Goodspeed, Andrew, Laura M Heiser, Joe W Gray, and James C Costello. 2016. "Tumor-Derived Cell Lines as Molecular Models of Cancer Pharmacogenomics." *Molecular Cancer Research : MCR* 14 (1): 3–13. <https://doi.org/10.1158/1541-7786.MCR-15-0189>.
- Granziero, Luisa, Paolo Ghia, Paola Circosta, Daniela Gottardi, Giuliana Strola, Massimo Geuna, Licia Montagna, Paola Piccoli, Marco Chilosi, and Federico Caligaris-Cappio. 2001. "Survivin is expressed on CD40 stimulation and interfaces proliferation and apoptosis in B-cell chronic lymphocytic leukemia." *Blood* 97 (9): 2777–83. <https://doi.org/10.1182/blood.V97.9.2777>.
- Grioni, Matteo, Arianna Brevi, Elena Cattaneo, Alessandra Rovida, Jessica Bordini, Maria Teresa Sabrina Bertilaccio, Maurilio Ponzoni, et al. 2021. "CD4+ T cells sustain aggressive chronic lymphocytic leukemia in E_{μ} -TCL1 mice through a CD40L-independent mechanism." *Blood Advances* 5 (14): 2817–28. <https://doi.org/10.1182/bloodadvances.2020003795>.

- Guarini, Anna, Sabina Chiaretti, Simona Tavolaro, Roberta Maggio, Nadia Peragine, Franca Citarella, Maria Rosaria Ricciardi, et al. 2008. "BCR ligation induced by IgM stimulation results in gene expression and functional changes only in IgVH unmutated chronic lymphocytic leukemia (CLL) cells." *Blood* 112 (3): 782–92. <https://doi.org/10.1182/blood-2007-12-127688>.
- Guo, Ailin, Pin Lu, Greg Coffey, Pamela Conley, Anjali Pandey, and Y Lynn Wang. 2017. "Dual SYK/JAK inhibition overcomes ibrutinib resistance in chronic lymphocytic leukemia: Cerdulatinib, but not ibrutinib, induces apoptosis of tumor cells protected by the microenvironment." *Oncotarget* 8 (8): 12953–67. <https://doi.org/10.18632/oncotarget.14588>.
- Guruharsha, K. G., Mark W. Kankel, and Spyros Artavanis-Tsakonas. 2012. "The Notch signalling system: Recent insights into the complexity of a conserved pathway." Nature Publishing Group. <https://doi.org/10.1038/nrg3272>.
- Hallek, M, K Fischer, G Fingerle-Rowson, A M Fink, R Busch, J Mayer, M Hensel, et al. 2010. "Addition of rituximab to fludarabine and cyclophosphamide in patients with chronic lymphocytic leukaemia: A randomised, open-label, phase 3 trial." *The Lancet* 376 (9747): 1164–74. [https://doi.org/10.1016/S0140-6736\(10\)61381-5](https://doi.org/10.1016/S0140-6736(10)61381-5).
- Hallek, Michael, Bruce D Cheson, Daniel Catovsky, Federico Caligaris-Cappio, Guillaume Dighiero, Hartmut Döhner, Peter Hillmen, et al. 2008. "Guidelines for the diagnosis and treatment of chronic lymphocytic leukemia: a report from the International Workshop on Chronic Lymphocytic Leukemia updating the National Cancer Institute-Working Group 1996 guidelines." *Blood* 111 (12): 5446–56. <https://doi.org/10.1182/blood-2007-06-093906>.
- Hamblin, Terry J., Zadie Davis, Anne Gardiner, David G. Oscier, and Freda K. Stevenson. 1999. "Unmutated Ig VH Genes Are Associated With a More Aggressive Form of Chronic Lymphocytic Leukemia." *Blood* 94 (6): 1848–54. <https://doi.org/10.1182/BLOOD.V94.6.1848>.
- Hamilton, Emma, Laurence Pearce, Liam Morgan, Sophie Robinson, Vicki Ware, Paul Brennan, N Shaun B Thomas, et al. 2012. "Mimicking the tumour microenvironment: Three different co-culture systems induce a similar phenotype but distinct proliferative signals in primary chronic lymphocytic leukaemia cells." *British Journal of Haematology* 158 (5): 589–99. <https://doi.org/10.1111/j.1365-2141.2012.09191.x>.

- Hayden, Rachel E, Guy Pratt, Claudia Roberts, Mark T Drayson, and Chris M Bunce. 2012. "Treatment of chronic lymphocytic leukemia requires targeting of the protective lymph node environment with novel therapeutic approaches." *Leuk Lymphoma*. <https://doi.org/10.3109/10428194.2011.610014>.
- Herbst, Sophie. 2020. "Systematic analysis of cell-intrinsic and extrinsic factors in chronic lymphocytic leukemia to understand functional consequences for drug response and clinical outcome." PhD diss., University of Heidelberg. <https://archiv.ub.uni-heidelberg.de/volltextserver/27438/1/Doktorarbeit.pdf>.
- Herishanu, Yair, Patricia Pérez-Galán, Delong Liu, Angélique Biancotto, Stefania Pitaluga, Berengere Vire, Federica Gibellini, et al. 2011. "The lymph node microenvironment promotes B-cell receptor signaling, NF- κ B activation, and tumor proliferation in chronic lymphocytic leukemia." *Blood* 117 (2): 563–74. <https://doi.org/10.1182/blood-2010-05-284984>.
- Herman, Sarah E. M., Amber L. Gordon, Erin Hertlein, Asha Ramanunni, Xiaoli Zhang, Samantha Jaglowski, Joseph Flynn, et al. 2011. "Bruton tyrosine kinase represents a promising therapeutic target for treatment of chronic lymphocytic leukemia and is effectively targeted by PCI-32765." *Blood* 117 (23): 6287–96. <https://doi.org/10.1182/blood-2011-01-328484>.
- Hernández-Lemus, Enrique. 2013. "Further steps toward functional systems biology of cancer." *Frontiers in Physiology* 4 SEP: 256. <https://doi.org/10.3389/fphys.2013.00256>.
- . 2014. "Systems Biology and Integrative Omics in Breast Cancer," 333–52. https://doi.org/10.1007/978-81-322-0843-3_17.
- Herndon, T M, S-S Chen, N S Saba, J Valdez, C Emson, M Gatmaitan, X Tian, et al. 2017. "Direct *in vivo* evidence for increased proliferation of CLL cells in lymph nodes compared to bone marrow and peripheral blood." *Leukemia* 31 (6): 1340–47. <https://doi.org/10.1038/leu.2017.11>.
- Hervé, Maxime, Kai Xu, Yen Shing Ng, Hedda Wardemann, Emilia Albesiano, Bradley T Messmer, Nicholas Chiorazzi, and Eric Meffre. 2005. "Unmutated and mutated chronic lymphocytic leukemias derive from self-reactive B cell precursors despite expressing different antibody reactivity." *Journal of Clinical Investigation* 115 (6): 1636–43. <https://doi.org/10.1172/JCI24387>.

- Hillmen, Peter, Tadeusz Robak, Ann Janssens, K Govind Babu, Janusz Kloczko, Sebastian Grosicki, Michael Doubek, et al. 2015. "Chlorambucil plus ofatumumab versus chlorambucil alone in previously untreated patients with chronic lymphocytic leukaemia (COMPLEMENT 1): a randomised, multicentre, open-label phase 3 trial." *Lancet (London, England)* 385 (9980): 1873–83. [https://doi.org/10.1016/S0140-6736\(15\)60027-7](https://doi.org/10.1016/S0140-6736(15)60027-7).
- Hoellenriegel, Julia, Sarah A Meadows, Mariela Sivina, William G Wierda, Hagop Kantarjian, Michael J Keating, Neill Giese, et al. 2011. "The phosphoinositide 3-kinase delta inhibitor, CAL-101, inhibits B-cell receptor signaling and chemokine networks in chronic lymphocytic leukemia." *Blood* 118 (13): 3603–12. <https://doi.org/10.1182/blood-2011-05-352492>.
- Hothorn, Torsten. 2017. *Maxstat: Maximally Selected Rank Statistics*. <https://CRAN.R-project.org/package=maxstat>.
- Huber, Wolfgang, Vincent J Carey, Robert Gentleman, Simon Anders, Marc Carlson, Benilton S Carvalho, Hector Corrada Bravo, et al. 2015. "Orchestrating high-throughput genomic analysis with Bioconductor." *Nature Methods* 12 (2): 115–21. <https://doi.org/10.1038/nmeth.3252>.
- Huber, Wolfgang, and Susan Holmes. 2019. "Modern Statistics for Modern Biology." <https://www.huber.embl.de/msmb/index.html>.
- Iacovelli, Stefano, Eva Hug, Sara Bennardo, Marcus Duehren-Von Minden, Stefania Gobessi, Andrea Rinaldi, Mirza Suljagic, et al. 2015. "Two types of BCR interactions are positively selected during leukemia development in the E μ -TCL1 transgenic mouse model of CLL." *Blood* 125 (10): 1578–88. <https://doi.org/10.1182/blood-2014-07-587790>.
- Iorio, Francesco, Theo A Knijnenburg, Daniel J Vis, Graham R Bignell, Michael P Menden, Michael Schubert, Nanne Aben, et al. 2016. "A Landscape of Pharmacogenomic Interactions in Cancer." *Cell* 166 (3): 740–54. <https://doi.org/10.1016/j.cell.2016.06.017>.
- Jassal, Bijay, Lisa Matthews, Guilherme Viteri, Chuqiao Gong, Pascual Lorente, Antonio Fabregat, Konstantinos Sidiropoulos, et al. 2020. "The reactome pathway knowledgebase." *Nucleic Acids Research* 48 (D1): D498–503. <https://doi.org/10.1093/nar/gkz1031>.

- Jayappa, Kallesh D., Konrad J. Cios, Vicki L. Gordon, Puja C. Arora, Timothy P. Bender, Michael E. Williams, Craig A. Portell, and Michael J. Weber. 2018. "A Multi-Drug Tolerant Phenotype Is Induced By Diverse Microenvironmental Agonists in Chronic Lymphocytic Leukemia and Mantle Cell Lymphoma." *Blood* 132 (Supplement 1): 4120–20. <https://doi.org/10.1182/blood-2018-99-119521>.
- Jayappa, Kallesh D, Craig A Portell, Vicki L Gordon, Brian J Capaldo, Stefan Bekiranov, Mark J Axelrod, L Kyle Brett, et al. 2017. "Microenvironmental agonists generate de novo phenotypic resistance to combined ibrutinib plus venetoclax in CLL and MCL." *Blood Advances* 1 (14): 933–46. <https://doi.org/10.1182/bloodadvances.2016004176>.
- Jensen, Caleb, and Yong Teng. 2020. "Is It Time to Start Transitioning From 2D to 3D Cell Culture?" *Frontiers*. <https://doi.org/10.3389/fmolb.2020.00033>.
- Kalachikov, S, A Migliazza, E Cayanis, N S Fracchiolla, M F Bonaldo, L Lawton, P Jelenc, et al. 1997. "Cloning and gene mapping of the chromosome 13q14 region deleted in chronic lymphocytic leukemia." *Genomics* 42 (3): 369–77. <https://doi.org/10.1006/geno.1997.4747>.
- Kanehisa, Minoru, Susumu Goto, Miho Furumichi, Mao Tanabe, and Mika Hirakawa. 2010. "KEGG for representation and analysis of molecular networks involving diseases and drugs." *Nucleic Acids Research* 38 (suppl_1): D355–60. <https://doi.org/10.1093/nar/gkp896>.
- Kassambara, Alboukadel, Marcin Kosinski, and Przemyslaw Biecek. 2021. *Survminer: Drawing Survival Curves Using Ggplot2*. <https://rpkgs.datanovia.com/survminer/index.html>.
- Kay, Neil E, Tait D Shanafelt, Ann K Strelge, Yean K Lee, Nancy D Bone, and Azra Raza. 2007. "Bone biopsy derived marrow stromal elements rescue chronic lymphocytic leukemia B-cells from spontaneous and drug induced cell death and facilitates an "angiogenic switch"." *Leukemia Research* 31 (7): 899–906. <https://doi.org/10.1016/j.leukres.2006.11.024>.
- Kienle, Dirk L, Christian Korz, Beate Hosch, Axel Benner, Daniel Mertens, Annett Habermann, Alexander Kröber, et al. 2005. "Evidence for distinct pathomechanisms in genetic subgroups of chronic lymphocytic leukemia revealed by quantitative expression analysis of cell cycle, activation, and apoptosis-associated genes." *Journal of Clinical Oncology : Official Journal of the American Society of Clinical Oncology* 23 (16): 3780–92. <https://doi.org/10.1200/JCO.2005.02.568>.

- Kipps, Thomas J, Freda K Stevenson, Catherine J Wu, Carlo M Croce, Graham Packham, William G Wierda, Susan O'Brien, John Gribben, and Kanti Rai. 2017. "Chronic lymphocytic leukaemia." *Nature Reviews. Disease Primers* 3: 16096. <https://doi.org/10.1038/nrdp.2016.96>.
- Kipps, Thomas J, E. Tomhave, L. F. Pratt, S. Duffy, P. P. Chen, and D. A. Carson. 1989. "Developmentally restricted immunoglobulin heavy chain variable region gene expressed at high frequency in chronic lymphocytic leukemia." *Proceedings of the National Academy of Sciences of the United States of America* 86 (15): 5913–17. <https://doi.org/10.1073/pnas.86.15.5913>.
- Kitada, S, J M Zapata, M Andreeff, and J C Reed. 1999. "Bryostatin and CD40-ligand enhance apoptosis resistance and induce expression of cell survival genes in B-cell chronic lymphocytic leukaemia." *British Journal of Haematology* 106 (4): 995–1004. <https://doi.org/10.1046/j.1365-2141.1999.01642.x>.
- Klein, Ulf, Yuhai Tu, Gustavo A Stolovitzky, Michela Mattioli, Giorgio Cattoretti, Hervé Husson, Arnold Freedman, et al. 2001. "Gene expression profiling of B cell chronic lymphocytic leukemia reveals a homogeneous phenotype related to memory B cells." *Journal of Experimental Medicine* 194 (11): 1625–38. <https://doi.org/10.1084/jem.194.11.1625>.
- Kö Ster, Johannes, and Sven Rahmann. 2012. "Genome analysis Snakemake-a scalable bioinformatics workflow engine." *BIOINFORMATICS APPLICATION NOTE* 28: 2520–22. <https://doi.org/10.1093/bioinformatics/bts480>.
- Kolde, Raivo. 2019. *Pheatmap: Pretty Heatmaps*. <https://CRAN.R-project.org/package=pheatmap>.
- Kondo, Motonari. 2010. "Lymphoid and myeloid lineage commitment in multipotent hematopoietic progenitors." *Immunological Reviews* 238 (1): 37–46. <https://doi.org/10.1111/j.1600-065X.2010.00963.x>.
- Kostareli, E., M. Gounari, A. Janus, F. Murray, X. Brochet, V. Giudicelli, S. Pospisilova, et al. 2012. "Antigen receptor stereotypy across B-cell lymphoproliferations: The case of IGHV4-59/IGKV3-20 receptors with rheumatoid factor activity." *Leukemia*. <https://doi.org/10.1038/leu.2011.311>.
- Kraus, Manfred, Marat B. Alimzhanov, Nikolaus Rajewsky, and Klaus Rajewsky. 2004. "Survival of resting mature B lymphocytes depends on BCR signaling via the Ig α/β

heterodimer." *Cell* 117 (6): 787–800. <https://doi.org/10.1016/j.cell.2004.05.014>.

Krysov, Sergey, Kathleen N. Potter, C. Ian Mockridge, Vania Coelho, Isla Wheatley, Graham Packham, and Freda K. Stevenson. 2010. "Surface IgM of CLL cells displays unusual glycans indicative of engagement of antigen in vivo." *Blood* 115 (21): 4198–4205. <https://doi.org/10.1182/blood-2009-12-254847>.

Kulakovskiy, Ivan V, Ilya E Vorontsov, Ivan S Yevshin, Anastasiia V Soboleva, Artem S Kasianov, Haitham Ashoor, Wail Ba-Alawi, et al. 2016. "HOCOMOCO: expansion and enhancement of the collection of transcription factor binding sites models." *Nucleic Acids Research* 44 (D1): D116–25. <https://doi.org/10.1093/nar/gkv1249>.

Kulis, Marta, Simon Heath, Marina Bibikova, Ana C Queirós, Alba Navarro, Guillem Clot, Alejandra Martínez-Trillo, et al. 2012. "Epigenomic analysis detects widespread gene-body DNA hypomethylation in chronic lymphocytic leukemia." *Nature Genetics* 44 (11): 1236–42. <https://doi.org/10.1038/ng.2443>.

Kumar, Dinesh. n.d. "A Complete understanding of LASSO Regression." Accessed October 3, 2021. <https://www.mygreatlearning.com/blog/understanding-of-lasso-regression/#introduction>.

Kurtova, Antonina V., Kumudha Balakrishnan, Rong Chen, Wei Ding, Susanne Schnabl, Maite P. Quiroga, Mariela Sivina, et al. 2009. "Diverse marrow stromal cells protect CLL cells from spontaneous and drug-induced apoptosis: development of a reliable and reproducible system to assess stromal cell adhesion-mediated drug resistance." *Blood* 114 (20): 4441–50. <https://doi.org/10.1182/blood-2009-07-233718>.

Lagneaux, L., A. Delforge, D. Bron, C. De Bruyn, and P. Stryckmans. 1998. "Chronic Lymphocytic Leukemic B Cells But Not Normal B Cells Are Rescued From Apoptosis by Contact With Normal Bone Marrow Stromal Cells." *Blood* 91 (7): 2387–96. <https://doi.org/10.1182/BLOOD.V91.7.2387>.

Lagneaux, L, A Delforge, C De Bruyn, M Bernier, and D Bron. 1999. "Adhesion to bone marrow stroma inhibits apoptosis of chronic lymphocytic leukemia cells." *Leukemia & Lymphoma* 35 (5-6): 445–53. <https://doi.org/10.1080/10428199909169609>.

Lam, K P, R Kühn, and K Rajewsky. 1997. "In vivo ablation of surface immunoglobulin on mature B cells by inducible gene targeting results in rapid cell death." *Cell* 90 (6):

1073–83. [https://doi.org/10.1016/s0092-8674\(00\)80373-6](https://doi.org/10.1016/s0092-8674(00)80373-6).

Landau, Dan A, Scott L Carter, Petar Stojanov, Aaron McKenna, Kristen Stevenson, Michael S Lawrence, Carrie Sougnez, et al. 2013. “Evolution and impact of subclonal mutations in chronic lymphocytic leukemia.” *Cell* 152 (4): 714–26. <https://doi.org/10.1016/j.cell.2013.01.019>.

Landau, Dan A, Kendell Clement, Michael J Ziller, Patrick Boyle, Jean Fan, Hongcang Gu, Kristen Stevenson, et al. 2014. “Locally Disordered Methylation Forms the Basis of Intratumor Methylome Variation in Chronic Lymphocytic Leukemia.” *Cancer Cell* 26 (6): 813–25. <https://doi.org/10.1016/j.ccr.2014.10.012>.

Landau, Dan A, Eugen Tausch, Amaro N Taylor-Weiner, Chip Stewart, Johannes G Reiter, Jasmin Bahlo, Sandra Kluth, et al. 2015. “Mutations driving CLL and their evolution in progression and relapse.” *Nature* 526 (7574): 525–30. <https://doi.org/10.1038/nature15395>.

Langmead, Ben, and Steven L Salzberg. 2012. “Fast gapped-read alignment with Bowtie 2.” *Nature Methods* 9 (4): 357–59. <https://doi.org/10.1038/nmeth.1923>.

Lebien, Tucker W., and Thomas F Tedder. 2008. “B lymphocytes: How they develop and function.” *Blood* 112 (5): 1570–80. <https://doi.org/10.1182/blood-2008-02-078071>.

Letai, Anthony. 2017. “Functional precision cancer medicine-moving beyond pure genomics.” *Nature Medicine* 23 (9): 1028–35. <https://doi.org/10.1038/nm.4389>.

Li, Heng, Bob Handsaker, Alec Wysoker, Tim Fennell, Jue Ruan, Nils Homer, Gabor Marth, et al. 2009. “The Sequence Alignment/Map format and SAMtools.” *BIOINFORMATICS APPLICATIONS NOTE* 25 (16): 2078–79. <https://doi.org/10.1093/bioinformatics/btp352>.

Li, Yang, Yu Wang, Zhuoyue Wang, Danhui Yi, and Shuangge Ma. 2015. “Racial differences in three major NHL subtypes: Descriptive epidemiology.” *Cancer Epidemiology* 39 (1): 8–13. <https://doi.org/10.1016/j.canep.2014.12.001>.

Lipsky, Andrew, Danny Luan, Shirley Chen, Ronan Chaligne, Neville Dusaj, Erica B Bhavsar, Chelston Ang, et al. 2020. “Single-Cell Multi-Omics Reveals Distinct Paths to Survival of Admixed BTKC481 Mutant Vs. Wild-Type Cells in Clinically Progressing Chronic Lymphocytic Leukemia.” *Blood* 136 (Supplement 1): 40–42.

<https://doi.org/10.1182/blood-2020-138374>.

Longo, P. G., L. Laurenti, S. Gobessi, A. Petlickovski, M. Pelosi, P. Chiusolo, S. Sica, G. Leone, and D. G. Efremov. 2007. “The Akt signaling pathway determines the different proliferative capacity of chronic lymphocytic leukemia B-cells from patients with progressive and stable disease.” *Leukemia* 21 (1): 110–20. <https://doi.org/10.1038/sj.leu.2404417>.

Lotz, M, E Ranheim, and T J Kipps. 1994. “Transforming growth factor beta as endogenous growth inhibitor of chronic lymphocytic leukemia B cells.” *Journal of Experimental Medicine* 179 (3): 999–1004. <https://doi.org/10.1084/jem.179.3.999>.

Love, Michael, Simon Anders, and Wolfgang Huber. 2021. *DESeq2: Differential Gene Expression Analysis Based on the Negative Binomial Distribution*. <https://github.com/mikelove/DESeq2>.

Love, Michael, Charlotte Soneson, Mark Robinson, Rob Patro, Andrew Parker Morgan, Ryan C. Thompson, Matt Shirley, and Avi Srivastava. 2021. *Tximport: Import and Summarize Transcript-Level Estimates for Transcript- and Gene-Level Analysis*. <https://github.com/mikelove/tximport>.

Lu, Desheng, Yandong Zhao, Rommel Tawatao, Howard B Cottam, Malini Sen, Lorenzo M Leoni, Thomas J Kipps, Maripat Corr, and Dennis A Carson. 2004. “Activation of the Wnt signaling pathway in chronic lymphocytic leukemia.” *Proceedings of the National Academy of Sciences of the United States of America* 101 (9): 3118–23. <https://doi.org/10.1073/pnas.0308648100>.

Lu, Junyan, Ester Cannizzaro, Fabienne Meier-Abt, Sebastian Scheinost, Peter-Martin Bruch, Holly Ar Giles, Almut Lütge, et al. 2021. “Multi-omics reveals clinically relevant proliferative drive associated with mTOR-MYC-OXPHOS activity in chronic lymphocytic leukemia.” *Nature Cancer* 2 (8): 853–64. <https://doi.org/10.1038/s43018-021-00216-6>.

Lukas, Marina, Britta Velten, Leopold Sellner, Katarzyna Tomska, Jennifer Hüellein, Tatjana Walther, Lena Wagner, et al. 2020. “Survey of ex vivo drug combination effects in chronic lymphocytic leukemia reveals synergistic drug effects and genetic dependencies.” *Leukemia* 34 (11): 2934–50. <https://doi.org/10.1038/s41375-020-0846-5>.

Lukenbill, Joshua, and Matt Kalaycio. 2013. “Fludarabine: A review of the clear benefits

and potential harms.” *Leuk Res.* <https://doi.org/10.1016/j.leukres.2013.05.004>.

Mallm, Jan-Philipp, Murat Iskar, Naveed Ishaque, Lara C Klett, Sabrina J Kugler, Jose M Muino, Vladimir B Teif, et al. 2019. “Linking aberrant chromatin features in chronic lymphocytic leukemia to transcription factor networks.” *Molecular Systems Biology* 15 (5): e8339. <https://doi.org/10.15252/msb.20188339>.

Mangolini, Maurizio, Frederik Götte, Andrew Moore, Tim Ammon, Madlen Oelsner, Gloria Lutzny-Geier, Ludger Klein-Hitpass, et al. 2018. “Notch2 controls non-autonomous Wnt-signalling in chronic lymphocytic leukaemia.” *Nature Communications* 9 (1): 3839. <https://doi.org/10.1038/s41467-018-06069-5>.

Mansouri, Larry, Nikos Papakonstantinou, Stavroula Ntoufa, Kostas Stamatopoulos, and Richard Rosenquist. 2016. “NF- κ B activation in chronic lymphocytic leukemia: A point of convergence of external triggers and intrinsic lesions.” *Semin Cancer Biol.* <https://doi.org/10.1016/j.semcan.2016.07.005>.

Mårtensson, Inga Lill, Nina Almqvist, Ola Grimsholm, and Angelina I. Bernardi. 2010. “The pre-B cell receptor checkpoint.” *FEBS Lett.* <https://doi.org/10.1016/j.febslet.2010.04.057>.

Martínez-Trillos, Alejandra, Alba Navarro, Marta Aymerich, Julio Delgado, Armando López-Guillermo, Elias Campo, and Neus Villamor. 2016. “Clinical impact of MYD88 mutations in chronic lymphocytic leukemia.” *Blood*. <https://doi.org/10.1182/blood-2015-10-678490>.

Matutes, E., K. Owusu-Ankomah, R. Morilla, J. G. García Marco, A. Houlihan, T. Que, and D. Catovsky. 1994. “The immunological profile of B-cell disorders and proposal of a scoring system for the diagnosis of CLL.” *Undefined*. <https://www.semanticscholar.org/paper/The-immunological-profile-of-B-cell-disorders-and-a-Matutes-41ab989ce5c271aa59bd588e88919f4bea23dce6>.

McKenna, Aaron, Matthew Hanna, Eric Banks, Andrey Sivachenko, Kristian Cibulskis, Andrew Kernytsky, Kiran Garimella, et al. 2010. “The genome analysis toolkit: A MapReduce framework for analyzing next-generation DNA sequencing data.” *Genome Research* 20 (9): 1297–1303. <https://doi.org/10.1101/gr.107524.110>.

McWilliams, Emily M, Christopher R Lucas, Timothy Chen, Bonnie K Harrington, Ronni Wasmuth, Amanda Campbell, Kerry A Rogers, et al. 2019. “Anti-BAFF-R anti-

body VAY-736 demonstrates promising preclinical activity in CLL and enhances effectiveness of ibrutinib.” *Blood Advances* 3 (3): 447–60. <https://doi.org/10.1182/bloodadvances.2018025684>.

Meier-Abt, Fabienne, Junyan Lu, Ester Cannizzaro, Marcel F Pohly, Sandra Kummer, Sibylle Pfammatter, Laura Kunz, et al. 2021. “The Protein Landscape of Chronic Lymphocytic Leukemia (CLL).” *Blood*, June. <https://doi.org/10.1182/blood.2020009741>.

Menyhárt, Otília, and Balázs Gyrrfy. 2021. “Multi-omics approaches in cancer research with applications in tumor subtyping, prognosis, and diagnosis.” *Comput Struct Biotechnol J*. <https://doi.org/10.1016/j.csbj.2021.01.009>.

Messmer, Bradley T, Emilia Albesiano, Dimitar G Efremov, Fabio Ghiotto, Steven L Allen, Jonathan Kolitz, Robin Foa, et al. 2004. “Multiple distinct sets of stereotyped antigen receptors indicate a role for antigen in promoting chronic lymphocytic leukemia.” *The Journal of Experimental Medicine* 200 (4): 519–25. <https://doi.org/10.1084/jem.20040544>.

Messmer, Bradley T, Davorka Messmer, Steven L Allen, Jonathan E Kolitz, Prasad Kudalkar, Denise Cesar, Elizabeth J Murphy, et al. 2005. “In vivo measurements document the dynamic cellular kinetics of chronic lymphocytic leukemia B cells.” *The Journal of Clinical Investigation* 115 (3): 755–64. <https://doi.org/10.1172/JCI23409>.

Messmer, Davorka, Jessie-F Fecteau, Morgan O’hayre, Ila S Bharati, Tracy M Handel, and Thomas J Kipps. 2011. “Chronic lymphocytic leukemia cells receive RAF-dependent survival signals in response to CXCL12 that are sensitive to inhibition by sorafenib.” <https://doi.org/10.1182/blood-2010>.

Migliazza, Anna, Francesc Bosch, Hirokazu Komatsu, Eftihia Cayanis, Stefano Martinotti, Elena Toniato, Ernesto Guccione, et al. 2001. “Nucleotide sequence, transcription map, and mutation analysis of the 13q14 chromosomal region deleted in B-cell chronic lymphocytic leukemia.” *Blood* 97 (7): 2098–2104. <https://doi.org/10.1182/blood.V97.7.2098>.

Miller, Kimberly D., Leticia Nogueira, Angela B. Mariotto, Julia H. Rowland, K. Robin Yabroff, Catherine M. Alfano, Ahmedin Jemal, Joan L. Kramer, and Rebecca L. Siegel. 2019. “Cancer treatment and survivorship statistics, 2019.” *CA: A Cancer Journal for Clinicians* 69 (5): 363–85. <https://doi.org/10.3322/caac.21565>.

- Minden, Marcus Dühren Von, Rudolf Übelhart, Dunja Schneider, Thomas Wossning, Martina P. Bach, Maike Buchner, Daniel Hofmann, et al. 2012. "Chronic lymphocytic leukaemia is driven by antigen-independent cell-autonomous signalling." *Nature* 489 (7415): 309–12. <https://doi.org/10.1038/nature11309>.
- Mittal, Amit K., Nagendra K. Chaturvedi, Karan J. Rai, Christine E. Gilling-Cutucache, Tara M. Nordgren, Margaret Moragues, Runqing Lu, et al. 2014. "Chronic Lymphocytic Leukemia Cells in a Lymph Node Microenvironment Depict Molecular Signature Associated with an Aggressive Disease." *Molecular Medicine* 20 (1): 290–301. <https://doi.org/10.2119/molmed.2012.00303>.
- Montresor, Alessio, Lara Toffali, Antonella Rigo, Isacco Ferrarini, Fabrizio Vinante, and Carlo Laudanna. 2018. "CXCR4-and BCR-triggered integrin activation in B-cell chronic lymphocytic leukemia cells depends on JAK2-activated Bruton's tyrosine kinase." *Oncotarget* 9 (80): 35123–40. <https://doi.org/10.18632/oncotarget.26212>.
- Moore, Victoria Del Gaizo, Jennifer R Brown, Michael Certo, Tara M Love, Carl D Novina, and Anthony Letai. 2007. "Chronic lymphocytic leukemia requires BCL2 to sequester prodeath BIM, explaining sensitivity to BCL2 antagonist ABT-737." *Journal of Clinical Investigation* 117 (1): 112–21. <https://doi.org/10.1172/JCI28281>.
- Moreau, Elisabeth J, Estella Matutes, Roger P A'Hern, Alison M Morilla, Ricardo M Morilla, Kwasi A Owusu-Ankomah, Ben K Seon, and Daniel Catovsky. 1997. "Improvement of the chronic lymphocytic leukemia scoring system with the monoclonal antibody SN8 (CD79b)." *American Journal of Clinical Pathology* 108 (4): 378–82. <https://doi.org/10.1093/ajcp/108.4.378>.
- Moreton, Paul, Ben Kennedy, Guy Lucas, Michael Leach, Saad M. B. Rassam, Andrew Haynes, Jane Tighe, et al. 2005. "Eradication of minimal residual disease in B-cell chronic lymphocytic leukemia after alemtuzumab therapy is associated with prolonged survival." *Journal of Clinical Oncology* 23 (13): 2971–79. <https://doi.org/10.1200/JCO.2005.04.021>.
- Mraz, Marek, Clive S Zent, Amy K Church, Diane F Jelinek, Xiaosheng Wu, Sarka Pospisilova, Stephen M Ansell, et al. 2011. "Bone marrow stromal cells protect lymphoma B-cells from rituximab-induced apoptosis and targeting integrin α -4- β -1 (VLA-4) with natalizumab can overcome this resistance." *British Journal of Haematology* 155 (1): 53–64. <https://doi.org/10.1111/j.1365-2141.2011.08794.x>.

- Muzio, Marta, Cristina Scielzo, Maria T. S. Bertilaccio, Michela Frenquelli, Paolo Ghia, and Federico Caligaris-Cappio. 2009. "Expression and function of toll like receptors in chronic lymphocytic leukaemia cells." *British Journal of Haematology* 144 (4): 507–16. <https://doi.org/10.1111/j.1365-2141.2008.07475.x>.
- Myhrinder, Anna Lanemo, Eva Hellqvist, Ekaterina Sidorova, Anita Söderberg, Helen Baxendale, Charlotte Dahle, Kerstin Willander, et al. 2008. "A new perspective: Molecular motifs on oxidized LDL, apoptotic cells, and bacteria are targets for chronic lymphocytic leukemia antibodies." *Blood* 111 (7): 3838–48. <https://doi.org/10.1182/blood-2007-11-125450>.
- Nabhan, Chadi, Briseis Aschebrook-Kilfoy, Brian C-H Chiu, Sonali M Smith, Tait D Shanafelt, Andrew M Evens, and Neil E Kay. 2014. "The impact of race, ethnicity, age and sex on clinical outcome in chronic lymphocytic leukemia: A comprehensive Surveillance, Epidemiology, and End Results analysis in the modern era." *Leukemia and Lymphoma* 55 (12): 2778–84. <https://doi.org/10.3109/10428194.2014.898758>.
- Nadeu, Ferran, Julio Delgado, Cristina Royo, Tycho Baumann, Tatjana Stankovic, Magda Pinyol, Pedro Jares, et al. 2016. "Clinical impact of clonal and subclonal TP53, SF3B1, BIRC3, NOTCH1, and ATM mutations in chronic lymphocytic leukemia." *Blood* 127 (17): 2122–30. <https://doi.org/10.1182/blood-2015-07-659144>.
- Nelder, J. A., and R. W. M. Wedderburn. 1972. "Generalized Linear Models." *Journal of the Royal Statistical Society. Series A (General)* 135 (3): 370. <https://doi.org/10.2307/2344614>.
- Nishio, Mitsufumi, Tomoyuki Endo, Nobuhiro Tsukada, Junko Ohata, Shinichi Kitada, John C Reed, Nathan J Zvaifler, and Thomas J Kipps. 2005. "Nurselike cells express BAFF and APRIL, which can promote survival of chronic lymphocytic leukemia cells via a paracrine pathway distinct from that of SDF-1alpha." *Blood* 106 (3): 1012–20. <https://doi.org/10.1182/blood-2004-03-0889>.
- Nutt, Stephen L., Philip D. Hodgkin, David M. Tarlinton, and Lynn M. Corcoran. 2015. "The generation of antibody-secreting plasma cells." *Nature Reviews Immunology* 2015 15:3 15 (3): 160–71. <https://doi.org/10.1038/nri3795>.
- Nwabo Kamdje, A H, G Bassi, L Pacelli, G Malpeli, E Amati, I Nichele, G Pizzolo, and M Krampera. 2012. "Role of stromal cell-mediated Notch signaling in CLL resistance to chemotherapy." *Blood Cancer Journal* 2 (5): e73–73. <https://doi.org/10.1038/bcj.2012.13>

bcj .2012.17.

- O'Brien, Susan, and Neil E Kay. 2011. "Maintenance therapy for B-Chronic lymphocytic leukemia." *Clinical Advances in Hematology and Oncology* 9 (1): 22–31. http://www.hematologyandoncology.net/files/2013/07/ho0111_obrien1.pdf.
- O'Hayre, Morgan, Catherina L. Salanga, Thomas J. Kipps, Davorka Messmer, Pieter C. Dorrestein, and Tracy M. Handel. 2010. "Elucidating the CXCL12/CXCR4 signaling network in chronic lymphocytic leukemia through phosphoproteomics analysis." Edited by Syed A. Aziz. *PLoS ONE* 5 (7): e11716. <https://doi.org/10.1371/journal.pone.0011716>.
- Oakes, Christopher C, Marc Seifert, Yassen Assenov, Lei Gu, Martina Przekopowitz, Amy S Ruppert, Qi Wang, et al. 2016. "DNA methylation dynamics during B cell maturation underlie a continuum of disease phenotypes in chronic lymphocytic leukemia." *Nature Genetics* 48 (3): 253–64. <https://doi.org/10.1038/ng.3488>.
- Oles, Małgorzata, Sascha Dietrich, Junyan Lu, Britta Velten, Andreas Mock, Vladislav Kim, and Wolfgang Huber. 2021. *BloodCancerMultiOmics2017: "Drug-Perturbation-Based Stratification of Blood Cancer" by Dietrich s, Oles m, Lu j Et Al. - Experimental Data and Complete Analysis*.
- Oppezzo, P, and G Dighiero. 2013. "Role of the B-cell receptor and the microenvironment in chronic lymphocytic leukemia". *Blood Cancer Journal* 3 (9): e149–49. <https://doi.org/10.1038/bcj.2013.45>.
- Os, Audun, Simone Bürgler, Anna Parente Ribes, Ane Funderud, Dong Wang, Keith M. Thompson, Geir E. Tjønnfjord, Bjarne Bogen, and Ludvig A. Munthe. 2013. "Chronic Lymphocytic Leukemia Cells Are Activated and Proliferate in Response to Specific T Helper Cells." *Cell Reports* 4 (3): 566–77. <https://doi.org/10.1016/J.CELREP.2013.07.011>.
- Palamarchuk, Alexey, Alexey Efanov, Natalya Nazaryan, Urmila Santanam, Hansjuerg Alder, Laura Rassenti, Thomas Kipps, Carlo M Croce, and Yuri Pekarsky. 2010. "13q14 deletions in CLL involve cooperating tumor suppressors." *Blood* 115 (19): 3916–22. <https://doi.org/10.1182/blood-2009-10-249367>.
- Palma, Marzia, Giusy Gentilcore, Kia Heimersson, Fariba Mozaffari, Barbro Näsman-Glaser, Emma Young, Richard Rosenquist, Lotta Hansson, Anders Österborg, and Håkan Mellstedt. 2017. "T cells in chronic lymphocytic leukemia display dysreg-

- ulated expression of immune checkpoints and activation markers.” *Haematologica* 102 (3): 562–72. <https://doi.org/10.3324/haematol.2016.151100>.
- Panayiotidis, P., D. Jones, K. Ganeshaguru, L. Foroni, and A. V. Hoffbrand. 1996. “Human bone marrow stromal cells prevent apoptosis and support the survival of chronic lymphocytic leukaemia cells in vitro.” *British Journal of Haematology* 92 (1): 97–103. <https://doi.org/10.1046/j.1365-2141.1996.00305.x>.
- Pascutti, Maria Fernanda, Margot Jak, Jacqueline M. Tromp, Ingrid A. M. Derkx, Esther B. M. Remmerswaal, Rachel Thijssen, Martijn H. A. van Attekum, et al. 2013. “IL-21 and CD40L signals from autologous T cells can induce antigen-independent proliferation of CLL cells.” *Blood* 122 (17): 3010–19. <https://doi.org/10.1182/blood-2012-11-467670>.
- Patel, Viralkumar, Lisa S. Chen, William G. Wierda, Kumudha Balakrishnan, and Varsha Gandhi. 2014. “Impact of bone marrow stromal cells on Bcl-2 family members in chronic lymphocytic leukemia.” *Leukemia and Lymphoma* 55 (4): 899–910. <https://doi.org/10.3109/10428194.2013.819573>.
- Patro, Rob, Geet Duggal, Michael I Love, Rafael A Irizarry, and Carl Kingsford. 2017. “Salmon provides fast and bias-aware quantification of transcript expression.” *Nature Methods* 14 (4): 417–19. <https://doi.org/10.1038/nmeth.4197>.
- Pedersen, Irene M., Shinichi Kitada, Lorenzo M. Leoni, Juan M. Zapata, James G. Karras, Nobuhiro Tsukada, Thomas J. Kipps, Yong Sung Choi, Frank Bennett, and John C. Reed. 2002. “Protection of CLL B cells by a follicular dendritic cell line is dependent on induction of Mcl-1.” *Blood* 100 (5): 1795–1801. https://doi.org/10.1182/BLOOD.V100.5.1795.H81702001795_1795_1801.
- Pedersen, Thomas Lin. 2020. *Patchwork: The Composer of Plots*. <https://CRAN.R-project.org/package=patchwork>.
- Pelanda, Roberta, and Raul M. Torres. 2012. “Central B-Cell tolerance: Where selection begins.” *Cold Spring Harbor Perspectives in Biology* 4 (4). <https://doi.org/10.1101/cshperspect.a007146>.
- Pemovska, Tea, Mika Kontro, Bhagwan Yadav, Henrik Edgren, Samuli Eldfors, Agnieszka Szwajda, Henrikki Almusa, et al. 2013. “Individualized systems medicine strategy to tailor treatments for patients with chemorefractory acute myeloid leukemia.” *Cancer Discovery* 3 (12): 1416–29. <https://doi.org/10.1158/2159-8290.CD-13-0350>.

- Puente, Xose S., Silvia Beà, Rafael Valdés-Mas, Neus Villamor, Jesús Gutiérrez-Abril, José I Martín-Subero, Marta Munar, et al. 2015. “Non-coding recurrent mutations in chronic lymphocytic leukaemia.” *Nature* 526 (7574): 519–24. <https://doi.org/10.1038/nature14666>.
- Puente, Xose S., Magda Pinyol, Victor Quesada, Laura Conde, Gonzalo R. Ordóñez, Neus Villamor, Georgia Escaramis, et al. 2011. “Whole-genome sequencing identifies recurrent mutations in chronic lymphocytic leukaemia.” *Nature* 475 (7354): 101–5. <https://doi.org/10.1038/nature10113>.
- Pua, Bartosz, Aleksandra Goos, Patryk Górnjak, and Krzysztof Jamroziak. 2019. “Overcoming ibrutinib resistance in chronic lymphocytic leukemia.” *Cancers* 11 (12). <https://doi.org/10.3390/cancers11121834>.
- Pulte, Dianne, Maria Theresa Redaniel, Jenny Bird, and Mona Jeffreys. 2015. “Survival for patients with chronic leukemias in the US and Britain: Age-related disparities and changes in the early 21st century.” *European Journal of Haematology* 94 (6): 540–45. <https://doi.org/10.1111/ejh.12468>.
- Purroy, Noelia, Pau Abrisqueta, Júlia Carabia, Cecilia Carpio, Carles Palacio, Francesc Bosch, and Marta Crespo. 2015. “Co-culture of primary CLL cells with bone marrow mesenchymal cells, CD40 ligand and CpG ODN promotes proliferation of chemoresistant CLL cells phenotypically comparable to those proliferating *in vivo*.” *Oncotarget* 6 (10): 7632–43. <https://doi.org/10.18632/oncotarget.2939>.
- Quesada, Víctor, Laura Conde, Neus Villamor, Gonzalo R. Ordóñez, Pedro Jares, Laia Bassaganyas, Andrew J. Ramsay, et al. 2012. “Exome sequencing identifies recurrent mutations of the splicing factor SF3B1 gene in chronic lymphocytic leukemia.” *Nature Genetics* 44 (1): 47–52. <https://doi.org/10.1038/ng.1032>.
- R Core Team. 2021. *R: A Language and Environment for Statistical Computing*. Vienna, Austria: R Foundation for Statistical Computing. <https://www.R-project.org/>.
- Ramírez, Fidel, Friederike D Í Undar, Sarah Diehl, Björn Bjí, Björn A Grüning, Grí Grüning, and Thomas Manke. 2014. “deepTools: a flexible platform for exploring deep-sequencing data.” *Nucleic Acids Research* 42: 187–91. <https://doi.org/10.1093/nar/gku365>.
- Ramsay, Andrew J, Víctor Quesada, Miguel Foronda, Laura Conde, Alejandra Martínez-

Trillo, Neus Villamor, David Rodríguez, et al. 2013. "POT1 mutations cause telomere dysfunction in chronic lymphocytic leukemia." *Nature Genetics* 45 (5): 526–30. <https://doi.org/10.1038/ng.2584>.

Rendeiro, André F., Thomas Krausgruber, Nikolaus Fortelny, Fangwen Zhao, Thomas Penz, Matthias Farlik, Linda C. Schuster, et al. 2020. "Chromatin mapping and single-cell immune profiling define the temporal dynamics of ibrutinib response in CLL." *Nature Communications* 2020 11:1 11 (1): 1–14. <https://doi.org/10.1038/s41467-019-14081-6>.

Rendeiro, André F., Christian Schmidl, Jonathan C. Strefford, Renata Walewska, Zadie Davis, Matthias Farlik, David Oscier, and Christoph Bock. 2016. "Chromatin accessibility maps of chronic lymphocytic leukaemia identify subtype-specific epigenome signatures and transcription regulatory networks." *Nature Communications* 7 (1): 11938. <https://doi.org/10.1038/ncomms11938>.

Robak, Tadeusz. 2005. "Therapy of chronic lymphocytic leukaemia with purine nucleoside analogues: Facts and controversies." *Drugs Aging*. <https://doi.org/10.2165/00002512-200522120-00002>.

Robak, Tadeusz, Anna Dmoszynska, Philippe Solal-Célyny, Krzysztof Warzocha, Javier Loscertales, John Catalano, Boris V Afanasiev, et al. 2010. "Rituximab plus fludarabine and cyclophosphamide prolongs progression-free survival compared with fludarabine and cyclophosphamide alone in previously treated chronic lymphocytic leukemia." *Journal of Clinical Oncology* 28 (10): 1756–65. <https://doi.org/10.1200/JCO.2009.26.4556>.

Roberts, Andrew W., Matthew S. Davids, John M. Pagel, Brad S. Kahl, Soham D. Puvvada, John F. Gerecitano, Thomas J. Kipps, et al. 2016. "Targeting BCL2 with Venetoclax in Relapsed Chronic Lymphocytic Leukemia." *New England Journal of Medicine* 374 (4): 311–22. <https://doi.org/10.1056/nejmoa1513257>.

Roessner, Philipp M, and Martina Seiffert. 2020. "T-cells in chronic lymphocytic leukemia: Guardians or drivers of disease?" *Leukemia* 34 (8): 2012–24. <https://doi.org/10.1038/s41375-020-0873-2>.

Rosenwald, Andreas, Ash A Alizadeh, George Widhopf, Richard Simon, R Eric Davis, Xin Yu, Liming Yang, et al. 2001. "Relation of gene expression phenotype to immunoglobulin mutation genotype in B cell chronic lymphocytic leukemia." *Journal of Experimental Medicine* 194 (11): 1639–47. <https://doi.org/10.1084/jem.194.11.1639>.

11.1639.

- Rossi, Davide, Michaela Cerri, Clara Deambrogi, Elisa Sozzi, Stefania Cresta, Silvia Rasi, Lorenzo De Paoli, et al. 2009. “The prognostic value of TP53 mutations in chronic lymphocytic leukemia is independent of Del17p13: Implications for overall survival and chemorefractoriness.” *Clinical Cancer Research* 15 (3): 995–1004. <https://doi.org/10.1158/1078-0432.CCR-08-1630>.
- Rossi, Davide, Silvia Rasi, Giulia Fabbri, Valeria Spina, Marco Fangazio, Francesco Forconi, Roberto Marasca, et al. 2012. “Mutations of NOTCH1 are an independent predictor of survival in chronic lymphocytic leukemia.” *Blood* 119 (2): 521–29. <https://doi.org/10.1182/blood-2011-09-379966>.
- Rossi, Davide, Silvia Rasi, Valeria Spina, Alessio Bruscaggin, Sara Monti, Carmela Ciardullo, Clara Deambrogi, et al. 2013. “Integrated mutational and cytogenetic analysis identifies new prognostic subgroups in chronic lymphocytic leukemia.” *Blood* 121 (8): 1403–12. <https://doi.org/10.1182/blood-2012-09-458265>.
- RStudio Team. 2020. “RStudio: Integrated Development Environment for R.” Boston, MA: RStudio, PBC. <http://www.rstudio.com/>.
- Scheffold, Annika, and Stephan Stilgenbauer. 2020. “Revolution of Chronic Lymphocytic Leukemia Therapy: the Chemo-Free Treatment Paradigm.” Springer. <https://doi.org/10.1007/s11912-020-0881-4>.
- Schulz, A., G. Toedt, T. Zenz, S. Stilgenbauer, P. Lichter, and M. Seiffert. 2011. “Inflammatory cytokines and signaling pathways are associated with survival of primary chronic lymphocytic leukemia cells in vitro: a dominant role of CCL2.” *Haematologica* 96 (3): 408–16. <https://doi.org/10.3324/haematol.2010.031377>.
- Scielzo, Cristina, and Paolo Ghia. 2020. “Modeling the Leukemia Microenvironment In Vitro.” Frontiers Media SA. <https://doi.org/10.3389/fonc.2020.607608>.
- Scrivener, S., R. V. Goddard, E. R. Kaminski, and A. G. Prentice. 2003. “Abnormal T-cell Function in B-cell Chronic Lymphocytic Leukaemia.” *Leukemia & Lymphoma* 44 (3): 383–89. <https://doi.org/10.1080/1042819021000029993>.
- Shiloh, Yosef, and Yael Ziv. 2013. “The ATM protein kinase: Regulating the cellular response to genotoxic stress, and more.” *Nat Rev Mol Cell Biol*. <https://doi.org/10.1038/nrm3546>.

- Shin, Chanseok, and James L Manley. 2004. "Cell signalling and the control of pre-mRNA splicing." *Nat Rev Mol Cell Biol*. <https://doi.org/10.1038/nrm1467>.
- Shlomchik, Mark J., and Florian Weisel. 2012. "Germinal center selection and the development of memory B and plasma cells." *Immunological Reviews* 247 (1): 52–63. <https://doi.org/10.1111/J.1600-065X.2012.01124.X>.
- Siegel, Rebecca, Carol DeSantis, Katherine Virgo, Kevin Stein, Angela Mariotto, Tenbroeck Smith, Dexter Cooper, et al. 2012. "Cancer treatment and survivorship statistics, 2012." *CA: A Cancer Journal for Clinicians* 62 (4): 220–41. <https://doi.org/10.3322/caac.21149>.
- Simonetti, Giorgia, Maria Teresa Sabrina Bertilaccio, Paolo Ghia, and Ulf Klein. 2014. "Mouse models in the study of chronic lymphocytic leukemia pathogenesis and therapy." American Society of Hematology. <https://doi.org/10.1182/blood-2014-05-577122>.
- Skowronska, Anna, Anton Parker, Gulshanara Ahmed, Ceri Oldrieve, Zadie Davis, Sue Richards, Martin Dyer, et al. 2012. "Biallelic ATM inactivation significantly reduces survival in patients treated on the United Kingdom leukemia research fund chronic lymphocytic leukemia 4 trial." *Journal of Clinical Oncology* 30 (36): 4524–32. <https://doi.org/10.1200/JCO.2011.41.0852>.
- Snijder, Berend, Gregory I Vladimer, Nikolaus Krall, Katsuhiro Miura, Ann Sofie Schmolke, Christoph Kornauth, Oscar Lopez de la Fuente, et al. 2017. "Image-based ex-vivo drug screening for patients with aggressive haematological malignancies: interim results from a single-arm, open-label, pilot study." *The Lancet Haematology* 4 (12): e595–606. [https://doi.org/10.1016/S2352-3026\(17\)30208-9](https://doi.org/10.1016/S2352-3026(17)30208-9).
- Srinivasan, Lakshmi, Yoshiteru Sasaki, Dinis Pedro Calado, Baochun Zhang, Ji Hye Paik, Ronald A DePinho, Jeffrey L Kutok, John F Kearney, Kevin L Otipoby, and Klaus Rajewsky. 2009. "PI3 kinase signals BCR-dependent mature B cell survival." *Cell* 139 (3): 573–86. <https://doi.org/10.1016/j.cell.2009.08.041>.
- Srinivasan, Vishrut K, Shano Naseem, Neelam Varma, Deepesh P Lad, and Pankaj Malhotra. 2020. "Genomic alterations in chronic lymphocytic leukemia and their correlation with clinico-hematological parameters and disease progression." *Blood Research* 55 (3): 131–38. <https://doi.org/10.5045/br.2020.2020080>.
- Stamatopoulos, Basile, Nathalie Meuleman, Cécile De Bruyn, Karlien Pieters, Philippe Mineur, Christine Le Roy, Stéphane Saint-Georges, et al. 2012. "AMD3100 disrupts

the cross-talk between chronic lymphocytic leukemia cells and a mesenchymal stromal or nurse-like cell-based microenvironment: pre-clinical evidence for its association with chronic lymphocytic leukemia treatments." *Haematologica* 97 (4): 608–15. <https://doi.org/10.3324/haematol.2011.052779>.

Stamatopoulos, Basile, Michaël Van Damme, Emerence Cromptot, Barbara Dessars, Hakim El Housni, Philippe Mineur, Nathalie Meuleman, Dominique Bron, and Laurence Lagneaux. 2015. "Opposite Prognostic Significance of Cellular and Serum Circulating MicroRNA-150 in Patients with Chronic Lymphocytic Leukemia." *Molecular Medicine* 21 (1): 123–33. <https://doi.org/10.2119/molmed.2014.00214>.

Stamatopoulos, B., N. Meuleman, C. De Bruyn, A. Delforge, D. Bron, and L. Lagneaux. 2010. "The histone deacetylase inhibitor suberoylanilide hydroxamic acid induces apoptosis, down-regulates the CXCR4 chemokine receptor and impairs migration of chronic lymphocytic leukemia cells." *Haematologica* 95 (7): 1136–43. <https://doi.org/10.3324/haematol.2009.013847>.

Stamatopoulos, Kostas, Chrysoula Belessi, Carol Moreno, Myriam Boudjogra, Giuseppe Guida, Tatjana Smilevska, Lynda Belhoul, et al. 2007. *Blood* 109 (1): 259–70. <https://doi.org/10.1182/blood-2006-03-012948>.

Stankovic, Tatjana, and Anna Skowronska. 2014. "The role of ATM mutations and 11q deletions in disease progression in chronic lymphocytic leukemia." *Leuk Lymphoma*. <https://doi.org/10.3109/10428194.2013.829919>.

Stark, Rory, and Gord Brown. 2021. *DiffBind: Differential Binding Analysis of ChIP-Seq Peak Data*. <https://www.cruk.cam.ac.uk/core-facilities/bioinformatics-core/software/DiffBind>.

Stevenson, Freda K, and Federico Caligaris-Cappio. 2004. "Chronic lymphocytic leukemia: Revelations from the B-cell receptor." *Blood*. <https://doi.org/10.1182/blood-2003-12-4312>.

Sthoeger, Z. M., M. Wakai, D. B. Tse, V. P. Vinciguerra, S. L. Allen, D. R. Budman, S. M. Lichtman, P. Schulman, L. R. Weiselberg, and N. Chiorazzi. 1989. "Production of autoantibodies by CD5-expressing B lymphocytes from patients with chronic lymphocytic leukemia." *Journal of Experimental Medicine* 169 (1): 255–68. <https://doi.org/10.1084/jem.169.1.255>.

Stilgenbauer, Stephan, Barbara Eichhorst, Johannes Schetelig, Steven Coutre, John F Seymour, Talha Munir, Soham D Puvvada, et al. 2016. "Venetoclax in relapsed

or refractory chronic lymphocytic leukaemia with 17p deletion: a multicentre, open-label, phase 2 study." *The Lancet Oncology* 17 (6): 768–78. [https://doi.org/10.1016/S1470-2045\(16\)30019-5](https://doi.org/10.1016/S1470-2045(16)30019-5).

Stilgenbauer, Stephan, Andrea Schnaiter, Peter Paschka, Thorsten Zenz, Marianna Rossi, Konstanze Döhner, Andreas Bühler, et al. 2014. "Gene mutations and treatment outcome in chronic lymphocytic leukemia: results from the CLL8 trial." *Blood* 123 (21): 3247–54. <https://doi.org/10.1182/blood-2014-01-546150>.

Ten Hacken, Elisa, and Jan A Burger. 2016. "Microenvironment interactions and B-cell receptor signaling in Chronic Lymphocytic Leukemia: Implications for disease pathogenesis and treatment." *Biochimica Et Biophysica Acta* 1863 (3): 401–13. <https://doi.org/10.1016/j.bbamcr.2015.07.009>.

Therneau, Terry M. 2021. *Survival: Survival Analysis*. <https://github.com/therneau/survival>.

Tibshirani, Robert. 1996. "Regression Shrinkage and Selection via the Lasso." 1. Vol. 58. <https://www.jstor.org/stable/pdf/2346178.pdf>.

Timp, Winston, and Andrew P Feinberg. 2013. "Cancer as a dysregulated epigenome allowing cellular growth advantage at the expense of the host." *Nat Rev Cancer.* <https://doi.org/10.1038/nrc3486>.

Totero, Daniela de, Raffaella Meazza, Simona Zupo, Giovanna Cutrona, Serena Matis, Monica Colombo, Enrico Balleari, et al. 2006. "Interleukin-21 receptor (IL-21R) is up-regulated by CD40 triggering and mediates proapoptotic signals in chronic lymphocytic leukemia B cells." *Blood* 107 (9): 3708–15. <https://doi.org/10.1182/blood-2005-09-3535>.

Trbusek, Martin, Jana Smardova, Jitka Malcikova, Ludmila Sebejova, Petr Dobes, Miluse Svitakova, Vladimira Vranova, et al. 2011. "Missense mutations located in structural p53 DNA-binding motifs are associated with extremely poor survival in chronic lymphocytic leukemia." *Journal of Clinical Oncology* 29 (19): 2703–8. <https://doi.org/10.1200/JCO.2011.34.7872>.

Trentin, Livio, Andrea Cerutti, Renato Zambello, Rosaria Sancetta, Cristina Tassinari, Monica Facco, Fausto Adami, Francesco Rodeghiero, Carlo Agostini, and Gianpietro Semenzato. 1996. "Interleukin-15 promotes the growth of leukemic cells of patients with B-cell chronic lymphoproliferative disorders." *Blood* 87 (8): 3327–35. <https://doi.org/10.1182/blood.87.8.3327>

//doi.org/10.1182/blood.v87.8.3327.bloodjournal8783327.

Trimarco, Valentina, Elisa Ave, Monica Facco, Giorgia Chiodin, Federica Frezzato, Veronica Martini, Cristina Gattazzo, et al. 2015. "Cross-talk between chronic lymphocytic leukemia (CLL) tumor b cells and mesenchymal stromal cells (MSCs): Implications for neoplastic cell survival." *Oncotarget* 6 (39): 42130–49. <https://doi.org/10.18632/oncotarget.6239>.

Tsukada, Nobuhiro, Jan A. Burger, Nathan J. Zvaifler, and Thomas J. Kipps. 2002. "Distinctive features of "nurselike" cells that differentiate in the context of chronic lymphocytic leukemia." *Blood* 99 (3): 1030–37. <https://doi.org/10.1182/blood.V99.3.1030>.

Turkistany, Shereen A, and Rodney P Dekoter. 2011. "The transcription factor PU.1 is a critical regulator of cellular communication in the immune system." <https://doi.org/10.1007/s00005-011-0147-9>.

Tyner, Jeffrey W, Wayne F Yang, Armand Bankhead, Guang Fan, Luke B Fletcher, Jade Bryant, Jason M Glover, et al. 2013. "Kinase pathway dependence in primary human leukemias determined by rapid inhibitor screening." *Cancer Research* 73 (1): 285–96. <https://doi.org/10.1158/0008-5472.CAN-12-1906>.

Vangapandu, Hima V., Mary L. Ayres, Christopher A. Bristow, William G. Wierda, Michael J. Keating, Kumudha Balakrishnan, Christine M. Stellrecht, and Varsha Gandhi. 2017. "The Stromal Microenvironment Modulates Mitochondrial Oxidative Phosphorylation in Chronic Lymphocytic Leukemia Cells." *Neoplasia (United States)* 19 (10): 762–71. <https://doi.org/10.1016/j.neo.2017.07.004>.

Vogelstein, Bert, Nickolas Papadopoulos, Victor E Velculescu, Shabin Zhou, Luis A Diaz, and Kenneth W Kinzler. 2013. "Cancer genome landscapes." *Science*. <https://doi.org/10.1126/science.1235122>.

Wahlfors, J., H. Hiltunen, K. Heinonen, E Hamalainen, L. Alhonen, and J. Janne. 1992. "Genomic hypomethylation in human chronic lymphocytic leukemia." *Blood* 80 (8): 2074–80. <https://doi.org/10.1182/blood.v80.8.2074.2074>.

Walker, Jeffrey A. 2018. "Elementary Statistical Modeling for Applied Biostatistics." https://www.middleprofessor.com/files/applied-biostatistics_bookdown/_book/index.html#what-is-unusual-about-this-book.

Walsby, Elisabeth, Andrea Buggins, Stephen Devereux, Ceri Jones, Guy Pratt, Paul

- Brennan, Chris Fegan, and Chris Pepper. 2014. "Development and characterization of a physiologically relevant model of lymphocyte migration in chronic lymphocytic leukemia." *Blood* 123 (23): 3607–17. <https://doi.org/10.1182/blood-2013-12-544569>.
- Wang, Lili, Michael S. Lawrence, Youzhong Wan, Petar Stojanov, Carrie Sougnez, Kristen Stevenson, Lillian Werner, et al. 2011. "SF3B1 and Other Novel Cancer Genes in Chronic Lymphocytic Leukemia." *New England Journal of Medicine* 365 (26): 2497–2506. <https://doi.org/10.1056/nejmoa1109016>.
- Wickham, Hadley, Winston Chang, Lionel Henry, Thomas Lin Pedersen, Kohske Takahashi, Claus Wilke, Kara Woo, Hiroaki Yutani, and Dewey Dunnington. 2021. *Ggplot2: Create Elegant Data Visualisations Using the Grammar of Graphics*. <https://CRAN.R-project.org/package=ggplot2>.
- Widhopf, George F., Laura Z. Rassenti, Traci L. Toy, John G. Gribben, William G. Wierda, and Thomas J. Kipps. 2004. *Blood* 104 (8): 2499–2504. <https://doi.org/10.1182/blood-2004-03-0818>.
- Wiestner, Adrian. 2015. "The role of b-cell receptor inhibitors in the treatment of patients with chronic lymphocytic leukemia." *Haematologica* 100 (12): 1495–1507. <https://doi.org/10.3324/haematol.2014.119123>.
- Wilkerson, Matt, and Peter Waltman. 2021. *ConsensusClusterPlus: ConsensusClusterPlus*.
- Willis, Simon N., Julie Tellier, Yang Liao, Stephanie Trezise, Amanda Light, Kristy O'Donnell, Lee Ann Garrett-Sinha, Wei Shi, David M. Tarlinton, and Stephen L. Nutt. 2017. "Environmental sensing by mature B cells is controlled by the transcription factors PU.1 and SpiB." *Nature Communications* 8 (1): 1426. <https://doi.org/10.1038/s41467-017-01605-1>.
- Woyach, Jennifer A., Richard R. Furman, Ta-Ming Liu, Hatice Gulcin Ozer, Marc Zapatka, Amy S. Ruppert, Ling Xue, et al. 2014. "Resistance Mechanisms for the Bruton's Tyrosine Kinase Inhibitor Ibrutinib." *New England Journal of Medicine* 370 (24): 2286–94. <https://doi.org/10.1056/nejmoa1400029>.
- Woyach, Jennifer A., and Amy J. Johnson. 2015. "Targeted therapies in CLL: Mechanisms of resistance and strategies for management." *Blood* 126 (4): 471–77. <https://doi.org/10.1182/blood-2015-03-585075>.
- Xu, Zhenhua, Donglian Xiong, Jushun Zhang, Jingyan Zhang, Xiuli Chen, Zhizhe Chen,

- and Rong Zhan. 2018. “Bone marrow stromal cells enhance the survival of chronic lymphocytic leukemia cells by regulating HES-1 gene expression and H3K27me3 demethylation.” *Oncology Letters* 15 (2): 1937–42. <https://doi.org/10.3892/ol.2017.7450>.
- Yosifov, Deyan Y, Christine Wolf, Stephan Stilgenbauer, and Daniel Mertens. 2019. “From biology to therapy: The CLL success story.” Wolters Kluwer Health. <https://doi.org/10.1097/HSC.0000000000000175>.
- Yu, Guangchuang. 2021. *clusterProfiler: A Universal Enrichment Tool for Interpreting Omics Data*. <https://yulab-smu.top/biomedical-knowledge-mining-book/>.
- Yu, Lijian, Haesook T Kim, Siddha N. Kasar, Parul Benien, Wei Du, Kevin Hoang, Andrew Aw, et al. 2017. “Survival of Del17p CLL depends on genomic complexity and somatic mutation.” *Clinical Cancer Research* 23 (3): 735–45. <https://doi.org/10.1158/1078-0432.CCR-16-0594>.
- Zenz, Thorsten, Alexander Kröber, Katrin Scherer, Sonja Häbe, Andreas Bühler, Axel Benner, Tina Denzel, et al. 2008. “Monoallelic TP53 inactivation is associated with poor prognosis in chronic lymphocytic leukemia: Results from a detailed genetic characterization with long-term follow-up.” *Blood* 112 (8): 3322–29. <https://doi.org/10.1182/blood-2008-04-154070>.
- Zenz, Thorsten, Almut Luetge, Junyan Lu, Huellein Jennifer, Sascha Dietrich, Leopold Sellner, and Wolfgang Huber. 2019. “Transcriptional Profiling Reveals Strong Impact of Major Molecular Disease Subgroups and Mixed Epistasis in Chronic Lymphocytic Leukemia.” *Blood* 134 (Supplement_1): 1742–42. <https://doi.org/10.1182/blood-2019-126388>.
- Zenz, Thorsten, Daniel Mertens, Ralf Küppers, Hartmut Döhner, and Stephan Stilgenbauer. 2010. “From pathogenesis to treatment of chronic lymphocytic leukaemia.” *Nature Reviews Cancer* 10 (1): 37–50. <https://doi.org/10.1038/nrc2764>.
- Zhang, Wan, Dunyaporn Trachootham, Jinyun Liu, Gang Chen, Helene Pelicano, Celia Garcia-Prieto, Weiqin Lu, et al. 2012. “Stromal control of cystine metabolism promotes cancer cell survival in chronic lymphocytic leukaemia.” *Nature Cell Biology* 14 (3): 276–86. <https://doi.org/10.1038/ncb2432>.
- Zhang, Yong, Tao Liu, Clifford A Meyer, Jérôme Eeckhoute, David S Johnson, Bradley E Bernstein, Chad Nussbaum, et al. 2008. “Model-based Analysis of ChIP-Seq

(MACS)." *Genome Biology* 9 (9): R137. <https://doi.org/10.1186/gb-2008-9-9-r137>.

Ziller, Michael J., Hongcang Gu, Fabian Müller, Julie Donaghey, Linus T.-Y. Tsai, Oliver Kohlbacher, Philip L. De Jager, et al. 2013. "Charting a dynamic DNA methylation landscape of the human genome." *Nature* 500 (7463): 477–81. <https://doi.org/10.1038/nature12433>.

Appendix

Figures

	1	2	3	4	5	6	7	8	9	10	11	12	13	14	15	16	17	18	19	20	21	22	23	24
A	DMSO																							DMSO
B	DMSO																							DMSO
C	DMSO																							DMSO
D	DMSO																							DMSO
E	DMSO																							DMSO
F	DMSO																							DMSO
G	DMSO																							DMSO
H	DMSO																							
I	DMSO																							DMSO
J	DMSO																							DMSO
K	DMSO																							DMSO
L	DMSO																							DMSO
M	DMSO																							DMSO
N	DMSO																							DMSO
O	DMSO																							DMSO
P	DMSO																							DMSO

Figure 7.1: Layout of the 15 drugs on each screening plate. *Plate plot generated by Peter-Martin Bruch.*

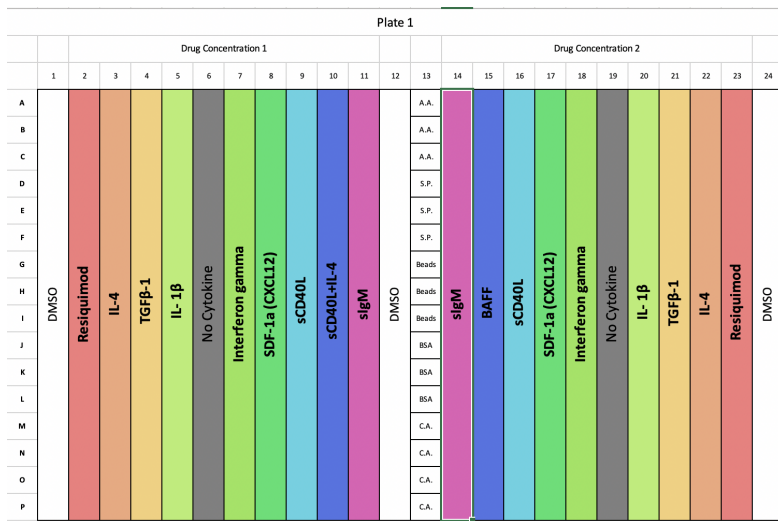


Figure 7.2: Layout of 9 / 18 stimuli on the first screening plate. A.A., S.P., Beads, B.S.A. and C.A. refer to additional agents tested in the screen which were not included in downstream analysis. *Plate plot generated by Peter-Martin Bruch.*

Tables

Table 7.1: Summary of the patient samples and selected genetic features included in this study. Table published in Bruch and Giles et al. 2021.

Patient ID	Sex	Treated before	IGHV status	Methylation Cluster	Del13q	Del11q	Trisomy 12	Del17p
Pat_001	f		1 U	LP	1	0	0	0
Pat_002	m		1 M	IP	1	0	0	0
Pat_003	m		0 M	HP	0	0	1	0
Pat_004	f		1 U	LP	0	1	0	0
Pat_005	m		0 U	LP	1	0	0	0
Pat_006	f		0 U	LP	0	0	0	0
Pat_007	f		0 M	HP	1	0	0	0
Pat_008	m		1 U	LP	1	0	0	0
Pat_009	m		1 U	LP	1	0	0	1
Pat_010	f		1 U	LP	1	0	0	1
Pat_011	f		0 U	NA	0	0	1	0
Pat_012	f		0 M	HP	1	0	0	0
Pat_013	f		1 U	IP	1	1	0	0
Pat_014	m		0 M	HP	0	0	0	0
Pat_015	m		0 M	HP	1	0	0	0
Pat_016	m		0 M	HP	1	0	0	0
Pat_017	m		0 M	NA	1	0	0	0
Pat_018	f		1 U	LP	1	1	0	0
Pat_019	m		0 M	HP	1	0	0	0
Pat_020	f		1 M	IP	1	0	0	0
Pat_021	m		0 U	LP	0	0	0	1

Table 7.1: Summary of the patient samples and selected genetic features included in this study. Table published in Bruch and Giles et al. 2021. (*continued*)

Patient ID	Sex	Treated before	IGHV status	Methylation Cluster	Del13q	Del11q	Trisomy 12	Del17p
Pat_022	f	0	M	IP	0	0	1	0
Pat_023	f	0	M	HP	0	0	0	0
Pat_024	f	1	M	HP	0	0	0	1
Pat_025	m	0	M	IP	1	0	0	0
Pat_026	m	0	M	HP	1	0	0	0
Pat_027	f	0	M	HP	1	0	0	0
Pat_028	f	0	M	IP	1	0	0	0
Pat_029	f	0	M	HP	1	0	0	0
Pat_030	m	1	M	HP	1	0	0	0
Pat_031	m	0	M	HP	0	0	0	0
Pat_032	f	1	U	LP	1	1	0	0
Pat_033	m	1	U	IP	0	1	0	0
Pat_034	m	1	U	LP	0	1	0	0
Pat_035	m	0	M	HP	1	0	0	0
Pat_036	m	1	U	LP	1	1	0	1
Pat_037	f	1	U	IP	1	0	0	0
Pat_038	m	0	M	IP	1	0	0	0
Pat_039	m	1	M	HP	1	0	0	0
Pat_040	f	0	M	HP	0	0	0	0
Pat_041	f	1	U	LP	0	0	1	0
Pat_042	f	0	M	IP	1	1	0	0
Pat_043	f	0	M	HP	1	0	0	0
Pat_044	m	0	M	HP	1	0	0	0
Pat_045	m	0	U	LP	0	0	0	0
Pat_046	m	0	M	IP	0	0	1	0
Pat_047	m	0	M	HP	1	0	0	0
Pat_048	m	0	M	HP	1	0	0	0
Pat_049	f	0	M	IP	0	1	0	0
Pat_050	m	0	M	HP	0	0	1	0
Pat_051	m	0	M	NA	1	0	0	0
Pat_052	f	0	M	IP	1	0	0	0
Pat_053	m	1	U	LP	1	1	0	0
Pat_054	f	1	U	LP	0	1	0	0
Pat_055	m	1	U	LP	0	0	0	0
Pat_056	f	0	U	LP	NA	NA	NA	NA
Pat_057	f	0	M	HP	1	0	1	0
Pat_058	f	1	U	LP	0	0	0	0
Pat_059	m	0	M	HP	1	0	0	0
Pat_060	m	1	M	IP	1	0	0	1
Pat_061	m	0	U	LP	0	0	1	0
Pat_062	m	1	U	LP	1	1	0	0
Pat_063	f	0	U	LP	1	0	0	0
Pat_064	m	1	U	LP	1	1	0	1
Pat_065	m	0	U	LP	0	1	0	0
Pat_066	m	1	U	LP	1	1	0	0
Pat_067	f	0	M	HP	1	0	0	0
Pat_068	m	0	M	HP	1	0	0	0
Pat_069	m	1	M	HP	1	0	0	0

Table 7.1: Summary of the patient samples and selected genetic features included in this study. Table published in Bruch and Giles et al. 2021. (*continued*)

Patient ID	Sex	Treated before	IGHV status	Methylation Cluster	Del13q	Del11q	Trisomy 12	Del17p
Pat_070	f	0	M	HP	0	0	0	0
Pat_071	f	0	U	LP	0	0	0	0
Pat_072	m	1	M	HP	0	0	1	0
Pat_073	f	0	U	LP	1	1	0	0
Pat_074	f	0	M	HP	0	0	0	0
Pat_075	f	0	M	HP	1	0	0	0
Pat_076	m	0	M	HP	1	0	0	0
Pat_077	f	0	U	NA	0	0	1	0
Pat_078	m	0	U	LP	0	0	0	0
Pat_079	m	0	M	HP	1	0	0	0
Pat_080	f	0	M	HP	0	0	0	0
Pat_081	m	0	M	HP	0	0	0	0
Pat_082	m	0	U	LP	0	0	0	0
Pat_083	m	0	M	HP	0	0	0	0
Pat_084	m	0	U	LP	0	0	1	0
Pat_085	m	0	M	HP	0	0	0	0
Pat_086	m	1	U	LP	1	1	0	0
Pat_087	m	0	M	IP	1	0	0	0
Pat_088	f	1	U	LP	1	0	0	1
Pat_089	m	0	M	HP	0	0	0	0
Pat_090	m	1	U	LP	0	0	1	0
Pat_091	m	1	M	NA	1	0	0	0
Pat_092	m	1	M	HP	0	0	0	0
Pat_093	m	0	M	HP	1	0	0	0
Pat_094	f	1	M	HP	0	0	0	0
Pat_095	m	1	U	LP	0	0	0	0
Pat_096	m	0	M	HP	0	0	0	0
Pat_097	f	1	U	LP	0	0	0	0
Pat_098	m	0	M	HP	1	0	0	0
Pat_099	f	0	U	LP	1	0	0	0
Pat_100	f	0	U	LP	1	0	0	0
Pat_101	f	0	U	LP	1	0	0	0
Pat_102	m	1	U	IP	0	0	0	0
Pat_103	f	0	M	HP	1	0	1	0
Pat_104	f	1	M	HP	0	0	0	0
Pat_105	m	0	U	LP	NA	NA	NA	NA
Pat_106	m	0	U	LP	1	1	0	1
Pat_107	f	0	M	NA	1	0	0	0
Pat_108	m	0	M	NA	1	0	1	0
Pat_109	m	0	M	HP	1	0	0	0
Pat_110	m	0	M	IP	1	1	0	0
Pat_111	f	1	U	LP	1	0	0	0
Pat_112	f	0	M	NA	0	0	1	0
Pat_113	f	0	M	HP	1	0	0	0
Pat_114	m	0	U	LP	1	0	0	0
Pat_115	m	1	U	LP	1	0	0	1
Pat_116	m	0	U	LP	1	0	0	0
Pat_117	m	0	U	IP	1	0	0	0

Table 7.1: Summary of the patient samples and selected genetic features included in this study. Table published in Bruch and Giles et al. 2021. (*continued*)

Patient ID	Sex	Treated before	IGHV status	Methylation Cluster	Del13q	Del11q	Trisomy 12	Del17p
Pat_118	f	0	M	HP	0	0	0	1
Pat_119	m	0	U	LP	NA	NA	NA	NA
Pat_120	f	0	U	LP	0	0	1	0
Pat_121	m	0	U	LP	0	0	0	1
Pat_122	m	0	U	LP	0	1	0	0
Pat_123	m	0	U	LP	1	0	0	1
Pat_124	f	0	M	HP	1	0	1	0
Pat_125	f	0	M	HP	1	0	0	0
Pat_126	m	1	NA	NA	0	0	1	0
Pat_127	m	0	U	LP	1	1	0	1
Pat_128	m	0	M	HP	1	0	0	0
Pat_129	m	1	U	LP	1	0	0	0
Pat_130	f	0	M	IP	1	0	0	0
Pat_131	f	0	U	LP	1	0	0	1
Pat_132	m	1	U	LP	1	0	0	1
Pat_133	m	1	U	LP	1	0	0	1
Pat_134	m	1	M	HP	1	0	0	1
Pat_135	m	0	M	HP	1	0	0	0
Pat_136	m	0	M	HP	1	0	0	0
Pat_137	f	0	U	LP	0	0	1	0
Pat_138	f	0	M	HP	1	0	0	0
Pat_139	f	0	M	HP	NA	NA	NA	NA
Pat_140	f	0	M	IP	1	0	0	0
Pat_141	m	0	M	IP	1	0	0	0
Pat_142	m	0	M	HP	1	0	0	0
Pat_143	f	0	U	LP	1	0	0	0
Pat_144	m	1	U	LP	0	0	0	1
Pat_145	f	0	M	HP	0	0	0	0
Pat_146	m	1	U	LP	NA	NA	NA	NA
Pat_147	m	1	U	LP	0	0	0	1
Pat_148	m	1	U	NA	1	0	0	0
Pat_149	m	1	U	LP	0	1	1	0
Pat_150	f	0	M	HP	1	0	0	NA
Pat_151	m	0	U	LP	0	0	1	0
Pat_152	m	0	NA	NA	0	1	1	0
Pat_153	m	1	U	LP	1	0	0	0
Pat_154	m	0	M	HP	1	0	0	0
Pat_155	m	0	M	HP	1	0	0	0
Pat_156	f	0	U	LP	1	0	0	0
Pat_157	f	0	U	LP	1	1	0	0
Pat_158	m	0	M	HP	1	0	0	0
Pat_159	f	0	U	LP	1	0	0	0
Pat_160	m	0	U	LP	NA	NA	NA	NA
Pat_161	m	1	U	LP	0	0	0	0
Pat_162	m	0	M	HP	0	0	0	0
Pat_163	m	0	M	HP	0	0	0	0
Pat_164	f	0	U	LP	0	0	0	0
Pat_165	m	1	U	LP	0	1	1	0

Table 7.1: Summary of the patient samples and selected genetic features included in this study. Table published in Bruch and Giles et al. 2021. (*continued*)

Patient ID	Sex	Treated before	IGHV status	Methylation Cluster	Del13q	Del11q	Trisomy 12	Del17p
Pat_166	m	0	U	LP	1	0	1	0
Pat_167	m	0	NA	IP	NA	NA	NA	NA
Pat_168	m	0	M	HP	1	1	0	0
Pat_169	m	0	M	HP	0	0	1	0
Pat_170	m	0	M	HP	1	0	0	0
Pat_171	m	0	M	HP	1	0	0	0
Pat_172	m	0	M	HP	1	0	0	0
Pat_173	m	0	M	HP	1	0	0	0
Pat_174	f	0	U	LP	NA	0	NA	0
Pat_175	m	0	U	LP	0	0	0	0
Pat_176	f	0	M	HP	NA	NA	NA	NA
Pat_177	f	0	NA	IP	NA	1	NA	NA
Pat_178	m	0	M	HP	1	0	0	0
Pat_179	m	0	U	LP	0	1	0	0
Pat_180	m	0	M	HP	NA	NA	NA	NA
Pat_181	f	0	M	HP	NA	NA	NA	NA
Pat_182	m	0	M	HP	1	0	0	0
Pat_183	f	1	NA	IP	1	0	0	0
Pat_184	m	0	U	LP	NA	NA	NA	NA
Pat_185	m	0	M	HP	NA	NA	NA	NA
Pat_186	m	0	M	HP	1	0	0	0
Pat_187	m	1	U	LP	NA	NA	NA	NA
Pat_188	m	0	NA	NA	NA	NA	NA	NA
Pat_189	m	0	NA	NA	NA	NA	NA	NA
Pat_190	m	0	NA	NA	NA	NA	NA	NA
Pat_191	f	0	NA	NA	0	0	0	0
Pat_192	f	0	NA	NA	1	0	0	0

Table 7.2: Characteristics of drugs included in the screen. Table published in Bruch and Giles et al. 2021.

Drug	Main targets	Target category	Drug Group	Company	Cat. No.	Conc. 1	Conc. 2
Ibrutinib	BTK	BCR	kinase inhibitor	Selleck Chemicals	S2680	500nM	50nM
Idelalisib	PI3K delta	BCR	kinase inhibitor	Selleck Chemicals	S2226	500nM	50nM
Fludarabine	Purine analogue	DDR	chemotherapeutic agent	Selleck Chemicals	S1491	2000nM	200nM
Nutlin-3a	MDM2	DDR	other	Selleck Chemicals	S8059	10000nM	1000nM
Selumetinib	MEK1/2	MAPK	kinase inhibitor	Selleck Chemicals	S1008	1000nM	100nM
BAY-11-7085	NFKB	NFKB	other	Selleck Chemicals	S7352	2000nM	200nM
Everolimus	mTOR	mTOR	other	Selleck Chemicals	S1120	500nM	50nM
PRT062607	SYK	BCR	kinase inhibitor	Selleck Chemicals	S8032	500nM	50nM
Pyridone-6	JAK1/2/3	JAK/STAT	kinase inhibitor	MedChemExpress	457021-03-7	500nM	50nM
Ralimetinib	p38 MAPK	MAPK	kinase inhibitor	Selleck Chemicals	S1494	1500nM	150nM
Luminespib	HSP90	HSP90	other	Selleck Chemicals	S1069	200nM	20nM
I-BET 762	BRD2/3/4	Epigenome	other	Selleck Chemicals	S7189	1000nM	100nM

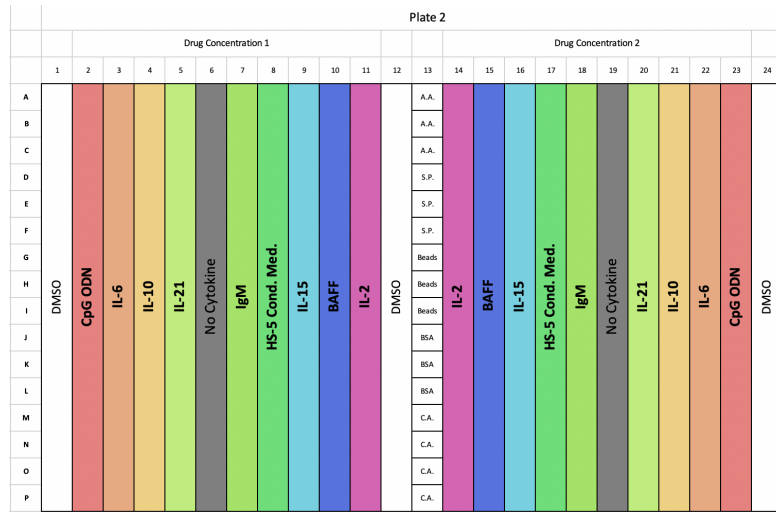


Figure 7.3: Layout of the remaining 9 / 18 stimuli on the second screening plate. A.A., S.P., Beads, B.S.A. and C.A. refer to additional agents tested in the screen which were not included in downstream analysis. *Plate plot generated by Peter-Martin Bruch.*

Table 7.3: Characteristics of the stimuli included in the screen. Table published in Bruch and Giles et al. 2021.

Stimulus	Name	Company	Concentration	Cat. No.	Lot No.	Source	Pathway
IL4 human recombinant animal component free	IL4	Sigma-Aldrich	10 ng/ml	SRP3093	0712AFC14	Company	JAK/STAT
IL10 human Animal component free	IL10	Sigma-Aldrich	10 ng/ml	SRP3312	1012AFC21	Company	JAK/STAT
IL2 human recombinant animal component free	IL2	Sigma-Aldrich	10 ng/ml	SRP3085	0416AFC12	Company	JAK/STAT
R-848	Resiquimod	Enzo Life Sciences	1000 ng/ml	ALX-420-038-M025	10211615	Company	TLR 7/8
Human IL-21	IL21	Peprotech	10 ng/ml	200-21	414226	Company	JAK/STAT
Human BAFF	BAFF	Peprotech	250 ng/ml	310-13	0706CY194	Company	NFkB
Human IL-\$\beta\$	IL1	Peprotech	10 ng/ml	200-01	0606B95	Company	NFkB
Human sCD40 Ligand	sCD40L	Peprotech	1000 ng/ml	310-02	1214145	Company	NFkB
Goat F(ab)2 Fragment to human IgM	soluble anti-IgM	MP Biomedicals	20000 ng/ml	55055	7227	Company	BCR
Human TGF\$\beta\$	TGF1	Peprotech	10 ng/ml	100-21	1117209	Company	MAPK
Human IL15	IL15	Peprotech	10 ng/ml	200-15	91624	Company	JAK/STAT
Human IL6	IL6	Peprotech	10 ng/ml	200-06	031316-2	Company	JAK/STAT
ODN 2006 (ODN 7909)	CpG ODN	Invivogen	1000 ng/ml	trtl-2006-1	3901-09T	Company	TLR 9
Human SDF-1\$\alpha\$(CXCL12)	SDF-1	Peprotech	200 ng/ml	300-28A	101492	Company	JAK/STAT
Human Interferon \$\gamma\$	Interferon	Peprotech	5 ng/ml	300-02	121527	Company	NFkB
HS-5 conditioned medium	HS-5 CM	self produced	20 %	NA	NA	self produced	NA

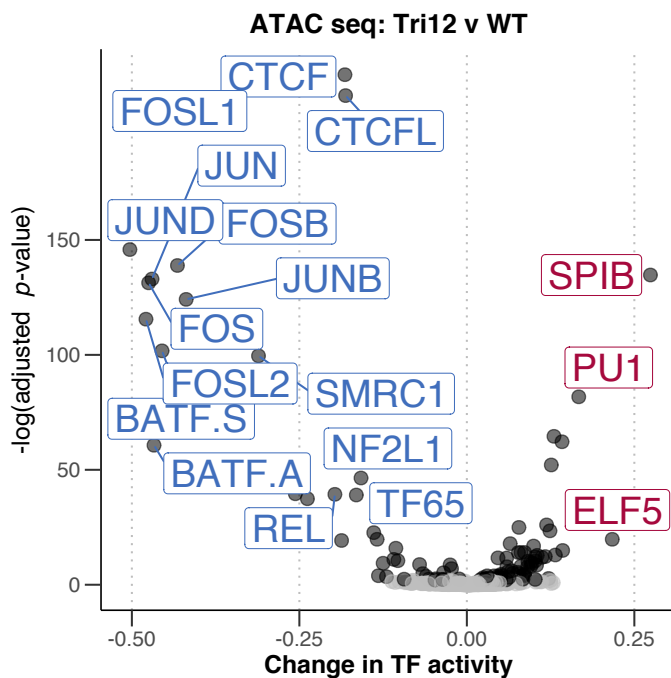


Figure 7.4: “Analysis of ATACseq dataset of two trisomy 12 and two non-trisomy 12 untreated CLL PMBC samples. The volcano plot depicts change in TF activity (x axis) versus BH-adjusted p-values (y axis) for 636 TFs, comparing trisomy 12 and non-trisomy 12 samples. The *diffTF* (Berest et al. 2019) software was run in analytical mode to calculate TF activity, measured as weighted mean difference. TFs are labelled if adjusted p-value < 0.01 and absolute weighted mean difference > 0.15.” *diffTF analysis ran by Ivan Berest, figure and caption published in Bruch and Giles et al. 2021.*

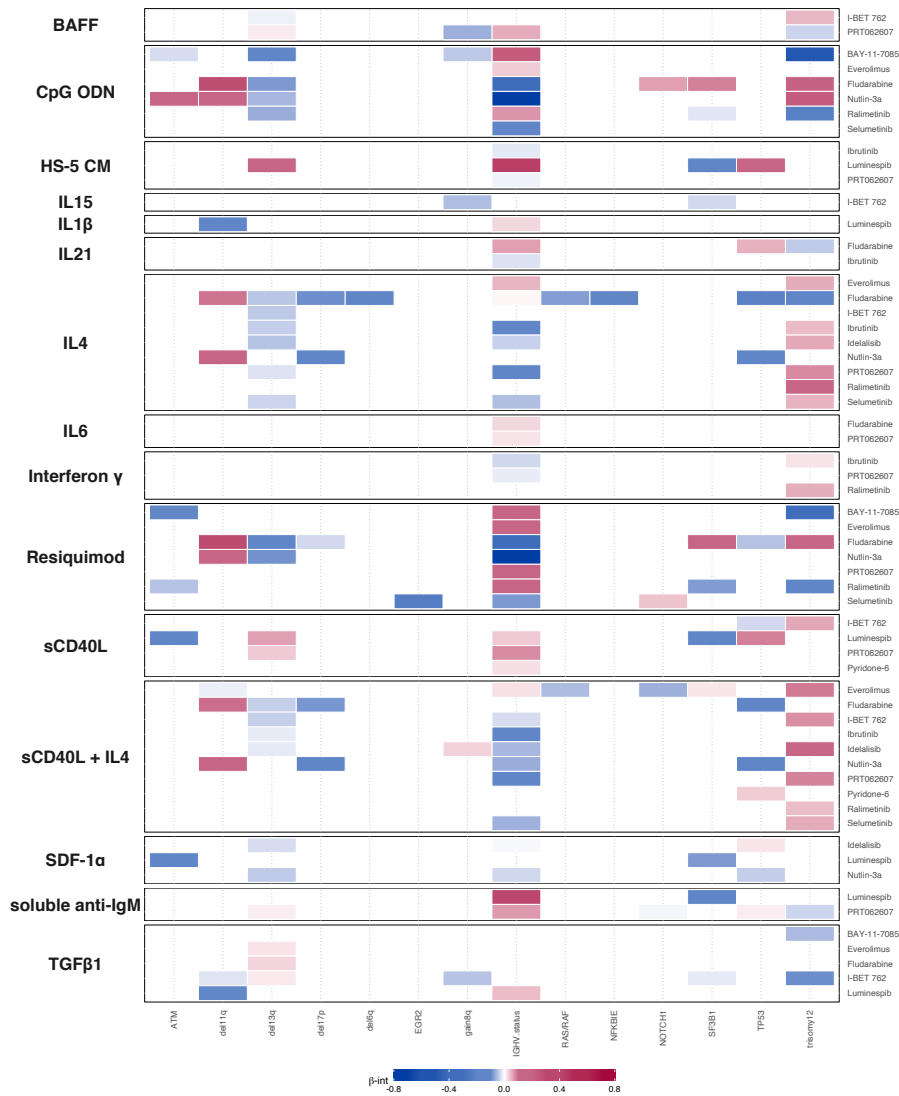


Figure 7.5: Heatmap depicting overview of genetic predictors of drug - stimulus interactions (each row represents the coefficients from fitting a single multivariate model). Stimuli are shown on left, and corresponding drugs on right. Drugs, stimuli and genetic alterations are alphabetically sorted. Coloured fields indicate that the β_{int} for given drug and stimulus is modulated by corresponding genetic feature. Positive coefficients are shown in red, indicating β_{int} is more positive for given drug and stimulus combination if the feature is present. *Figure and caption generated with Peter-Martin Bruch for the manuscript Bruch and Giles et al. 2021.*

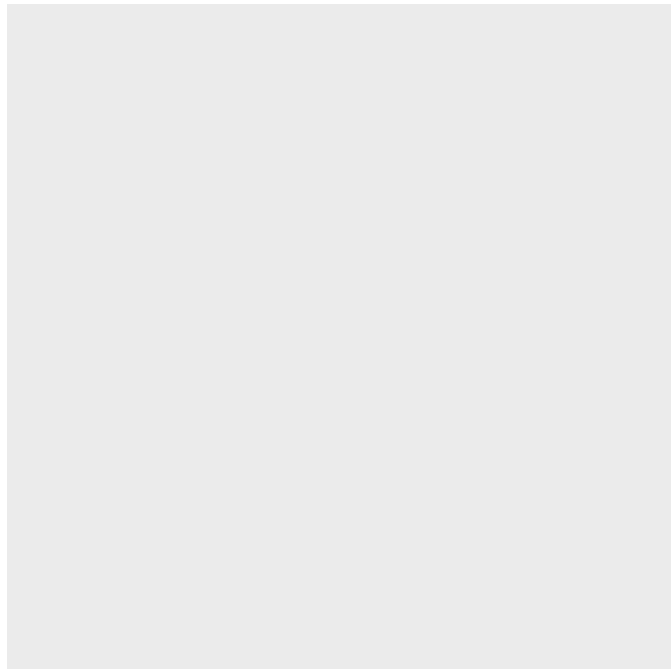


Figure 7.6: Add NUTLIN-3A Predictor profile

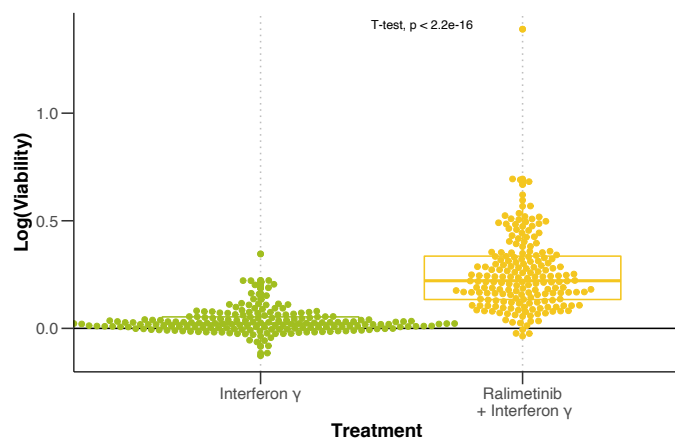


Figure 7.7: Beeswarm-boxplots of log-transformed control-normalised viability values for $\text{IFN}\gamma$ and Ralimetinib + $\text{IFN}\gamma$ treated samples.

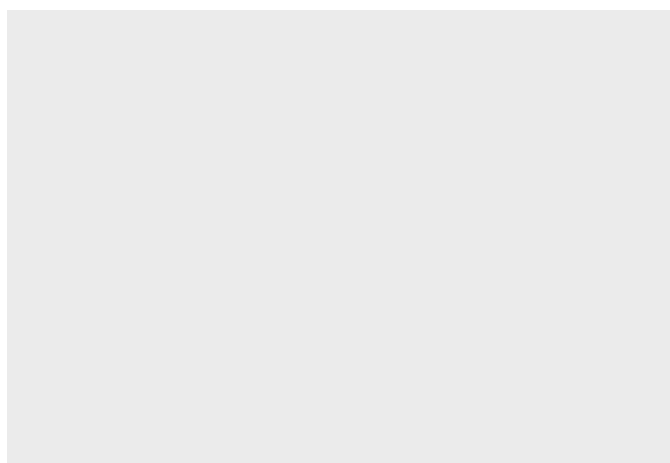


Figure 7.8: Differential TF binding site accessibility (y axis) in trisomy 12 vs non-trisomy 12 CLL samples (purple) and for IBET-762 vs DMSO treated CLL samples (green). Direction of differential accessibility values are shown for two independent datasets comparing trisomy 12 vs non-trisomy 12 CLL and IBET-762 vs control-treated CLL, for all TFs with adjusted p value <0.05 in the trisomy 12 comparison. Absolute change in TF accessibility can not be compared between the two experiments. See Methods section 2.1.2 and 2.4.2. *Figure and caption from Bruch and Giles et al. 2021.*

Table 7.4: Table depicting stimulus and receptor pairs used in stimulus response - stimulus receptor expression analysis.

Cytokine	Receptor	ENSEMLID	Kegg
SDF-1a	CXCR 4	ENSG00000121966	7852
SDF-1a	CXCR 7	ENSG00000144476	57007
IL-6	IL-6 R	ENSG00000160712	3570
IL-6	IL-6 ST	ENSG00000134352	3572
IL-15	IL-15 R alpha	ENSG00000134470	3601
IL-15	IL-2 R beta	ENSG00000100385	3560
IL-15	IL-2 R gamma	ENSG00000147168	3561
IL-21	IL-21 R	ENSG00000103522	50615
IL-21	IL-21 R gamma	ENSG00000147168	3561
IL-2	IL-2 R alpha	ENSG00000134460	3559
IL-2	IL-2 R beta	ENSG00000100385	3560
IL-2	IL-2 R gamma	ENSG00000147168	3561
IL-10	IL-10 R alpha	ENSG00000110324	3587
IL-10	IL-10 R beta	ENSG00000243646	3588
IL-4	IL-4 R	ENSG00000077238	3566
IL-4	IL-2 R gamma	ENSG00000147168	3561
IL-4	IL-13 R A1	ENSG00000131724	3597
soluble anti-IgM	B cell receptor	ENSG00000275063	102723407
soluble anti-IgM	CD79A	ENSG00000105369	973
soluble anti-IgM	CD79B	ENSG0000007312	974
Resiquimod	TLR 7	ENSG00000196664	51284ä
Resiquimod	TLR 8	ENSG00000101916	51311
CpG ODN	TLR9	ENSG00000239732	54106
BAFF	BAFF R	ENSG00000159958	115650
BAFF	TACI	ENSG00000240505	23495
BAFF	BCMA	ENSG00000048462	608
IL-1b	IL-1 R1	ENSG00000115594	3554
IL-1b	IL-1 R2	ENSG00000115590	7850
sCD40L	CD40	ENSG00000101017	958
Interferon gamma	IFN-gamma R1	ENSG00000027697	3459
Interferon gamma	IFN-gamma R2	ENSG00000159128	3460
TGF-b1	TGF-beta R1	ENSG00000106799	7046
TGF-b1	TGF-beta R2	ENSG00000163513	7048

Table 7.5: Number of cases of each gene mutation within the cohort used in this study.

	0	1
del13q	66	108
TP53	157	30
del11q	148	28
SF3B1	161	26
trisomy12	149	25
NOTCH1	137	24
del17p	154	20
ATM	164	16
gain8q	159	13
del8p	135	11
MED12	170	10
gain2p	137	9
KRAS	177	7
BRAF	180	7
del6q	166	7
POT1	174	6
del9p	140	6
NFKBIE	175	5
FAT2	175	5
CSMD3	175	5
del1q	141	5
del18p	141	5
del15q	141	5
del14q	145	5
IKZF3	176	4
FAT4	176	4
EGR2	176	4
gain19q	142	4
gain19p	142	4
gain18q	144	4
del9q	142	4
MYD88	184	3